Федеральное государственное автономное образовательное учреждение
высшего образования «Уральский федеральный университет
имени первого Президента России Б. Н. Ельцина»

*На правах рукописи*

Кифле Александр Берхане

# ВЛИЯНИЕ «ЗЕЛЕНЫХ» МЕТАЛЛОВ, КАК МОДИФИКАТОРОВ, НА ЭЛЕКТРОХИМИЧЕСКИЕ И ЭЛЕКТРОАНАЛИТИЧЕСКИЕ СВОЙСТВА ТОЛСТОПЛЕНОЧНЫХ УГЛЕРОДСОДЕРЖАЩИХ ЭЛЕКТРОДОВ НА ПРИМЕРЕ ВОЛЬТАМПЕРОМЕТРИЧЕСКОГО ОПРЕДЕЛЕНИЯ ФОРМАЛЬДЕГИДА И НИКЕЛЯ

1.4.2. Аналитическая химия

Диссертация на соискание ученой степени
кандидата химических наук

Научный руководитель:
Доктор химических наук, профессор
Козицина Алиса Николаевна

Екатеринбург – 2024

Federal State Autonomous Educational Institution of Higher Education “Ural Federal University named after the First President of Russia B. N. Yeltsin”

*On the rights of the manuscript*

Kifle Alexander Berhane

# THE INFLUENCE OF “GREEN” METALS, AS MODIFIERS, ON THE ELECTROCHEMICAL AND ELECTROANALYTICAL PROPERTIES OF THICK FILM CARBON-CONTAINING ELECTRODES USING THE EXAMPLE VOLTAMMETRIC DETERMINATION OF FORMALDEHYDE AND NICKEL

1.4.2. Analytical Chemistry

Dissertation for the degree
of Candidate of Chemical Sciences

Scientific supervisor:
Doctor of Chemical Sciences, Professor
Kozitsina Alisa Nikolaevna

Ekaterinburg – 2024

# TABLE OF CONTENTS

INTRODUCTION…….....5
CHAPTER 1 LITERATURE REVIEW……...…14
1.1 Physicochemical properties of formaldehyde……14
1.2 Formaldehyde toxicity and mechanism of action……...15
1.3 Sources of formaldehyde entering the environment, sanitary, hygienic and medical products……17
1.4 Methods for quantitative determination of formaldehyde ..... 22
1.4.1 Spectrophotometry and Chemiluminescence methods ..... 23
1.4.2 Chromatographic methods ..... 25
1.4.3 Electrochemical methods..... 28
1.4.3.1 Electrocatalytic conversion of formaldehyde with participation of the electrode material ..... 28
1.4.3.2 Voltammetry of electrochemically active derivatives of formaldehyde at mercury and carbon-containing electrodes ..... 30
1.5 Influence of plating conditions on the surface morphology of “green” metals-modified electrodes……..35
1.6 Evaluation of electrochemical performance of bismuth-modified electrodes ..... 48
1.7 Neutral Red as a near-reversible redox couple ..... 53
1.8 Statement of the research problem..... 55
CHAPTER 2 EXPERIMENTAL SECTION……59
2.1 Instrumentation and electrodes ..... 59
2.2 Reagents and preparation of solutions ..... 60
2.3 Preparation of “green” metals-modified screen-printed carbon-containing electrodes……..61
2.4 Objects of analysis and their preparation..... 62
CHAPTER 3 STUDY OF ELECTROCHEMICAL BEHAVIOR AND ELECTROANALYTICAL PERFORMANCE OF FORMALDEHYDE HYDRAZONE

ON BISMUTH-MODIFIED SCREEN-PRINTED CARBON-CONTAINING ELECTRODE……...64
3.1. Electrochemical behavior of formaldehyde hydrazone on bismuth-modified screen-printed carbon-containing electrode..... 64
3.2. Electroanalytical performance of bismuth-modified screen-printed carbon-containing electrode towards formaldehyde ..... 74
Conclusions to chapter 3 ..... 83
CHAPTER 4 STUDY OF “GREEN” METALS-MODIFIED SCREEN-PRINTED CARBON-CONTAINING ELECTRODES WITH PHYSICOCHEMICAL METHODS……...…84
4.1 Morphological characterization of the “green” metals-modified electrodes..... 84
4.2 Neutral Red as a redox probe for evaluation of electrochemical performance of “green” metals-modified electrodes..... 89
Conclusions to chapter 4 ..... 101
CHAPTER 5 ELECTROANALYTICAL PERFORMANCE OF “GREEN” METALS-MODIFIED SCREEN-PRINTED CARBON-CONTAINING ELECTRODES ……..…..102
5.1 Electroanalytical performance of the bismuth-modified screen-printed carbon-containing electrodes towards nickel (II) and formaldehyde..... 102
5.2 Electroanalytical performance of the antimony-modified screen-printed carbon-containing electrodes towards nickel (II)..... 108
Conclusions to chapter 5 ..... 112
CONCLUSION……..113
LIST OF SYMBOLS AND ABBREVIATIONS……116
LIST OF REFERENCES……118
Appendix A (Mandatory) Implementation information……147

# INTRODUCTION

## The relevance of the research topic

Formaldehyde is ubiquitously found in the environment due to natural sources and anthropogenic activities. Accordingly, a large portion of the human population is exposed to it environmentally and occupationally. This compound possesses significant health risks, causing severe respiratory and dermatological complications. Many cases of poisoning, allergy, asthma, pulmonary damage, cancer and even death linked to FA exposure from various sources have been reported. In addition, it was reported that FA exhibits mutagenic and genotoxic effects in several experimental models in vivo and in vitro. In its anhydrous form, FA is a potent reactive small electrophile that can bind covalently with biological nucleophiles in proteins, DNA and other molecules, which might lead to the formation of formaldehyde-specific antibodies and facilitates the formation of intrastrand and DNA-protein cross-links. It is probable that related reactions of FA in cells are responsible for its toxic and carcinogenic effects.

Formaldehyde is used in the production of phenol-formaldehyde, urea-formaldehyde and melamine-formaldehyde resins, which are subsequently used to manufacture chipboard and plywood for furniture. Consequently, FA is a main indoor air pollutant. Additionally, these resins serve as auxiliary reagents in the textile, leather, rubber, cement and other building materials industries. As a preservative, FA can be used in wood processing, the production of paints, cosmetics, personal hygiene products and pharmaceutical products to prevent mold and bacterial growth. Remarkably, FA has been detected in water at wastewater treatment plants and even in purified bottled drinking water, mainly due to the oxidation of organic substances during ozonation and chlorination processes. Such widespread use of FA in various fields creates the need for the development of simple and sensitive methods for its detection and control in environmental objects, drinking water, consumer products, pharmaceutical raw materials and medicines.

Electroanalytical approaches, due to their high sensitivity, rapid response, selectivity, simplicity, low cost, potential for miniaturization and capacity for real-time measurements in small laboratories, are particularly attractive for this purpose. These methods are considered as good alternatives to the expensive and time-consuming standard laboratory techniques such UV-Vis spectrophotometry, liquid chromatography, gas chromatography and chemiluminescence for the detection of traces of FA.

In voltammetry, bismuth-based electrodes have been developed as low toxic eco-friendly working electrodes for the detection of heavy metal ions and electroactive organic compounds. These “green” bismuth-based electrodes exhibit suitable electrochemical characteristics, such as a wide cathodic potential window, high electrocatalytic activity, the capability to adsorb organic compounds and insensitivity to dissolved oxygen. These characteristics make them a viable and environmentally sound alternative to toxic mercury and mercury film electrodes. Notably, screen-printed carbon-containing electrodes modified with bismuth films in a potentiostatic mode are widely used as working electrodes in voltammetry due to their simple modification process and favorable electroanalytical properties. Fabricated from carbon inks and pastes, SPCEs offer several advantages: low cost, easy mass production capability, high versatility in modification and excellent surface reproducibility. Unlike glassy-carbon electrodes, SPCEs do not require multi-stage mechanical surface regeneration. These characteristics make them suitable for developing new methods for the quantitative determination of FA using Bi/SPCEs.

Antimony, along with bismuth, is used as a modifier of carbon-containing electrodes due to its low environmental toxicity relative to mercury and its electrochemical/electroanalytical characteristics. Bismuth and antimony, like other modifiers, contribute to the change in the properties of the interface between the electrode and the electrolyte, the kinetics of electron transfer, the area of the electroactive surface and improving the electroanalytical characteristics of the electrode. Cyclic voltammetry and electrochemical impedance spectroscopy are used to keep track

of these changes using well-reversible redox couples, primarily $[Fe(CN)_6]^{3-/4-}$ or $[Ru(NH_3)_6]^{3+/2+}$.

However, bismuth and antimony start to oxidize at a potential of approximately minus 0.2 V in solutions with pH of 5 – 6, which are the typical operating conditions for these “classic” redox couples. Consequently, these redox couples are not suitable for studying the electrochemical characteristics of bismuth or antimony-based “green” metal electrodes due to their redox potentials falling within the metal dissolution range. For this reason, the search for alternative redox couples to effectively monitor the modification of SPCE surfaces with bismuth or antimony is quite relevant at this stage for advancing “green” electroanalysis.

**The degree of development of the research topic**

It is known that FA in aqueous solutions is found mainly in its hydrated form of methyl glycol ($CH_2(OH)_2$), which is electrochemically inactive. The electrochemically active (dehydrated) aldehyde form of FA ($CH_2O$) makes up a very small fraction of its analytical concentration. In this regard, a frequently used signal-forming process is the selective catalytic conversion of FA with the participation of the electrode material, mainly, noble metals or carbon-containing substrates modified with highly dispersed nanoparticles of specified metals that offer active sites and high surface area. In this instance, in most cases, electrochemical oxidation of FA is used to detect FA in various matrices by voltammetry like cyclic voltammetry, differential-pulse voltammetry and chronoamperometry (CA) methods. A common drawback of these sensor approaches is the surface fouling and passivation caused by some intermediate products generated during the reaction. Furthermore, determining FA using these methods suffers from low sensitivity, the formation of oxide layers on the metal surface complicating voltammogram interpretation and a strong dependence of kinetic behavior on the electrode surface state, leading to ambiguous results. It is important to note that modified electrodes are usually quite difficult to prepare and use in routine analysis.

Indirect methods of quantitative determination of FA employing a hanging mercury drop electrode are known. In these methods, FA is completely converted into its electrochemically active derivative via a chemical reaction with an amino compound. For instance, FA reacts with trimethylaminoacetohydrazide chloride (Girard T-reagent) in a neutral medium to form an electroactive adduct (formaldehyde-Girard T adduct, FGA). Alternatively, FA can be converted to formaldehyde hydrazone by reacting with hydrazine sulfate. The latter method is preferred due to its simplicity, fastness and ability to perform measurements at room temperature in the presence of dissolved oxygen without the need for preliminary exposure of the analyzed solutions for the formation of FAH. Results of a study of the electrochemical behavior of FAH on bismuth-modified SPCEs could lead to the development of a safe (“green”), very simple, low-cost, reliable and fast voltammetric methods for the quantitative determination of FA.

As well-reversible redox couples such as $[Fe(CN)_6]^{3-/4-}$ or $[Ru(NH_3)_6]^{3+/2+}$ are in some cases unsuitable for evaluating the electrochemical performance of bismuth-based electrodes within the framework of commonly used approaches, researchers have proposed original conditions for carrying out EIS measurements on these electrodes, for example, in the region of discharge of ions to be determined or hydrogen evolution. To calculate the electroactive surface area of these electrodes using the Randles-Ševćik equation, it was suggested to utilize the currents associated with the irreversible and adsorption-complicated electroconversion processes of the analyte in cyclic voltammograms, rather than those from well-reversible redox pairs. Unlike bismuth film electrodes, systematic studies evaluating the electrochemical performance of antimony-based electrodes are lacking.

However, it is known that monoprotonated 3-Amino-7-dimethylamino-2-methylphenazine hydrochloride (Neutral Red) in aqueous media undergoes a reversible redox process in the cathodic region where bismuth and antimony are electroinactive. Therefore, it makes sense to try NR, a well-known electronic mediator, for instance in the construction of biosensors, in a new capacity as a redox probe for evaluating the

electrochemical performance of bismuth and antimony-modified screen-printed carbon-containing electrodes.

**The dissertation work aims** to investigate the electrochemical behavior of formaldehyde hydrazone on bismuth-modified screen-printed carbon-containing electrodes for the development of a new voltammetric method for the quantitative determination of FA in medicinal product and pharmaceutical raw material, waste, melt, bottled waters, and to study the possibilities of using NR as an alternate well-reversible redox probe to monitor the efficiency of electrode modification processes with “green” metals.

To achieve this goal, it is necessary to solve several **tasks**.

1. To study the electrochemical behavior of FA in the form of FAH on Bi/SPCE.

2. To investigate the morphology of the Bi/SPCEs surface as a function of bismuth film deposition time and select optimized operating conditions for obtaining the electroactive form of the FA and establishing a reliable analytical response.

3. To develop a method for the quantitative determination of FA on Bi/SPCEs by voltammetry in the medicinal dug "Endofalk®" and technical urotropin, waste, melt and bottled waters.

4. To characterize the morphology of the bismuth and antimony coatings on the surface of the SPCEs as a function of changing chemical and instrumental conditions during the potentiostatic preplating process.

5. To study the electrochemical behavior of NR on SPCEs before and after their modification with bismuth or antimony.

6. To evaluate the electrochemical characteristics of unmodified and bismuth- or antimony-modified SPCEs, with significantly different surface morphologies, using CV and EIS methods, employing NR as a redox probe.

7. To compare the electroanalytical characteristics of the “green” metals-modified SPCEs with different surface morphologies towards FA and Ni(II) ions for Bi/SPCEs and towards Ni(II) ions for Sb/SPCEs.

**Methodology and methods of dissertation research**

Screen-printing technology was used to produce thick-film carbon-containing electrodes. For modification of the SPCEs surface with “green” metals, a potentiostatic preplating procedure was applied.

The surface morphology of the modified electrodes was studied by scanning electron microscopy. The average sizes of the metal particles and the surface area of the SPCE substrates covered with metals (%) were estimated using the program Image Processing and Analysis in Java (https://imagej.nih.gov/ij/download.html).

Electrochemical impedance spectroscopy was used to quantitatively assess the electron transport characteristics of the electrodes. CV was used to study the degree of reversibility of oxidation/reduction processes of an electroactive substance and to calculate the electroactive surface area of the electrodes. In this case, NR was used as an alternative well-reversible redox pair. Evaluation of the electroanalytical characteristics of the electrodes and analysis of real samples were performed using direct and stripping DP VA.

**Provisions submitted for the defense**

1. Results of the investigation of the electrochemical behavior of FA in the form FAH on Bi/SPCEs.

2. Results of the study of the effects of operating conditions and bismuth film deposition time on FA reduction current at Bi/SPCE.

3. Electroanalytical characteristics of Bi/SPCEs towards FA and the methods of its voltammetric determination in the drug "Endofalk®" and technical urotropin, waste, melt and bottled waters.

4. Results of comparative evaluation of the electrochemical characteristics of bare-SPCE, Bi/SPCEs and Sb/SPCEs, with significantly different morphologies, using NR as a redox probe.

5. Correlation between the morphological, electrochemical and electroanalytical characteristics of Bi/SPCEs and Sb/SPCEs.

**Scientific novelty of the research results**

The electrochemical behavior of FA in the form of its electroactive hydrazone on the Bi/SPCEs was studied. It was shown that the process of its electrochemical reduction is irreversible and is controlled primarily by diffusion.

Cyclic voltammetry method showed that NR in the protonated form undergoes quasi-reversible one-electron oxidation-reduction transformations on the surface of SPCE before and after its modification with “green” metals. It was shown that the process of electrochemical conversion of NR on unmodified SPCE is controlled by diffusion, while for SPCEs modified with bismuth or antimony, the diffusion process is accompanied by adsorption.

Neutral red is used for the first time as an alternative redox couple for comparative evaluation of electrochemical characteristics of SPCE modified with bismuth or antimony under different potentiostatic conditions of metal predeposition. It is shown that electrochemical impedance spectroscopy data obtained using NR as a redox couple allows estimating the degree of coverage of the carbon-containing substrate with metal films, which is confirmed by micrographs of Bi/SPCE and Sb/SPCE surfaces with different morphology. A significant correlation is established between the degree of substrate coverage with “green” metals and the dispersion of their particles with the surface roughness factor of the modified electrodes and the sensitivity of Bi/SPCE and Sb/SPCE to Ni(II) ions and FA as model analytes.

**Theoretical and practical significance of the work**

The possibility of electrochemical transformations of electrochemically active derivative of FA on the surface of bismuth was investigated. The relationship between the morphology of the modifier and the reduction current (response) of FAH was quantitatively characterized.

The possibility of using NR as a quasi-reversible redox couple for quantitative evaluation of the electrochemical characteristics of SPCEs modified with bismuth or

antimony, instead of “classical” redox couples in the case when their redox potentials fall into the region of dissolution of these metals, has been proven.

The practical significance of the developed approach utilizing NR as an alternative redox probe lies in the possibility of simple and rapid monitoring of the effectiveness of the modification process when creating novel sensors based on “green” metals.

A voltammetric method for the sensitive determination of traces of FA has been developed using Bi/SPCE. The method exhibited a fairly wide linear range (0.33–167 μM), a low limit of detection (LOD) of 0.07 μM, and a limit of quantification (LOQ) of 0.33 μM. These performance metrics surpass those reported in the literature for direct electrocatalysis on solid electrodes and indirect methods with HMDEs. Bi/SPCE differs from many known approaches in the extreme simplicity of the modification procedure, demonstrating high electroanalytical performance. The developed voltammetric methods offer an environmentally safe, inexpensive, very simple and fast manner for determining FA in medicinal products, pharmaceutical raw materials and environmental objects with satisfactory indicators of recovery and precision.

The method of electrochemical analysis of pharmaceuticals to determine FA content has been implemented and used in the educational process in the training of pharmaceutical personnel at the Department of Pharmacy of the Federal State Educational Institution of Higher Education of the Ural State Medical University of the Ministry of Health of Russia within the framework of the disciplines “Analytical Chemistry”, “General and Inorganic Chemistry”.

**Degree of reliability of the obtained results**

The reliability of the obtained results is confirmed using modern physical, chemical and analytical research methods in the work, the correspondence between the results obtained by different methods on high-tech equipment from well-known global manufacturers, the publication of the main experimental data in highly rated specialized journals, good agreement between the results of FA determination in real samples by the

proposed method and independent certified methods. The mass concentration of FA in the analyzed samples is characterized by good reproducibility under conditions of intralaboratory precision.

**Approval of the work**

The main provisions of the dissertation work were reported at scientific conferences: IV Congress of Russian Analysts (Moscow, 2022), XXXIV Russian Youth Scientific Conference with International Participation “Problems of Theoretical and Experimental Chemistry” (Ekaterinburg, 2024), XI All-Russian Conference on Electrochemical Methods of Analysis (Ekaterinburg, UrFU, 2024).

**Publications**

The main results based on the dissertation materials are presented in 6 scientific papers, of which 3 articles are in peer-reviewed scientific publications determined by the Higher Attestation Commission of the Russian Federation and the Certification Council of UrFU and indexed in the international databases Scopus and Web of Science.

**The author's personal contribution** consists of direct participation in the implementation of research and the general formulation of problems, in conducting analysis and statistical processing of the obtained results; in the writing of articles and reports, testing and implementation of research results in the development of voltammetric methods for determining FA in the drug "Endofalk®" and technical urotropin, waste, melt and bottled waters.

**Structure and volume of the dissertation**

The dissertation consists of an introduction, five chapters, a conclusion, and a list of references. The work is presented on 147 pages and contains 42 figures and 19 tables. The list of literature includes 245 titles of works by Russian and foreign authors.

# CHAPTER 1 LITERATURE REVIEW

## 1.1 Physicochemical properties of formaldehyde

Formaldehyde (also known as methanal) is a low-molecular-weight gas characterized by its high reactivity, toxicity and irritant properties at ambient temperature. It exhibits substantial water solubility (around 0.4 mg/cm$^3$ at 20 °C) and is miscible with common organic solvents such as benzene, ether, acetone and chloroform. Despite being slightly denser than air (with a relative density of 1.03-1.07 compared to air), FA can accumulate in poorly ventilated, low-lying areas [1].

Under ambient conditions (temperatures up to 80 °C) and in the presence of air and moisture, FA readily undergoes self-polymerization to form various polymeric structures (Figure 1.1) [2]. In aqueous solutions, FA primarily exists as methylenediol or methyl glycol, a hydrated form that equilibrates with a range of short polymer chains (oligomers). In the absence of methanol, FA further converts to an insoluble, white cyclic trimer (1,3,5-trioxane) and ultimately polymerizes into solid polyoxymethylene glycol (paraformaldehyde) within aqueous solutions [3]. To prevent polymerization and stabilize the solution, FA is commonly stored or transported as a 30 – 50% (w/w) aqueous solution containing 10 – 15% methanol, known as formalin [1, 3].

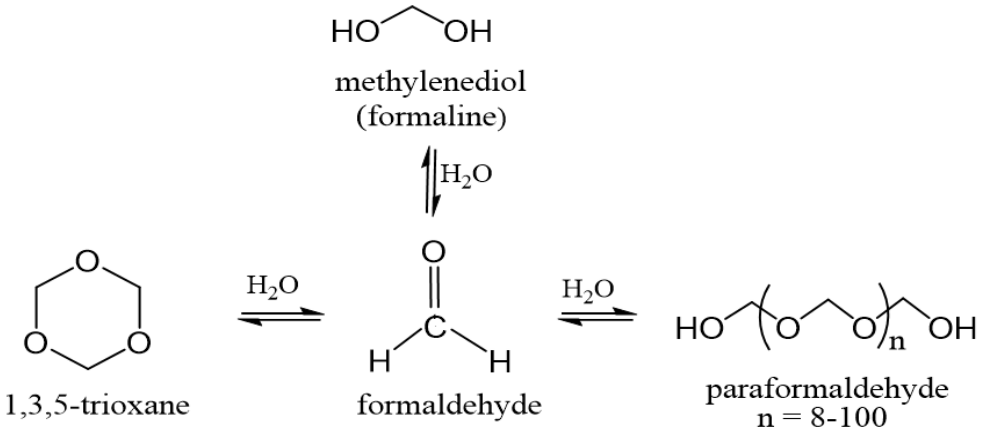


Figure 1.1 – Polymerization of Formaldehyde

Formaldehyde exhibits moderate thermal stability at ambient temperatures. However, its stability diminishes at elevated conditions. Above 150 °C, it decomposes to form methanol and carbon monoxide. Further increasing the temperature to exceed 350 °C results in the formation of carbon dioxide and hydrogen [4]. In environmental contexts, FA undergoes rapid transformation. It is readily photo-oxidized by sunlight to produce carbon dioxide and reacts instantaneously with hydroxyl radicals, a prevalent atmospheric constituent, to generate formic acid [1].

## 1.2 Formaldehyde toxicity and mechanism of action

Given its widespread environmental presence, a substantial portion of the human population is exposed to FA through both environmental and occupational routes [5-7]. Extensive documentation links FA exposure to a range of adverse health effects, including poisoning, allergies, asthma, pulmonary damage, cancer and even fatalities [5-9]. FA is a mutagenic and genotoxic compound that readily forms bonds with critical cellular components such as proteins and DNA [1, 5]. The International Agency for Research on Cancer (IARC), the World Health Organization (WHO) and the Risk Assessment Committee (RAS) have classified FA as a carcinogen (IARC, WHO) and a potential mutagen (RAS) [1, 6, 10].

Primary routes of FA exposure include inhalation and dermal/ocular contact [11, 12]. Individuals working in construction, furniture manufacturing and pathology laboratories are at heightened risk of occupational exposure [1]. Exposure to FA can induce a range of health effects. Low-level exposure may manifest as irritation and respiratory difficulties, while prolonged or repeated exposure can lead to severe respiratory conditions, skin ailments and potentially cancer [1, 4]. Moreover, long-term FA exposure raises concerns regarding reproductive health in both males (reduced sperm quality) and females (increased menstrual irregularities and pregnancy complications) [8, 13]. Children are particularly susceptible to it due to their physiology, inhaling

proportionately more relative to their body weight and being exposed to higher concentrations closer to ground level [14]. Figure 1.2 illustrates the diverse organ toxicity associated with FA exposure [1].

To mitigate FA health risks due to its high toxicity and volatility, regulatory agencies have established exposure limits for FA. The WHO and the US Occupational Safety and Health Administration (OSHA) have implemented strict workplace exposure limits 0.08 mg/L (WHO) and 0.75 mg/L (OSHA) [15-17]. For indoor air with a 30-minutes exposure, the recommended limit is 0.10 mg/m³ (WHO) and 0.05 mg/m³ (Russian Federation) [18, 19]. As for drinking water the limit is set as 0.05 mg/L (Russian Federation) and 0.90 mg/L (WHO) [19, 20].

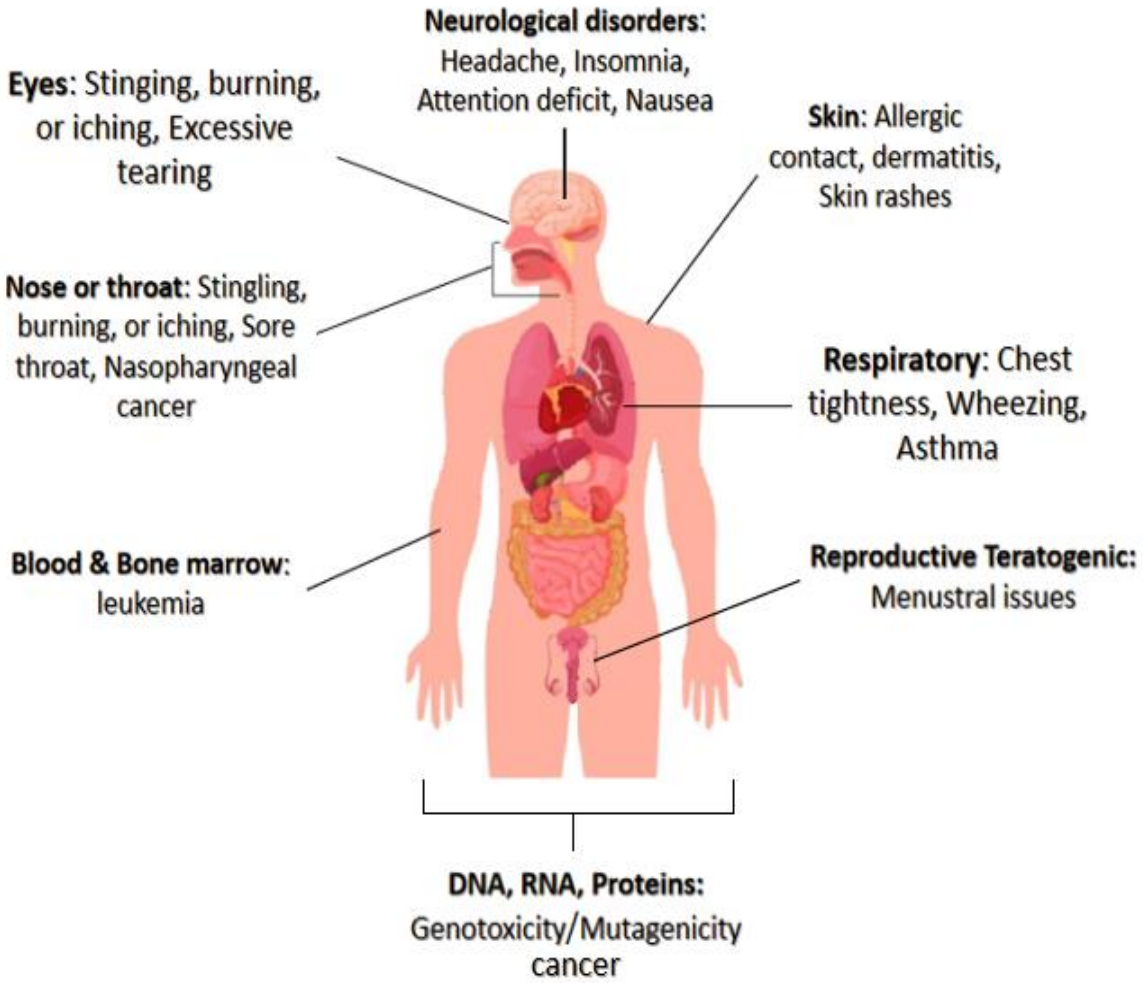


Figure 1.2 – Toxic effect of formaldehyde in different body organs [1]

## 1.3 Sources of formaldehyde entering the environment, sanitary, hygienic and medical products

Formaldehyde, a ubiquitous environmental compound, originates from both natural and anthropogenic sources. Natural processes, including biomass burning (forest fires and wildfires), decomposition of organic matter (dead plants and animals) and volcanic eruptions, are significant contributors to atmospheric FA levels [1]. Living organisms themselves also release trace amounts of FA as a natural metabolic byproduct [4, 21].

Human activities significantly contribute to elevated environmental FA levels. Industrial facilities, fossil fuel combustion for energy generation and fuel burning in vehicles and power plants directly release FA into the atmosphere [22]. Additionally, the atmospheric oxidation of volatile organic compounds (VOCs) such as methane, isoprene and terpenes, emitted from both anthropogenic and natural sources, indirectly contributes to FA formation. These VOCs undergo photo-oxidation through reactions with atmospheric hydroxyl radicals and ozone, producing FA and other aldehydes as intermediates. Ultimately, these intermediates break down into carbon monoxide, carbon dioxide, hydrogen and water [23, 24].

Formaldehyde is also a widely produced industrial chemical, with global annual production reaching 30 million tons, primarily concentrated in China, the United States and Germany [9]. Its extensive production is driven by its unique properties, including solubility, polymerization potential, cost-effectiveness, thermal stability and chemical reactivity. Over 65% of FA production is dedicated to the manufacturing of essential resins (phenol-formaldehyde, urea-formaldehyde, melamine-formaldehyde and polyacetal) used in various sectors such as construction materials, coatings, wood products, textiles, adhesives and automotive components [4, 25]. These applications constitute major indirect sources of FA, particularly indoors, where concentrations are

often highest due to the combined effects of off-gassing from these materials and limited ventilation [9].

Formaldehyde, in its formalin form, is a cornerstone in the biological and medical fields. Its applications encompass long-term storage of biological samples, embalming, disinfection, dental coatings and the preservation of medical instruments during hemodialysis [4, 7]. The pharmaceutical industry utilizes FA as a preservative and an alkylating agent [26, 27], while the cosmetics industry incorporates low concentrations as a preservative in products like mouthwashes (approximately 0.1%) and antiperspirants (< 0.5%) [28]. Notably, FA is also used in vaccine manufacturing to inactivate viruses and neutralize bacterial toxins. However, these quantities are minute and undergo rigorous purification, with the final product containing negligible traces well below safety limits [29].

It is essential to note that FA can also be unintentionally generated as a degradation byproduct of active pharmaceutical ingredients during storage. For instance, "Macrogol 3350", also known as polyethylene glycol (PEG) or polyethylene oxide (PEO), is a high-molecular-weight (3350 kDa), water-soluble, nonionic polymer of ethylene glycol. Widely employed in pharmaceuticals, cosmetics, food, chemicals and various other industries, PEG, in combination with electrolytes, found its first clinical application in the United States in 1984. Currently, Macrogol is the most commonly used bowel preparation solution for colonoscopy and a constituent of numerous medications, particularly ointments [30-33].

"Endofalk®", one such drug, contains PEG with a molecular weight of 3350. This powder-free, odorless substance is neither metabolized nor absorbed and the bacterial flora does not ferment it [34]. Macrogol's laxative effect stems from its ability to retain water molecules in the intestine through hydrogen bonding, consequently increasing osmotic pressure and fluid volume. This heightened intestinal activity stimulates peristalsis (gut contractions), promoting bowel movements and preventing irritation [30]. Its efficacy and safety have been substantiated through extensive clinical trials

involving both children and adults [35]. According to Pelham et al. [31], utilizing ultra-sensitive high performance liquid chromatography coupled with mass spectrometry (HPLC-MS), orally administered "Macrogol 3350" is minimally absorbed, rapidly eliminated from the body and primarily excreted in feces.

The polymer, when exposed to atmospheric oxygen at elevated temperatures, undergoes unintended FA formation, potentially altering drug properties and reducing shelf life. Consequently, meticulous control of FA content in medications containing "Macrogol 3350" becomes crucial to ensure their efficacy and safety throughout their designated shelf life [36]. Studies have demonstrated that drug decomposition through oxidative degradation generates FA and formic acid as byproducts [37], further accelerating degradation and subsequent FA formation [38]. While the precise mechanism of FA formation remains elusive, a potential autooxidation pathway is proposed (Figure 1.3) [37, 39]. The State Pharmacopoeia of the Russian Federation, XIV edition (FS.2.1.0127.18) [40] outlines a quantitative determination method for FA in Macrogol, establishing a maximum permissible FA content of 0.003% for safety assurance. This underscores the importance of monitoring carcinogenic FA levels to safeguard the drug's safety profile.

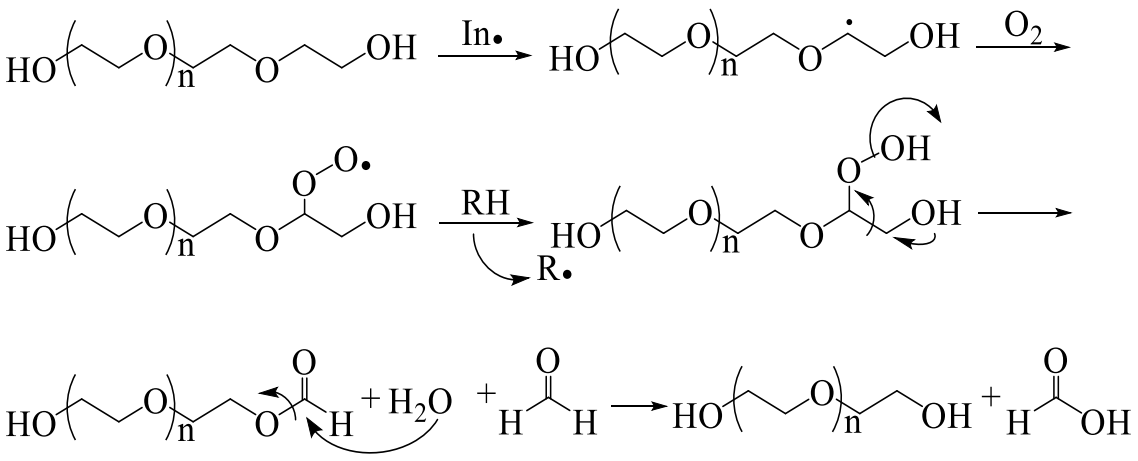


Figure 1.3 – Possible mechanism of PEG oxidation with the formation of FA and formic acid [37, 39]

Another pharmaceutical formulation that generates FA is urotropin (also known as methenamine, hexamine, hexamethylenetetramine). This heterocyclic tertiary amine, highly soluble in water and polar solvents like alcohol, chloroform, methanol and acetone, was first synthesized by Butlerov in 1859 from FA and ammonia [41, 42]. Interestingly, only 35 years after its discovery, the first medical use of urotropin was recorded, demonstrating its exceptional efficacy as an antiseptic for urine, including sterilization in patients with typhoid fever [42].

The recent emergence of antibiotic-resistant bacteria that cause urinary tract infections has led to a resurgence of interest in urotropin as a potential therapeutic agent [42, 43]. Its mechanism of action is due to the formation of bactericidal FA, which has non-specific antimicrobial activity due to the denaturation of bacterial proteins and nucleic acids. Under acidic cellular conditions, urotropin hydrolyzes, releasing six molecules of FA (Figure 1.4) [44]. These FA molecules trigger cell death by forming irreversible -$CH_2$ cross-links between the primary amino groups of proteins and nearby nitrogen atoms in proteins or DNA [44, 45].

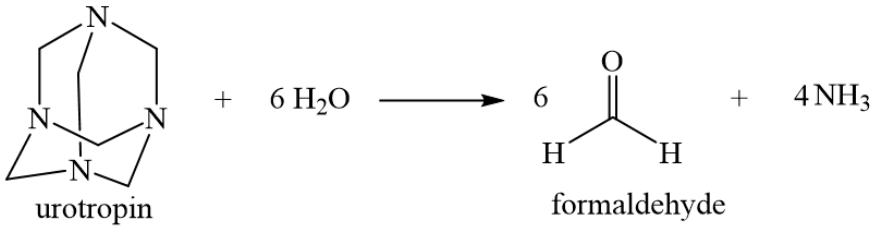


Figure 1.4 – Hydrolysis of urotropin [44]

Urotropin's activity is pH dependent. It is only active in acidic environment (below pH 6) where it releases FA with its antibacterial properties [46]. Almost no hydrolysis of urotropin occurs at physiological pH (around 7.4) and it is therefore virtually inactive in the body at neutral pH [46, 47]. With a half-life of approximately 4 hours, it is rapidly and almost completely eliminated in the urine [46]. Studies have not shown harmful reactions at doses used for antiseptic purposes (4 - 6 g daily for weeks) [48]. This safety profile allows urotropin to continue being used as an antibacterial

agent, most commonly found in foot care cosmetics (creams, lotions, deodorants, etc.) [49]. However, ointments containing 5% FA are not recommended for application to the skin of the face, since there are known cases of allergic reactions to this component [50, 51]. The Russian pharmaceutical market sells ointments for external use with the trade names "Formagel" and "Teymurova paste", which have an antiseptic effect and contain FA [52].

Urotropin has demonstrated promising antitumor activity against systemic cancers and glioblastomas, making it a subject of ongoing research [42]. However, this potential clinical application necessitates stricter control of free FA content. The current method outlined in the State Pharmacopoeia of the Russian Federation, XIV edition (FS 2.1.0131.18) [53], relies on a visual assessment of free FA content in the substance “Urotropin”, limiting its accuracy. The maximum permitted concentration of free FA is 0.005%.

Formaldehyde contamination is a potential issue in drinking water supplies. Primarily, it originates from two sources. The first is the disinfection processes used in water treatment plants and bottled water production. While ozonation and chlorination effectively eliminate harmful microorganisms, they can inadvertently oxidize naturally occurring organic matter (humic substances) in the water, producing FA as a byproduct [54, 55]. Median FA concentration in ozonated drinking water samples is close to 50 µg/L [56, 57]. Another source is FA leaching into drinking water from the degradation of polyacetal plastic fittings in water infrastructure over time [58]. A Taiwanese study by Tsai et al. [59] detected FA levels of 129 µg/L in plastic bottle drinking water.

Formaldehyde is also detectable in snow due to its high-water solubility. This is significant as snow acts as a complex photochemical reactor, actively exchanging chemicals with the atmosphere [60]. The presence of FA in snowpack is primarily attributed to two sources: the absorption of atmospheric FA and the direct photolysis of light-absorbing organic compounds within the snow itself [61]. Furthermore, snow

facilitates FA production by generating photo-formed oxidants, such as hydroxyl radicals, which can oxidize existing organic matter [62].

The ecological consequences of snowmelt are well-established. Extensive research has demonstrated its impact on the chemical composition of rivers and lakes, especially during spring floods [63, 64]. This melting process can release organic contaminants, including FA, posing potential risks to aquatic and terrestrial ecosystems [65]. Furthermore, in regions with seasonal snow cover, contaminated snowmelt can adversely affect human health through polluted drinking water and food production [64].

Research conducted in Russian cities underscores the role of snowmelt as a potential pollutant for urban water and soil systems during snowmelt periods [38]. This is especially significant for Nordic countries and Russia, where meltwater is a primary water source. Consequently, monitoring FA content in snowpack is essential for assessing the extent of this contaminant and mitigating its risks to aquatic and terrestrial ecosystems, as well as human health.

## 1.4 Methods for quantitative determination of formaldehyde

The increasing prevalence of FA in the environment, driven by its widespread use in various products and industrial processes, poses significant public health concern. Consequently, rapid, sensitive and field-deployable FA detection methods are essential for effective monitoring. Through consideration of the physicochemical properties of FA, several analytical methods have been proposed to address this challenge. Traditional methods, such as spectrophotometry, chromatography and chemiluminescence, have been the mainstay of FA detection for years [66-68]. However, the optimal method for FA detection depends on specific factors such as the application (e.g., indoor air quality monitoring, leak detection, environmental sampling), required sensitivity and accuracy, as well as cost-effectiveness. Each method presents distinct advantages and limitations, necessitating careful selection based on these considerations.

### 1.4.1 Spectrophotometry and Chemiluminescence methods

Spectrophotometry remains a widely used technique for FA detection in environmental samples due to its relative simplicity, affordability and adequate sensitivity [69, 70]. These methods typically employ chromogenic reagents, mainly chromotropic acid and acetylacetone. These reagents react with FA to form colored derivatives that can be readily measured using spectrophotometry [71].

The chromotropic acid method, favored for its simplicity and high sensitivity of FA determination in aqueous solutions [72], possesses limitations that diminish its broader applicability. A key drawback is the lack of selectivity. Phenols, ethanol, various aldehydes, hydrogen sulfide, ammonia, nitrates and nitrites can hinder FA determination [73]. For complex matrices like natural and waste waters, this necessitates additional sample preparation steps, such as steam distillation, to remove interfering substances before chromotropic acid analysis, significantly reducing the efficiency of the method [73]. Furthermore, the method utilizes a concentrated sulfuric acid medium for the reaction between FA and disodium salt of chromotropic acid, leading to the formation of a chromogenic product (mono-cationic dibenzoxanthylium) (Figure 1.5) [74]. This raises safety concerns due to sulfuric acid's hazardous and corrosive nature [75]. Additionally, the required prolonged heating (30 – 60 minutes) in a steam bath at 100 °C for color development [71, 76], renders the method cumbersome and less suitable for routine analysis.

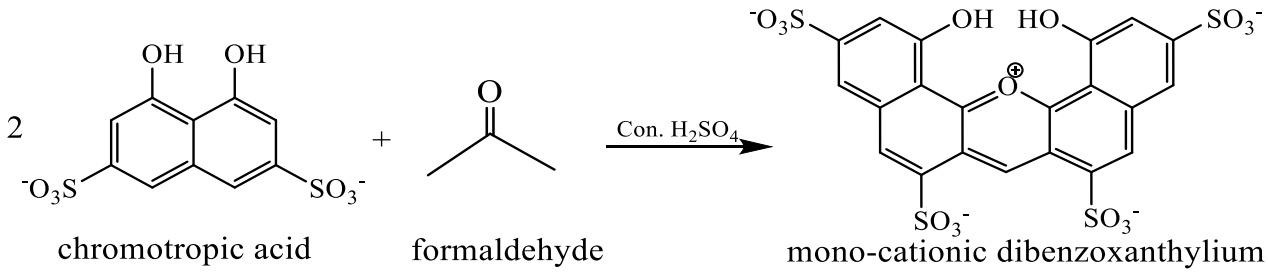


Figure 1.5 – Interaction scheme between chromotropic acid and FA [74]

The reaction between FA and acetylacetone in ammonium acetate solution proceeds under heating (10 minutes) in a water bath (60 – 65 °C) with the formation of a lemon-yellow colored reaction product 3,5-diacetyl-1,4-dihydrolutidine (DDL) (Figure 1.6) [77]:

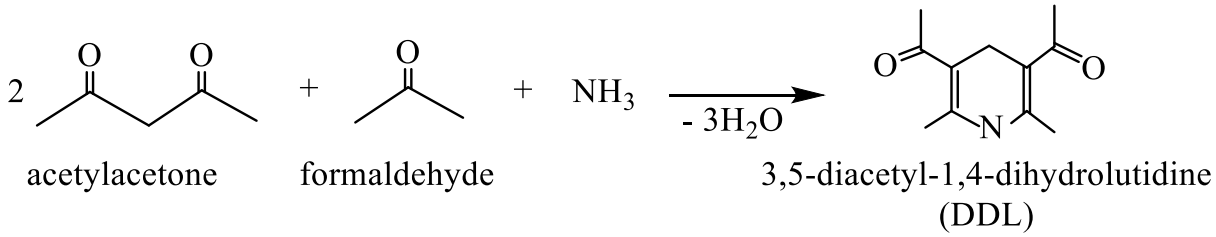


Figure 1.6 – Interaction scheme between acetylacetone and FA [77]

The acetylacetone method is more selective than the chromotropic acid method. The determination is not interfered by up to 10-fold excess of phenol, 1000-fold excess of methanol, any amount of ammonia, or 60-fold excess of acetaldehyde and propionaldehyde. The interfering influence exerted by the color of the analyzed samples, as well as the presence of metal ions that form colored complexes with acetylacetone, is eliminated by distilling off FA with water vapor [78].

Chemiluminescence (CL) is a valuable technique for real-time monitoring of extremely low FA levels in environmental samples owing to its exceptional sensitivity and simplicity [79]. This method involves detecting light emitted from the reaction between FA and specific derivatizing agents, such as luminol or gallic acid [68, 79]. The FA-derived product reacts with an oxidizing agent, releasing energy as light. The intensity of this emitted light directly correlates with the initial FA concentration in the sample. While CL offers exceptional possibilities for real-time FA monitoring, it presents certain challenges. A primary limitation is its susceptibility to interferences from other compounds present in the sample, leading to inaccurate FA concentration measurements. Additionally, complex samples can exhibit quenching effects, diminishing the CL signal and compromising data reliability [68].

To address these issues, CL methods often require elaborate sample pretreatment steps, such as filtration, extraction, or ion removal, which can be time-consuming and laborious. For instance, Khataee et al. [80] describe a complex pretreatment process for water samples involving column filtration to remove interfering metal cations. In this study, the derivatization process between FA and methyl acetoacetate in the presence of ammonia to form a color product, 2,6-dimethyl1,4-dihydropyridine-3,5-di(methylcarboxylate) required heating for 10 minutes at 60 °C in a water bath, followed by cooling down in water for 5 minutes. Another study [81] utilized 1,3-cyclohexanedione and ammonium acetate to form a compound that fluoresces between 450 and 480 nm when excited at 380 – 410 nm. To eliminate interfering influences, FA is distilled off with steam. These complexities hinder the suitability of CL for routine FA analysis in environmental samples.

### 1.4.2 Chromatographic methods

Chromatographic techniques, including HPLC and gas chromatography (GC), are among the most widely used methods for FA detection due to their high accuracy, sensitivity, specificity, and ability to separate complex mixtures [82]. These techniques often employ detectors like mass spectrometers (MS) or ultraviolet (UV) detectors to enhance sensitivity.

High-performance liquid chromatography is the predominant method for FA quantification. Due to FA's high reactivity, polarity and lack of intrinsic UV absorption, derivatization with reagents like chromotropic acid or 2,4-dinitrophenylhydrazine (DNPH) is crucial for generating detectable derivatives [26, 83]. The effectiveness and versatility of HPLC coupled with derivatization for FA analysis in diverse matrices, including dairy products [84], pharmaceuticals [26] and cosmetics [85], is well-established. A prevalent approach involves the formation and subsequent separation of DNPH derivatives for both FA and other carbonyl compounds using HPLC [86]. The

resulting FA-DNPH derivative exhibits UV-detectable properties. For atmospheric FA sampling, cartridges containing silica gel impregnated with DNPH are commonly employed [87]. Despite its versatility and sufficient selectivity HPLC with derivatization often involves laborious and time-consuming extraction procedures and analysis [88]. In addition, most HPLC methods employ a toxic organic solvent, methanol, as a mobile phase, which negatively affects the environment and human health [89].

Gas chromatography is another option for FA determination owing to its effectiveness in analyzing volatile compounds. For FA determination by GC, chromatographic columns packed with various stationary phases are utilized. These sorbents include porous polymers (Porapak N, T, Q) [90], Chromosorb [91] and molecular sieves (Tenax TA) [92]. Notably, carbon molecular sieves offer advantages in terms of ready availability and the ability to be directly employed without further modifications, while exhibiting comparable ease of preparation and reproducibility to porous polymers. However, a drawback of molecular sieves is their susceptibility to adsorption of atmospheric gases, necessitating careful protection from impurities [93].

Oxygenate impurities can impede FA determination, necessitating alternative analytical approaches. Capillary columns [94] and associated systems [95] are routinely employed for FA separation. GC can utilize various detectors for FA analysis. While thermal conductivity detectors (TCDs) [96] have been employed, flame ionization detectors (FIDs) are generally favored due to their superior efficiency. However, the low sensitivity of FIDs to FA results in underestimated concentrations.

To address the low sensitivity of FIDs to FA, a prevalent strategy involves derivatizing FA into acetyls via reaction with alcohols under acidic conditions prior to analysis. Capillary columns are primarily employed for the indirect quantification of FA, coupled with detectors such as MS, FIDs, or photoionization detectors (PIDs). The optimal temperature for analyzing FA-containing samples typically ranges between 110 and 140 °C [97].

Like HPLC, existing GC methods for FA analysis often involve complex and time-consuming derivatization reactions, extractions, or sample preparation steps [98]. Furthermore, FA's thermal instability at the high temperatures used in GC limits its direct quantification [82].

In general, despite their numerous advantages, standard methods often suffer from high costs, time-consuming procedures and complex operational requirements. Moreover, they typically necessitate large quantities of reagents, which can pose environmental and health risks. These factors collectively limit their suitability for real-time monitoring applications.

It is important to emphasize that traditional analytical methods have shown limited application in quantifying free FA in urotropin. The spectrophotometric methods described above [74, 77] require heating of the test solutions which lead to urotropin hydrolysis with the formation of ammonia and FA [99-101]. Wang et al. [102] employed gas chromatography method which requires elevated temperatures (200-300 °C) for the determination of FA in urotropin pharmaceutical product. While the exact temperature can vary based on factors like purity and the presence of catalysts, these high temperatures can induce hydrolysis of urotropin, leading to the formation of additional FA [99-101]. Moreover, the use of strong acids like concentrated hydrochloric or sulfuric acid [40], commonly employed in these methods, can completely decompose aqueous solutions of urotropin (Figure 1.7) [103, 104], further complicating the analysis process.

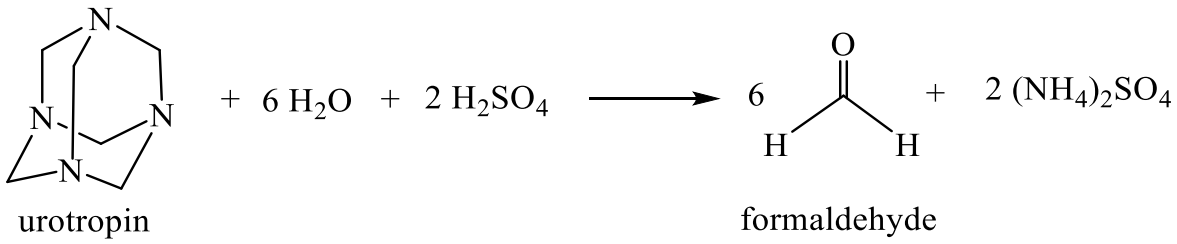


Figure 1.7 – Hydrolysis of urotropin by the action of concentrated sulfuric acid [104]

Colorimetric or potentiometric titration methods, involving the reaction between FA and hydroxylamine hydrochloride under optimal conditions (pH 3-4), have been found to be convenient methods for determining FA content [105, 106]. The reaction liberates one mole of hydrochloric acid for each mole of FA in the solution. The liberated hydrochloric acid is back titrated with standard sodium hydroxide solution, allowing for the determination of the initial FA concentration based on the moles of sodium hydroxide added [105]. Nevertheles, these titrimetric methods are not suitable for determining FA in urotropin. The acidic pH conditions and the hydrochloric acid formed during the reaction cause the hydrolysis of urotropin, leading to the formation of additional FA and subsequent overestimation of the FA concentration [103, 104]. Furthermore, these titrimetric methods are susceptible to interference from other aldehydes and ketones, which can interact with hydroxylamine hydrochloride [107].

### 1.4.3 Electrochemical methods

Electroanalytical methods such as voltammetry and amperometry offer a promising alternative for trace FA detection due to their high sensitivity, rapid response, selectivity, simplicity and cost-effectiveness. These techniques enable miniaturization and real-time measurements, providing a significant advantage over traditional, often expensive and time-consuming methods [69, 108]. Electroanalytical methods exploit the electron transfer between an electrode and FA molecules or FA-adducts, generating an electrical current proportional to FA concentration [109]. The performance of these methods is heavily influenced by the electrode material employed.

#### 1.4.3.1 Electrocatalytic conversion of formaldehyde with participation of the electrode material

It is noteworthy that FA predominantly exists as an electrochemically inactive

hydrated form ($CH_2(OH)_2$) in aqueous solutions. In this regard, one of the keys to its electrochemical detection lies in its highly selective conversion facilitated by the participation of the electrode material as catalyst with the formation of FA oxidation products ($H_2O$ and $CO_2$) or reduction ones ($CH_3OH$).

Noble metals such as Au [110], Pt [111], Pd [24, 90], Ag [112] and Ni [113], favored for their inherent catalytic activity, have been used as working electrodes for direct FA detection. Additionally, metallic [114] or carbon-based substrates modified with metal nanoparticles (as Pd [24], Pt [111] etc.), or their combination with carbon nanomaterials as graphene oxide (GO) [115] are widely employed to enhance active surface area and catalytic activity [116]. Notably, unmodified carbon electrodes exhibit no electrochemical activity towards FA [77, 117].

To enhance FA sensing, various electrode modification approaches have been introduced. These approaches involve modifying the electrode surface with different materials to improve its sensitivity, selectivity and stability. For instance, Nellaiappan et al. [118] developed a GCE modified by combining carbon nanofibers and chitosan with gold nanoparticles. Xi et al. [119] further optimized this concept by incorporating polypyrrole into the electrode structure. While gold-based materials have shown promise, platinum has also attracted significant attention due to its electrocatalytic properties. Chou et al. [120] designed a screen-printed ultramicroelectrode sensor (SPUME) ex-situ electrodeposited with Pt nanoparticles at -0.6 V (vs. Ag/AgCl) for 190 seconds in 50 ppm $H_2PtCl_6$ followed by Nafion casting. Chen et al. [121] introduced graphene–Pt (Pt/EG) nanocomposite electrode by dispersion of graphene-Pt nanocomposite liquid on GCE followed by electrodeposition via CV. Palladium-based materials have also emerged as a viable alternative. Zhang et al. [122] fabricated a Pd nanoparticle-modified GCE prepared by the electrochemical deposition method of CV and the potentiostatic technique. Zhang et al. [123] introduced a sensor for the detection of FA based on Pd nanowire arrays, in which arrays were obtained via the direct electrodeposition of Pd on a GCE within the pores of anodized aluminum oxide

membrane. These advancements contribute to the development of efficient and reliable FA sensors.

The size, composition, structure and support materials of the chosen electrode modifiers significantly influence their catalytic performance, highlighting the crucial role of careful material selection and optimization for achieving sensitive and efficient FA detection [124, 125]. In most cases, electrochemical oxidation of FA is predominantly employed for its detection in various matrices using voltammetric methods (VA) such as CV, DP VA, square wave voltammetry (SqW VA) and CA.

Several challenges hinder the optimal performance of these electrode approaches for FA detection. A common issue is their susceptibility to rapid metal surface fouling, due to the strong adsorption of intermediate species, such as carbon monoxide ($CO_{ads}$) and formic acid ($H_2COO_{ads}$), which are generated during the FA electrooxidation process [121]. This leads to passivation and hinders the electrodes effectiveness over time [126]. In addition, anodic reactions are accompanied by the formation of oxide layers on the metal surface, which complicates the interpretation of voltammograms. Having studied the same reaction, the authors of [127] obtained a strong dependence of the kinetic behavior on the state of the electrode surface, which subsequently led to ambiguous results. These factors necessitate continuous research and development efforts to address these limitations and improve the overall efficiency and reliability of FA sensors.

Alternatively, biosensors have been developed to enhance sensitivity and selectivity and avoid redundant interferences from the matrices [128]. However, enzyme-modified electrodes often suffer from complex fabrication processes, low stability and poor reproducibility during immobilization and storage [129].

### 1.4.3.2 Voltammetry of electrochemically active derivatives of formaldehyde at mercury and carbon containing electrodes

Formaldehyde oxidation was observed at -0.1 V on a dropping mercury electrode

in an alkaline medium [116]. This is close to the dissolution potential of mercury. The reduction signal of FA to alcohol was recorded at a potential of -1.6 V relative to a saturated calomel electrode (s.c.e) [130]. During the experiment the solution temperature must be maintained constant with accuracy of ±0.1 °C, since even a 1 °C temperature fluctuation can significantly distort results. The method allows determination up to 0.15 mg/L FA [131].

Indirect methods are used for the quantitative determination of FA using a hanging mercury drop electrode or unmodified glassy carbon electrode and SPCE. As for HMDE, FA is completely converted into its electrochemically active derivatives by a chemical reaction with an amino compound into FGA by reaction with Girard T-reagent in a neutral medium (equation 1.1) [132, 133], or formaldehyde hydrazone by interaction with hydrazine sulfate (equation 1.3) [134].

The FA reduction current on the surface of the mercury electrode corresponds to the electroreduction of the double bond of the electrochemically active FA derivative (equations 1.2, 1.4) [133, 134].

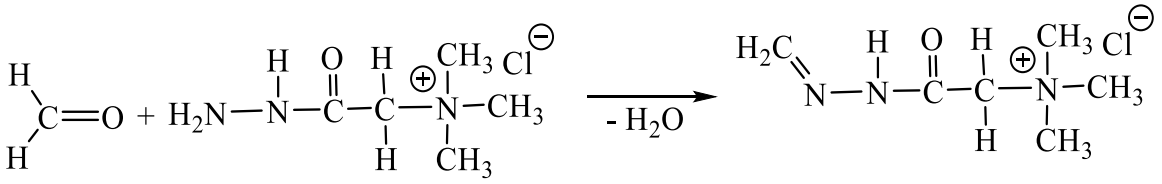

(1.1)

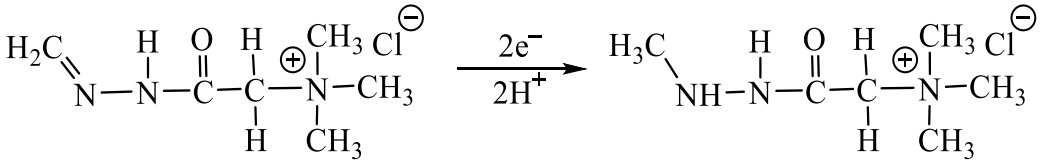

(1.2)

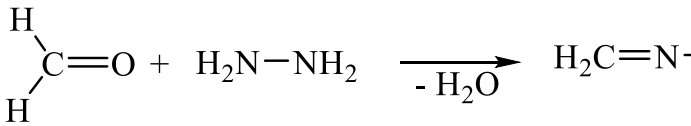

(1.3)

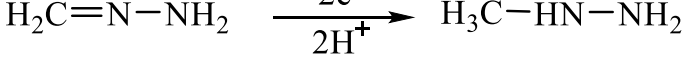

(1.4)

Alternatively, DDL as the reaction product of FA interactions with acetylacetone in the presence of ammonium salt (Figure 1.6), is electrochemically active at unmodified GCE and SPCE, generating a selective oxidation peak at +0.8 V and +0.4 V, respectively [77, 117]. This indirect approach offers enhanced selectivity for FA determination due to the specific chemical transformation involved.

Indirect methods [132, 133] suffer from limitations including a lengthy derivatization procedure (30 – 40 minutes) and the requirement for oxygen removal by nitrogen purging for 5 minutes. For dilute FA solutions (below 1 μM), 90 seconds preconcentration step at -0.7 V (vs Ag/AgCl) followed by a 30 – 40 minutes derivatization reaction at 50 °C is required [132]. Due to slow reaction kinetics at room temperature, DDL formation requires 10 minutes of heating (60 – 80 °C) to reach chemical equilibrium (Figure 1.6) [77, 117].

In contrast, the method in [134] offers a simpler, faster and more suitable approach, allowing measurements in the presence of dissolved oxygen and eliminating the need for prederivatization to form FAH exhibiting electrochemical activity on the mercury surface. However, inherent mercury toxicity poses significant health and environmental risks, necessitating a shift towards safer and more sustainable electrode materials in contemporary research and analytical practices.

“Green” bismuth/antimony-based electrodes exhibit suitable electrochemical characteristics, such as a wide cathodic potential window due to negative overvoltage of hydrogen evolution, low background currents, high electrocatalytic activity, the capacity to adsorb organic compounds and insensitivity to dissolved oxygen [135], may turn out to be a worthy alternative to toxic mercury electrodes for the indirect determination of FA after conversion to FAH.

Table 1.1 displays the details of various electroanalytical methods for FA detection at different electrodes.

Table 1.1 – Comparison of various electroanalytical methods for FA detection

| Electrode (Substrate)/ modifier* | Electrolyte (pH) | Method/ Process | $E_{peak}$, V | LOD/Linear Range, µM | Samples | Reference |
|---|---|---|---|---|---|---|
| *1* | *2* | *3* | *4* | *5* | *6* | *7* |
| SPCE/Pd doped carbon ink | 0.04 M NaOH | CA/ECR** | -0.10 | 2/10–1000 | River water | [135] |
| GCE/Pd nanowire arrays | 0.1 M KOH | CA/ECO*** | 0.05 | 0.5/2–1000 | — | [123] |
| GCE/PdNPs on poly (acrylic acid)-functionalized GO | 0.1 M KOH | CA/ECO | -0.07 | 16/50–50000 | Vegetables, Fruits, Seafood | [115] |
| GCE/Ni-Pd NPs | 0.5 M NaOH | CV/ ECO | 0.43 | 5.4/10–1000 | Bottled water | [56] |
| GCE/polypyrrole-coated Pd-Pt/ N-doped rGO/carbon NPs | 0.1 M $H_2SO_4$ | DP VA/ECO | 0.45 | 2.7/10–900 | Wastewater | [111] |
| GCE/Nafion/Pt-Pd | 0.1 M $H_2SO_4$ | LS VA/ECO | 0.6 | 3.3/10–5000 | Lake water | [144] |
| SPE/rGO/Pt-Ag | 0.1 M NaOH | CA/ECO | 0.12 | 1/1–100 | Tap water, Orange juice, Beer | [145] |
| GCE/graphene/Pt-carbon NPs | 1 M $H_2SO_4$ | CA/ECO | 0.35 | 40/125–2000 | — | [121] |
| Ni | 0.1M NaOH | Staircase VA/ECO | 0.47 | 0.8/1.6–54.6 | Fishes, Shrimps, Wastewater | [113] |
| GCE/Ni | 1 M KOH | CA/ECO | 0.46 | 11/10–1000 | Pond water | [136] |
| CPE/$NiWO_4$-NPs | 0.1M NaOH | CA/ECO | 0.75 | 3.6/8–1000 | Well water | [137] |
| Ni-NWs/$Ni(OH)_2$ /NiOOH | 0.1M NaOH | CA/ECO | 0.80 | 0.8/10–2000 | — | [114] |
| Ni(II)/ionic liquid/ CNT paste electrode | 0.1M NaOH | CVA/ECO | 0.62 | 0.9/7–96 and 96–32000 | Formalin | [138] |

Continuation of table 1.1

| *1* | *2* | *3* | *4* | *5* | *6* | *7* |
|---|---|---|---|---|---|---|
| GCE/carbon nanofiber/ Chitosan/AuNPs | 0.1 M PBS (pH 7) | CA/ECO | 0.50 | $1.5 \cdot 10^4$ / $(0.1–1.8) \cdot 10^6$ | Commercial hair dye formulation | [118] |
| GCE/polypyrrole\| AuNPs | 0.1M NaOH | DP VA/ECO | -0.50 | 20/400–2400 | Milk | [119] |
| CPE/$CeO_2$NPs | 0.1M NaOH | DP VA/ECO | 1.50 | 1/25–1000 | Mushroom | [139] |
| Carbon cloth/ultrathin $Co(OH)_2$ nanosheet arrays | 0.1M NaOH | CA/ECO | 0.60 | 0.6/4–5500 | — | [140] |
| Ti/CuO/Cu/$TiO_2$ NT arrays | 0.1 M KOH | CA/ECO | 0.65 | 25/65–7800 | — | [141] |
| SPCE/copper–porous silicon nanostructure | 0.1 M NaOH | CA/ECO | -0.28 | 12/400–4000 | River water | [142] |
| Stainless steel/ electrodeposited polydopamine | PBS (pH 7) | CV/ECO | -0.13 | 0.1/0.4–1.6 | Fish samples | [143] |
| HMDE | $NH_4$ buffer + 0.2 mM Girard T- (pH 9.7) | Adsorptive DP VA/FGA reduction | -1.28 | 0.08/0.2–8 | Rainwater | [132] |
| HMDE | $NH_4$ buffer + 2.5 mM Girard T- reagent (pH 6-8) | DP VA /FGA reduction | -1.22 | 1.3/10–90 | — | [133] |
| HMDE | 0.2 M PBS + 0.01-0.2 M HRZ (pH 5.6 ± 0.4) | AC VA/FAH reduction | -0.93 | 6.7/6.7–500 | — | [134] |

Continuation of table 1.1

| *1* | *2* | *3* | *4* | *5* | *6* | *7* |
|---|---|---|---|---|---|---|
| GCE | 1.95 M $NH_4$ acetate + 0.0195 M acetylacetone (pH 5.5) | SqW VA/DDL oxidation | +0.8 | 3.9/13.3–1300 | Mushroom | [77] |
| SPCE | 1.2 M $NH_4$ acetate + 0.05% acetylacetone | SqW VA/DDL oxidation | +0.4 | 0.6/15–500 (mg/kg) | Wood-based products | [117] |

*Note* – * CPE - Carbon paste electrode; GCE - Glassy carbon electrode; NPs - nanoparticles; rGO – reduced graphene oxide; CNT - Carbon nanotubes

** ECR - electrocatalytic reduction of FA

*** ECO - electrocatalytic oxidation of FA

## 1.5 Influence of plating conditions on the surface morphology of "green" metals-modified electrodes

Due to their environmentally friendly nature and comparable analytical performance to mercury electrodes, "green" metals such as bismuth and antimony have emerged as attractive options for modifying electrode surfaces in electrochemistry. The morphology of electrodeposited bismuth or antimony films, which can vary from nanoparticles to nanowires or thin films with diverse surface structures, significantly influences the electrochemical performance of the electrode by affecting factors such as active surface area, mass transport and reaction kinetics [147, 148]. The morphology of these metal deposits is highly dependent on electroplating conditions, including electrode substrate, metal deposition potential, metal deposition time, modifier ion concentration and the composition of plating solutions and additives [149-152].

Bismuth and antimony can be electrodeposited onto various substrates, with carbon-based materials being particularly favored. These metal films can be prepared using either physical or electrochemical methods, depending on the desired thickness

and application. Examples of deposition techniques include sputtering [151] and electrodeposition [153].

Electrodeposition is the preferred method for preparing bismuth and antimony-modified electrodes due to its several advantages. This method offers high reproducibility, cost-effectiveness, scalability, rapid synthesis and precise control over the micro and nanostructures of the resulting material [154, 155].

Electrodeposition can be broadly categorized into two approaches: ex-situ and in-situ. Each approach offers distinct advantages and limitations. Ex-situ electrodeposition involves a two-step process. First, a modifier metal salt is reduced onto a working electrode immersed in a plating solution. The modified electrode is then transferred to the sample solution for analysis. This step offers precise control over plating potential, optimizing film properties without interference from the sample matrix. A key benefit of the ex-situ approach is the ease of optimizing the plating potential; plating potential can be freely adapted and optimized solely with respect to the behavior/performance and stability of the film. This approach provides flexibility, especially when the plating metal ions might disrupt speciation studies [156] and is preferred for analysis of complex sample matrices where tailored film properties are crucial [153]. Despite offering control and flexibility, ex-situ electrodeposition faces limitations such as weak film adhesion, potential damage during transfer and contamination [157]. Real-time monitoring is also precluded.

In contrast to ex-situ electrodeposition, the in-situ approach involves directly adding modifier metal ions to the sample solution itself. These ions are then co-deposited onto the electrode surface alongside the target analyte. Following analysis, the metal film is removed from the electrode using positive potential. The primary advantages of in-situ electrodeposition are its simplicity and speed. By eliminating the need for a separate plating step, it offers a more efficient electrode modification process. Additionally, in-situ electrodeposition allows for continuous electrode surface regeneration as a fresh film during each measurement [157]. However, there is a trade-

off associated with this convenience. Primarily, in-situ electrodeposition often requires acidic or highly alkaline sample solutions to prevent hydrolysis of Bi(III) or Sb(III) ions, restricting its applicability to neutral or alkaline media [158, 159]. Additionally, the plating conditions (plating potential and time) are intrinsically dictated by the conditions used for the actual analytical cycle, limiting independent optimization.

Comparative studies have demonstrated that in-situ modified electrodes can outperform their ex-situ counterparts for determination of heavy metal ions by anodic stripping voltammetry. This can be justified by the fact that a greater amount of co-deposited metal alloy with bismuth is present in the whole metal film when the in-situ methodology is used, while only the outer layer of metal film is involved in the formation of this alloy in the ex-situ approach [160]. As for cathodic stripping voltammetry ex-situ preplating is preferable [150, 161].

To address the limitations of direct electrodeposition, an alternative approach involves incorporating metal precursors like $Bi_2O_3$ [162] or $Sb_2O_3$ [163] into the electrode material during fabrication. These precursors are typically mixed with graphite ink before printing and subsequently reduced to their respective metal deposits through electrochemical means [156]. While this method enhances the mechanical stability of the electrode film, it presents challenges in preparing the metal oxide-modified ink. The hardness and large particle size of metal oxides hinder uniform mixing with graphite ink, leading to inconsistencies in electrode preparation, particularly for hand-made screen-printed electrodes. This variability ultimately results in irreproducible electrode performance [155].

Common methods for depositing bismuth films onto carbon-containing electrodes have been documented. Table 1.2 presents a number of specific bismuth preplating protocols.

Table 1.2 - Conditions for potentiostatic preplating of bismuth films

| Substrate | Analyte | Bismuth plating solution | Deposition conditions | | Reference |
|---|---|---|---|---|---|
| | | | $E_{el}$, V | $t_{el}$, s | |
| *1* | *2* | *3* | *4* | *5* | *6* |
| SPCE | Pb(II) | 0.1 M ac. buffer (pH 4.5) + 100 mg/L Bi(III) | -0.8 | 240 | [164] |
| GCE | Co(II) | 0.1 M ac. buffer (pH 4.5) + 100 mg/L Bi(III) | -1.0 | 300 | [165] |
| GCE/Nafion | Cd(II), Pb(II) | 0.1 M ac. buffer (pH 4.5) + 0.4 mg/L Bi(III) | -1.1 | 600 | [166] |
| GCE | testosterone | 0.1 M ac. buffer (pH 4.8) + 5 mg/L Bi(III) | -1.0 | 150 | [167] |
| Carbon film electrical resistors | Zn(II), Cd(II), Pb(II) | 0.1 M ac. buffer (pH 4.5) + 1 mg/L Bi(III) | -1.4 | 300 | [168] |
| GCE | $Ru(NH_3)_6^{3+/2+}$ or $Fe(CN)_6^{3-/4-}$ | 0.1 M ac. buffer (pH 4.5) + 100 mg/L Bi(III) | -1.0 | 300 | [169] |
| | | 0.1 M ac. buffer (pH 4.5) + 50 mg/L NaBr + 50 mg/L Bi(III) | -0.3 | 60 | |
| Carbon fiber microelectrode (CFME) | Cd(II), Pb(II), Co(II), Ni(II) | 0.1 M ac. buffer (pH 4.5) + 50 mg/L NaBr + 50 mg/L Bi(III) | -0.3 | 60 | [170] |
| GCE | Co(II), Ni(II) | 1 M ac. buffer (pH 4.5) + 100 mg/L Bi(III) | -1.0 | 300 | [171] |
| GCE | Co(II), Ni(II) | 0.1 M ac. buffer (pH 4.5) + 100 mg/L Bi(III) | -1.0 | 300 | [172] |
| GCE | Ni(II) | 0.1 M ac. buffer (pH 4.5) + 100 mg/L Bi(III) | -1.0 | 480 | [173] |
| SPCE | Ni(II) | 0.2 M ac. buffer (pH 4.5) + 100 mg/L Bi(III) | -0.8 | 300 | [153] |

Continuation of table 1.2

| *1* | *2* | *3* | *4* | *5* | *6* |
|---|---|---|---|---|---|
| SPCE | Ni(II) | 1 M ac. buffer (pH 4.5) + 100 mg/L Bi(III) | -1.0 | 300 | [174] |
| SPCE | Ni(II) | 0.1 M ac. buffer (pH 4.5) + 100 mg/L Bi(III) | -1.0 | 300 | [175] |
| GCE | Co(II) | 1 M HCl + 0.5 M LiBr + 0.02 M (4 g/L) Bi(III), without stirring | -0.28 | 20 (35) | [150] |
| GCE | Co(II) | 1 M HCl + 0.5 M LiBr + 0.02 M (4 g/L) Bi(III) | -0.25 | 45 | [176] |
| GCE | glutathione and folic acid | 0.1 M ac. buffer (pH 4.5) + 200 mg/L Bi(III) + 1 mM EDTA | -0.9 | 600 | [161] |

*Note* – ac.– acetic

These techniques generally entail submerging the electrode in a Bi(III) plating solution with a concentration of 0.4 – 100 mg/L. An acetate buffer, adjusted to a pH of 4.5, is often used to control the acidity of the solution [156]. Electrodeposition is conducted at potentials ranging from -0.3 V to -1.4 V for 30 seconds to 10 minutes with continuous stirring. A post-deposition equilibration period of 15 – 20 seconds without stirring is often employed. To enhance the mechanical resistance of the bismuth film, GCE can be further coated with a Nafion membrane using 0.5 – 1% Nafion solution in ethanol [166].

In the process of electroplating, the applied deposition potential is one of the most crucial parameters, which exerts a powerful influence on two key processes: nucleation and deposition rate [150]. The balance between these processes determines the morphology of the deposit. Shifting the potential towards more negative values favors the formation of new nuclei over crystal growth on existing nuclei, leading to finer-grained and more homogeneous films [147]. This influence of deposition potential on particle morphology is evident in studies like Bobrowski et al. [147], which

demonstrated the formation of various bismuth film morphologies (from fern-like dendrites to spindle-shaped crystallites) by varying the deposition potential between -0.3 V and -1.0 V. However, under conditions of dominance of the competing process of hydrogen evolution, the degree of coverage of the substrate surface with metal is critically reduced (Figure 1.8, B) [177].

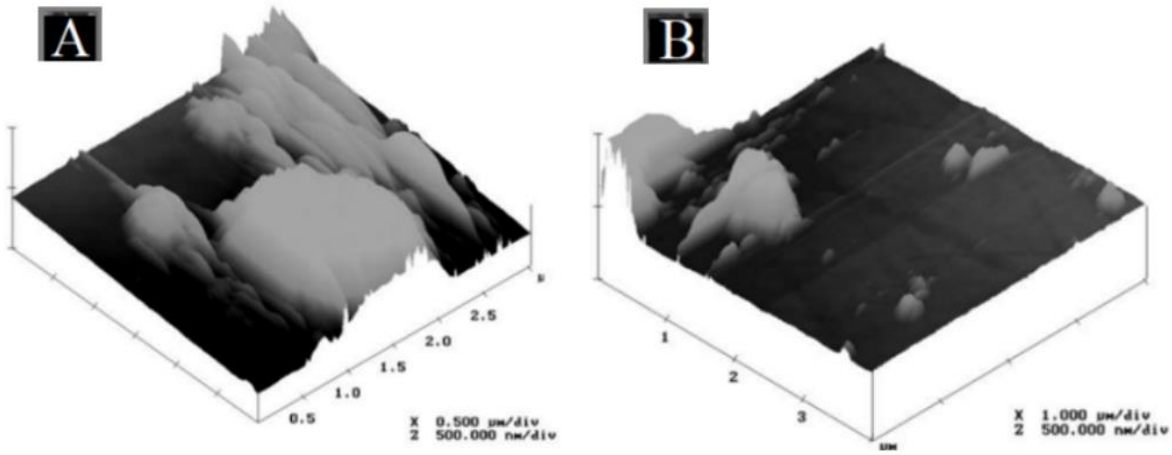


Figure 1.8 – Atomic force microscopic (AFM) images of GCE covered with bismuth film obtained after 30 s electrolysis of the stirred solution of 0.1 M acetic buffer and 10 mM $Bi(NO_3)_3$ at potential of -1.2 V (A) and -1.7 V (B) [177]

Deposition time, alongside deposition potential, is another critical factor influencing the morphology of electrodeposited materials. Svancara et al. [178] effectively demonstrated that increasing deposition time from 30 to 120 seconds led to increased deposit abundance and surface coverage, resulting in distinct morphological changes (Figure 1.9). Zhong et al. [179] also observed a progressive evolution of bismuth structures with increasing deposition time on treated carbon paper.

Wang et al. [180] observed distinct bismuth film morphologies on different carbon substrates. Glassy carbon electrodes yielded porous, three-dimensional fibril-like structures, while carbon-fiber microelectrodes produced thicker, more uniform and nonporous films (Figure 1.10). Additionally, surface defects on the substrate can act as nucleation sites, further impacting the resulting structure [181].

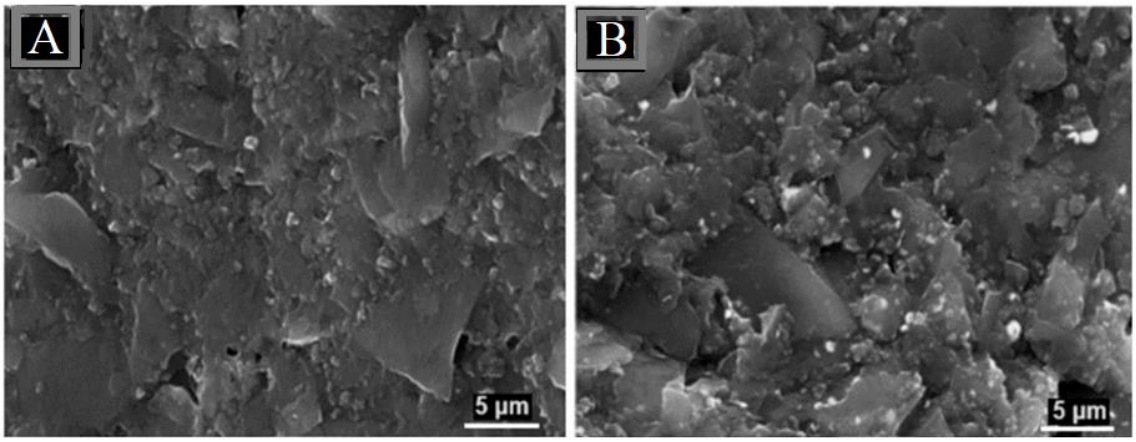


Figure 1.9 – SEM images of bismuth film (whitish, tiny objects) deposited on a carbon paste electrode in acetate buffer under conditions in-situ at 30 s (A) and 120 s (B) [178]

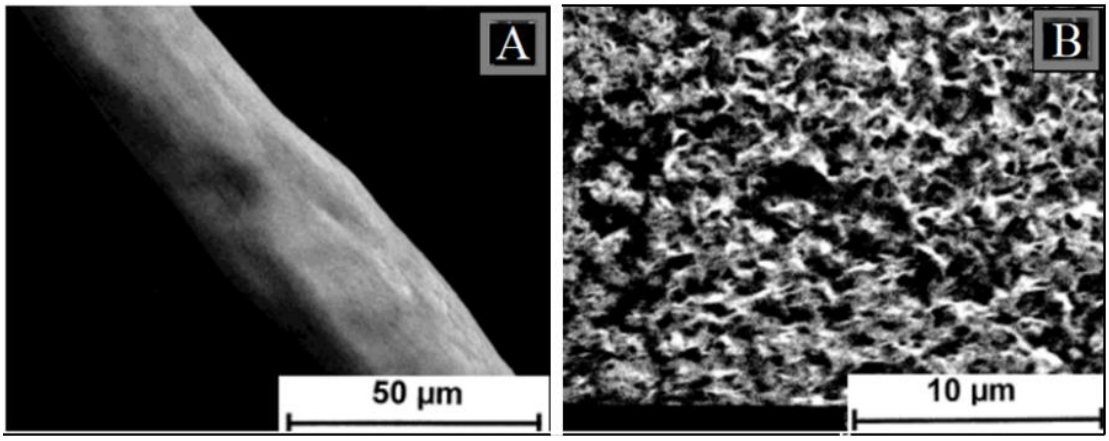


Figure 1.10 – SEM images of carbon-fiber (A) and glassy-carbon (B) electrodes with bismuth deposited for 10 min at -1.2 V from an acetate buffer solution (pH 4.5) containing 50 mg/L Bi(III) ions. Accelerating voltage, 20 kV [180]

The morphology of electrodeposited films was also influenced significantly by the composition of the plating solution [150]. Factors such as bismuth precursor salt concentration, acid type used for bismuth salt dissolution (affecting solution pH) and the presence of additives play essential roles [88]. In solution, metal ions can either contribute to existing nuclei growth or initiate new nuclei formation [181]. Stronger substrate-metal ion interactions favor nucleation, while stronger metal-metal interactions promote existing nuclei growth [178, 182] (Figure 1.11**)**.

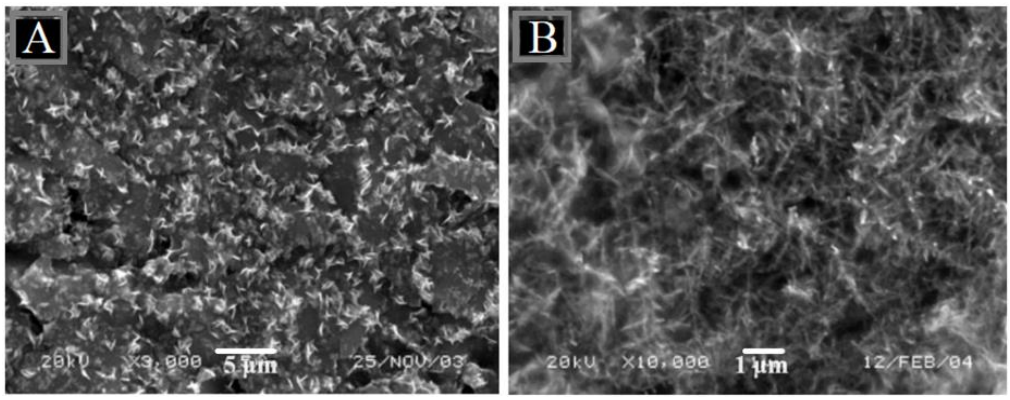


Figure 1.11 – SEM image of Bi-film deposited from 0.5 M HCl solution containing 0.001 M Bi(III) ions (A) and 0.005 M Bi(III) ions (B) at 0.5 V [178, 182]

It was observed that higher Bi(III) ion concentrations promoted 3-D progressive nucleation, resulting in formation of denser and more uniform bismuth films with smaller and less crystallites [183, 184].

Additives are employed to modify various aspects of the electrodeposition process, including particle agglomeration, volume fraction and crystallite dispersion [185]. Examples of additives used in bismuth electrodeposition include EDTA [161, 186] and bromide ions [169, 170, 187, 188]. These additives demonstrate the ability to influence the morphology of deposited bismuth particles.

The inclusion of bromide ions in the plating solution significantly influences bismuth film on the carbon substrate electrode morphology by complexing with Bi(III) ions [188, 189]. These bromide ions preferentially adsorb onto the growing bismuth deposit, forming a non-uniform blocking layer that inhibits crystal growth, leading to denser films with smaller, more uniformly distributed bismuth particles [170]. Additionally, the complexation of bromide ions enhances both the physical and electrochemical stability of the deposited film.

Hočevar et al. [169] demonstrated this effect by comparing bismuth films deposited with and without bromide ions in the plating solution. In the absence of bromide ions, the resulting bismuth film exhibits sparse and relatively large crystals,

while the inclusion of bromide ions leads to a denser structure with smaller, uniformly distributed bismuth particles (Figure 1.12).

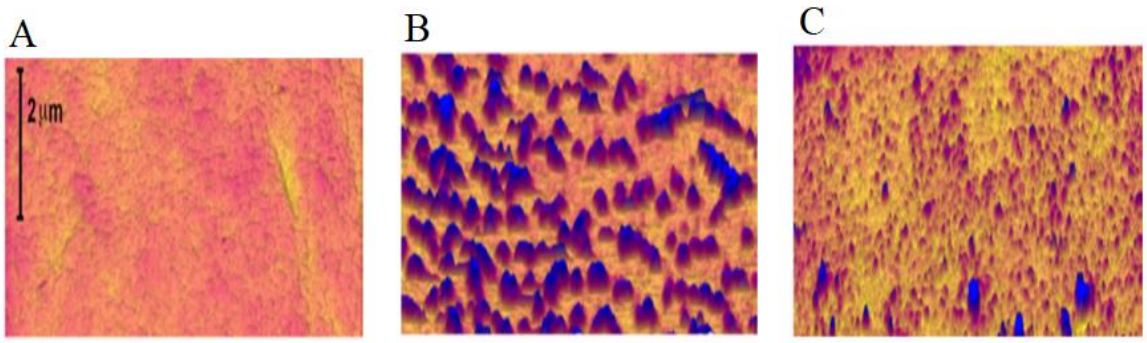


Figure 1.12 − Atomic force microscopy images of bare-GCE (A), bismuth films deposited onto GCE prepared in 0.1 M acetate buffer solution (pH 4.5) containing 50 mg/L Bi(III) without (B) and with (C) 50 mg/L NaBr. Plating conditions: $E_{el}$ = -0.3 V; $t_{el}$ = 60 s. [169]

A significantly improved bismuth film was formed on GCE from the unstirred acid solution with extremely high concentration of Bi(III), in the presence of bromide ions [150]. At plating potential -0.28 V, an adhesive bismuth film is formed on GCE, characterized with fine (1 µm thick), lumpy, perpendicular crystallites (Figure 1.13) which showed good performance in the determination of $Co^{2+}$ with dimethylglyoxime (DMG) as complex agent by adsorptive stripping VA.

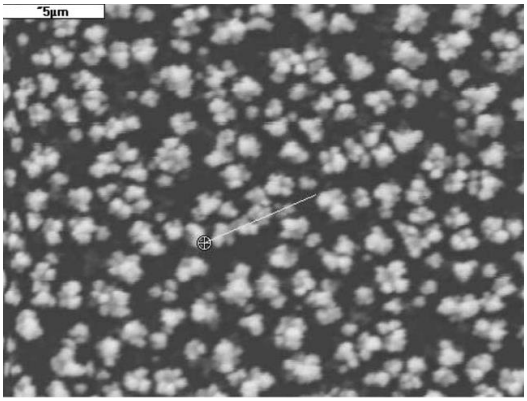


Figure 1.13 − SEM images of the GCE covered by bismuth deposited in a plating solution containing 1 M HCl + 0.02 M $Bi(NO_3)_3$ + 0.5 M LiBr at $E_{el}$ = -0.28 V, $t_{el}$ = 20 s [150]

At slightly negative potentials ($E_{el}$ = -0.25 V) the rate of deposition is slow, and the growth of earlier formed crystallites is favored. As the plating potential becomes more negative (< -0.35 V) the process of reduction of bismuth ions becomes quicker and the microstructure of bismuth film changes to small, pure shaped crystallites.

The influence of additives extends beyond bromide ions. EDTA acts as a complexing agent, forming complexes with Bi(III) ions and reducing the concentration of free Bi(III) available for immediate electrodeposition [190]. This complexation leads to slower and more controlled crystal growth, resulting in smoother and more compact bismuth films [161, 190]. Vladislavić et al. [161] demonstrated the significant influence of EDTA on bismuth film morphology. In this study, the film formed in acetate buffer at -0.7 V was characterized by irregular dendritic crystals (around 1 μm), resulting in a thick, quite uniform, non-porous layer (Figure 1.14, A), while the film at -0.9 V suffered from a spongy-like morphology (Figure 1.14, B).

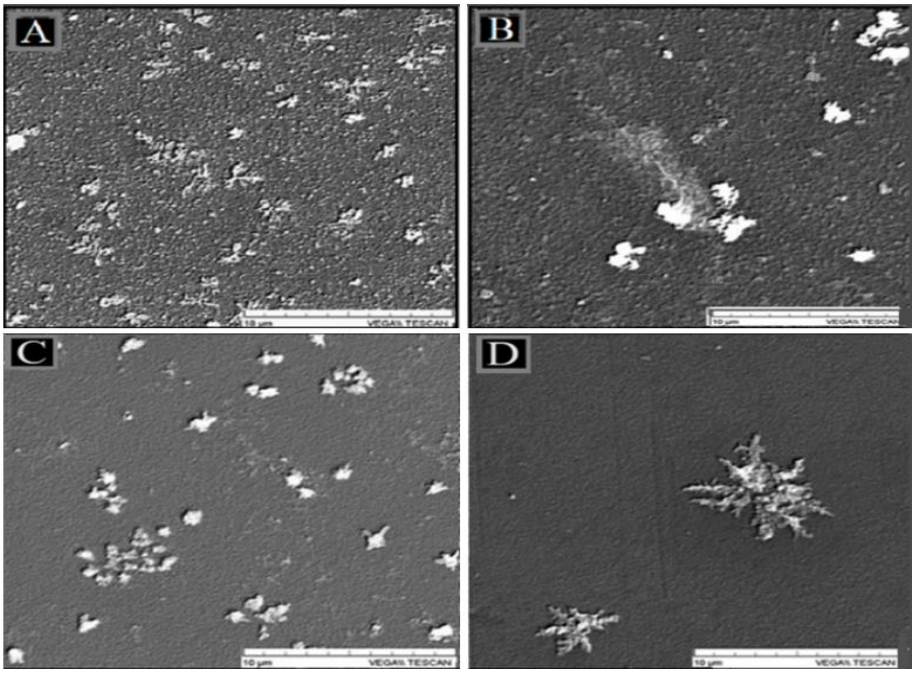


Figure 1.14 − SEM images of the bismuth films formed on GCE in 0.1 M acetate buffer solution (pH 4.5) containing 1mM Bi(III) without (A, B) and with 1mM EDTA (C, D) at -0.7 V for 60 s (A, C), -0.9 V for 60 s (B, D) [161]

In contrast, Figure 1.14, C illustrates the impact of EDTA on bismuth film morphology. In an acetate buffer containing EDTA, bismuth deposited at -0.7 V exhibited a crystalline structure with large, flake-like dendrites. At -0.9 V, an increased surface coverage was observed.

Unlike bismuth films, the influence of plating conditions on antimony film morphology has been less extensively studied. The protocols proposed for antimony preplating on carbon-containing substrates are presented in Table 1.3.

Table 1.3 − Conditions for potentiostatic preplating of the antimony films

| Substrate | Analyte | Antimony plating solution | Deposition conditions | | Reference |
|---|---|---|---|---|---|
| | | | $E_{el}$, V | $t_{el}$, s | |
| GCE | Ni(II) | 0.01 M HCl + 10 mg/L Sb(III) | -0.5 | 60 | [191] |
| SPCE | Ni(II) | 0.01 M HCl + 50 mg/L Sb(III) | -0.5 | 300 | [153] |
| GCE/Nafion | Pb(II), Cd(II) | 0.5 M HCl + 100 mg/L Sb(III) | -1.2 | 50 | [192] |
| GCE | Ni(II) | 0.01 M HCl + 10 mg/L Sb(III) | -1.0 | 120 | [193] |
| SPCE | Pd(II) | 0.01 M HCl + 50 mg/L Sb(III) | -0.5 | 300 | [189] |
| GCE | Pantoprazole | 0.01 M HCl + 20 mg/L Sb(III) | -0.7 | 60 | [194] |
| GCE | 4,6-dinitro-o-cresol | acetic buffer (pH 4.5) + 6 mg/L Sb(III) | -1.0 | 60 | [195] |
| GCE | Sulfasalazine | 0.01 M HCl + 20 mg/L Sb(III) | -0.7 | 60 | [125] |

Sosa et al. [196] demonstrated the significant impact of plating method and substrate on antimony particle morphology (shape, size and distribution) (Figure 1.15). Their study compared in-situ, ex-situ and sputtered antimony films. In-situ deposited antimony particles appeared nearly indistinguishable in their SEM images (Figure 1.15 A), whereas ex-situ particles were larger, brighter and more randomly dispersed (Figure 1.15, B). Sputtered antimony films exhibited a wider particle size distribution and a more compact appearance (Figure 1.15, C). Supporting these findings, Ashrafi et al. [197] observed distinct antimony film morphologies on in-situ and ex-situ antimony-

modified screen-printed carbon-containing electrodes (Sb/SPCEs) prepared from 100 mg/L antimony solutions, further confirming the influence of plating method on morphology.

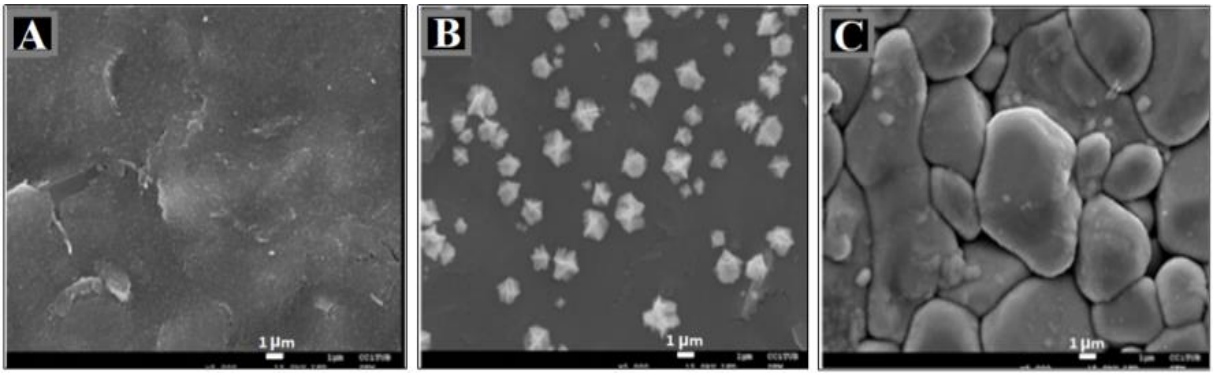


Figure 1.15 − SEM images of antimony film coated in-situ on a commercial SPCE (A), antimony film coated ex-situ on a commercial SPCE (B) and commercial antimony sputtered SPCE (C). Resolution: 1 mm; magnification: 5000x and accelerating potential: 15.0 kV [196]

Pérez-Ràfols et al. [198] investigated the impact of substrate nature on the morphology of in-situ modified antimony films using carbon nanofibers, carbon nanotubes, graphene and commercial screen-printed electrodes as substrates. In all cases, the antimony film consisted of randomly dispersed antimony particles of varying sizes on the carbon-based substrate surface. These particles did not cover the entire surface but resulted in a reasonably uniform Sb film, as observed in Figures 1.16, (A−D).

These investigations demonstrate that covering, visual aspect, particle dimensions of “green” metals films, obtained by different approaches, have been studied in detail by structural techniques (e.g., SEM, AFM).

Plating conditions play a vital role in tailoring the surface morphology, thickness and homogeneity of “green” metal-modified electrodes. By changing and optimizing these conditions, researchers can produce metal films with desired morphologies and structures. And while it is well known that the electroanalytical properties of “green” metal films are strongly influenced by its nature (structure, morphology, adherence, etc.)

and it is desirable to obtain a highly developed bismuth surface in order to improve analytical performance of the electrodes, it is difficult to predict comprehend their satisfactory correlation because suitable analytical properties (even for identical analytes) were obtained with a different morphology and structure of bismuth films [161]. Electrochemical performance of “green” metals-modified electrodes, especially electroactive surface area, need to be considered in the process of their development. However, there are few works concerning these issues. This will be discussed in the next section.

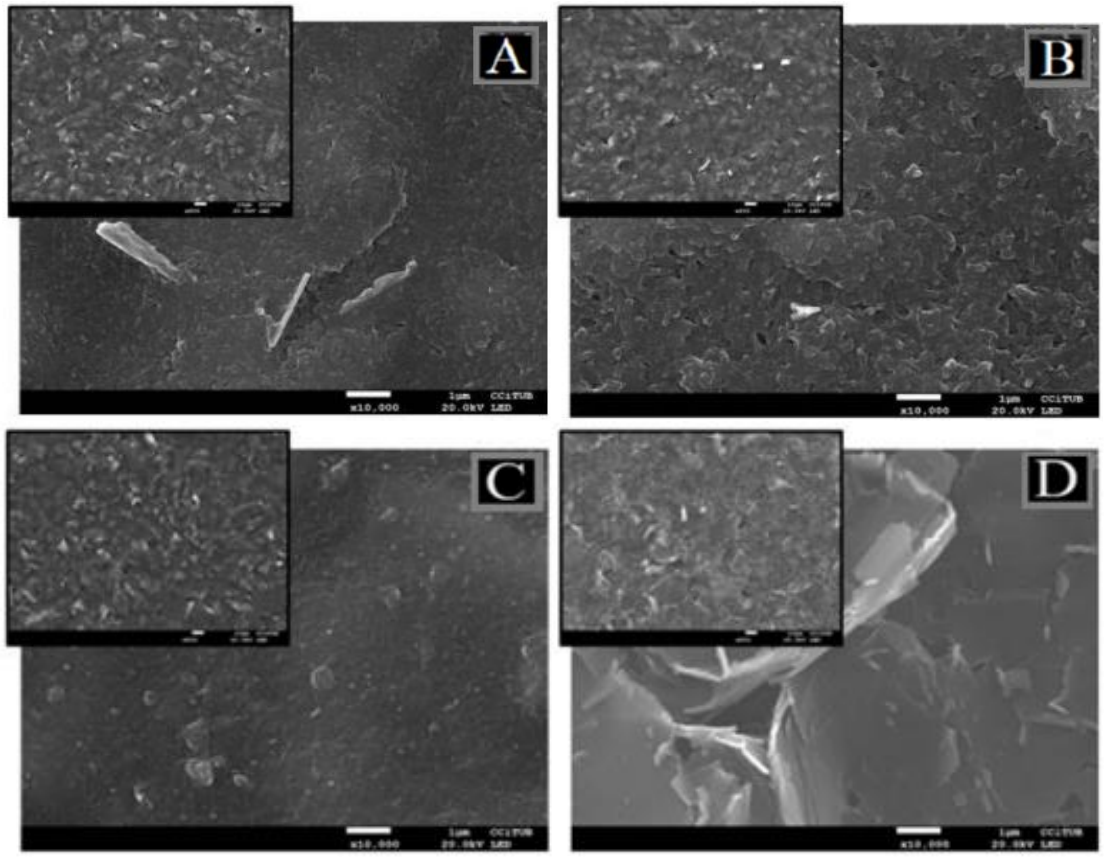


Figure 1.16 – SEM images of in-situ antimony-modified carbon nanofibers (A), carbon nanotubes (B), graphene (C) and commercial screen-printed electrodes (D). Resolution: 1 µm, accelerating potential: 20.0 kV and magnification: 10,000×, and 500× (insets A−D) [198]

## 1.6 Evaluation of electrochemical performance of bismuth-modified electrodes

Modified electrodes, where the surface of the electrode substrate is altered with specific materials, hold significant potential in various applications. Electrode modifiers contribute to the change in the interface between an electrode and electrolyte, the change in electron transfer kinetics, the electroactive surface area, and the improvement of the electroanalytical performance of a sensor [199]. Understanding the impact of these modifications on electrode properties is crucial for their successful implementation [188]. CV and EIS are powerful techniques for electrodes characterization [200].

Cyclic voltammetry can be used for evaluating modified electrodes due to its ability to provide insights into redox potential, reaction kinetics and surface properties [201-204]. EIS stands as a powerful complement to CV, providing insights into the complex interactions between the modified electrode and the surrounding electrolyte [205, 206]. By applying a small alternating current potential and measuring the resulting current response across a range of frequencies, EIS unveils valuable information to understanding electrode behavior, including double layer capacitance, charge transfer resistance, mass transport processes which are represented by the Warburg diffusion element [185] and the extent of metal coverage over the underlying electrode material [161, 207].

Traditionally, these techniques rely on “classical” near-reversible redox couples such as $[Fe(CN)_6]^{3-/4-}$ or $[Ru(NH_3)_6]^{3+/2+}$ [208, 209]. However, “green” metals (bismuth and antimony) start to oxidize at a potential of about -0.2 V in solutions with a pH of 5 − 6 [150, 180, 203], which are typical working conditions for these “classic” redox couples. In such situations, the characteristic redox potential of these redox couples falls within the range of metal’s dissolution. For this reason, these redox probes are not suited for studying the electrochemical characteristics of “green” metal electrodes.

There are certain exceptions to this case, electrodes with trace amount of bismuth deposited in-situ from solutions with 5 – 6 μM bismuth ions for detection of

cadmium(II), lead(II), copper(II) and zinc(II) using anodic stripping voltammetry [210] or preplated at under-voltage conditions with an applied potential of -0.18 V vs. Ag/AgCl for 200 seconds from a solution containing 0.02 M $Bi(NO_3)_3$, 0.15 M sodium citrate and 1 M HCl at GCE modified with reduced graphene oxide and chitosan to determine 3-Methylmorphine [211]. In case of bismuth bulk electrodes, coated with a thin conductive $Bi_2O_3$ film, dissolution process of metallic bismuth was blocked completely, allowing for the establishment of near-reversible electrode behavior using both “classical” redox couples [204]. Tohidinia et al. [212] studied electrochemical behavior of graphite paste electrodes modified with low concentration (0.15%) of poly(quercetin)-bismuth nanowires for simultaneous determination of hydroquinone, catechol, resorcinol in the presence of nitrite. In contrast, tin film electrodes do not face this limitation due to their stability in solutions with a pH of 5 – 6 [213].

Several authors proposed original conditions for carrying out EIS measurements on bismuth-containing electrodes without using “classical” well-reversible redox couples. Petovar et al. [214] reported a systematic EIS analysis at different potentials of an in-situ prepared bismuth-film GCE in 0.1M acetate buffer solution for the determination of trace amounts of the heavy metals (Zn(II), Cd(II), Pb(II)) by anodic square wave stripping voltammetry (SqW ASV). To investigate the characteristics of this sensor, EIS measurements were carried out at slightly more negative potentials than the potentials at which each individual stripping signal is detected, after the deposition step at different deposition potentials. For comparison, EIS measurements were also performed at open circuit potential. The selected equivalent electrical circuit (EEC) models consist of a combination of cell resistances ($R_\Omega$): the charge transfer resistance ($R_{ct}$), the constant phase element ($Q$) and the Warburg element (W). $Q$ represents the non-ideal capacitance and has no physical meaning, but it is only used for the fitting procedure.

The studied trace metal concentration range (5 – 20 ppb) did not significantly influence the capacitive and resistive behavior of the bismuth film electrode which

explains why the performance of this sensor is superior compared with the bare-GCE. The higher sensitivity of the SqW ASV method for bismuth film electrodes compared with the bare-GCE was explained by the lower polarization resistance values of the former. Moreover, the potential of zero charge was also determined and an explanation whether the system is under kinetic- and/or diffusion-controlled process is given. The proposed approach was later used for EIS measurements for in-situ prepared bismuth-copper-film electrodes to determine Zn(II), Cd(II) and Pb(II) traces in 0.1 M acetate buffer [215]. The main goal was to clarify if the electroanalytical system is under a kinetic-controlled or mixed kinetic- and diffusion-controlled process. EIS measurements with and without the analytes as Z(II), Cd(II) and Pb(II) present in 0.1 M acetate buffer were performed for the same two electrodes. As conductive material, GCE covered by a metal film was under investigation, the Randles EEC was chosen as the most likely model to describe the surface phenomena. It was shown that the most resistive contribution among all analytes can be ascribed to Pb, whereas Cd produced significantly lower resistance, followed by Zn. EIS measurements demonstrated that the SqW ASV mainly follows a kinetic-controlled process for such an electroanalytical experiment.

Carbon film resistor electrodes modified with bismuth films, deposited onto substrate electrochemically by different methods: at constant applied potential (ex-situ and in-situ), galvanostatically or by potential cycling were characterized by EIS [216]. Impedance spectra were recorded at bare-carbon electrodes and at bismuth film electrodes deposited in different ways at applied potentials of -0.7 V, -1.0 V and -1.4 V. EEC for modelling comprised the cell resistance, $R_{\Omega}$, $R_{ct}$, at the electrode solution interface with one or two (depends on values of applied potential) parallel combinations of *Q*. Differences between film formation methods become more apparent at -1.0 V, probably reflecting the beginning of a tiny amount of hydrogen evolution. At -1.4 V, hydrogen evolution begins to become more significant in acetate buffer solution. The

more negative potential leads to lower values of capacity as well as to lower charge transfer resistances.

The proposed model of EIS measurements was also applied to Nafion coating bismuth-modified carbon film resistor electrodes [217]. Bi films have been deposited in-situ for cadmium and lead ions determination at constant applied potential. A protective layer of Nafion has also been applied to decrease the adsorption of surface-active substances (SAS). To throw light on the influence of the Nafion coating and of Triton-X-100 on the SqW ASV of cadmium and lead ions on Bi film electrode before and after modification in solutions without and with Triton as SAS were investigated by EIS. Impedance spectra were recorded at applied potentials of -1.2, -0.8, -0.6, and -0.2 V. Fitting of spectra was done using an equivalent electrical circuit, described in [216]. The spectra clearly shows that Triton alters the interfacial characteristics at all potentials studied, but the SqW ASV experiments show that it does not occur sufficiently to block passage of the metal ions. A further important point is that the $R_{ct}$ at Nafion-coated Bi film electrodes with addition of Cd(II) and Pb(II) ions is significantly lower than at the Nafion coated carbon film, showing that Bi films facilitate heavy metal deposition. This suggests that it should be a better electrode for the electroanalysis of cadmium and lead than the Nafion-coated carbon film electrode. The $R_{ct}$ tends to increase with less negative applied potential, since more negative potentials secondary processes can occur such as oxide reduction and metal deposition/reoxidation.

Potentiostatically prepared bismuth films in 0.5 M nitric acid and or 0.1 M acetate buffer (pH 4.5) at Bi(III) concentration of 1 mM without and after EDTA addition in order to obtain satisfactory electroanalytical tools were characterized by EIS and SEM [182]. GCE as a substrate and glutathione and folic acid as model analytes were used. Impedance spectra were recorded in 0.5 M nitric acid at the potential of the evolution of hydrogen (E = -0.9 V) for different electrodes: GCE, bismuth film electrode formed in nitric acid at -0.7 V for 60 seconds (circles), bismuth film electrode formed in acetate buffer at -0.7 V for 60 seconds. Thus, EIS, coupled with a real-time hydrogen evolution,

was performed to gain further insight into the extent of surface coverage with bismuth. The impedance spectra were evaluated using two different EEC. The first-time constant arising from the $R_{ct}$ (due to the hydrogen evolution) in parallel with the double-layer capacitance is represented by the parameters n and $Q_{dl}$, while the second time constant can be described by the surface-related kinetic parameters concerning an evolution of hydrogen on the GCE, as it probably follows Volmer-Heyrovsky mechanism [218]. Information obtained from impedance analysis suggests improved surface coverage in the case of the films prepared in acetic buffer, especially in the presence of EDTA, when compared with films obtained from $HNO_3$. This data is in accordance with SEM images. Film prepared in acetate buffer spiked with EDTA exhibits attractive stripping performance and provides enhanced sensitivity to model analytes.

The above methods of carrying out EIS measurements and interpreting the results obtained are quite complex and time-consuming.

Cyclic voltammetry application for quantitative evaluating of electrochemical characteristics of “green” metals-modified electrodes without using “classic” well-reversible redox pairs is not described. As example [219], for measuring the electroactive surface area of bismuth-film plated GCE via the Randles-Ševćik equation for reversible process, it was proposed to use the currents of the irreversible and complicated by adsorption process of electroconversion of the analyte (cetirizine dihydrochloride - viable antihistamine) on cyclic voltammograms (CVs) instead of the currents of well-reversible redox pair.

As for antimony-modified electrodes, we were unable to find any systematic studies of their electrochemical performance.

For this reason, the search for alternative well-reversible redox couples to evaluate the electrochemical characteristics bismuth and antimony-modified electrodes and control the effectiveness of the procedure for modifying the surface of the electrode with bismuth or antimony is quite relevant at this stage of the development of “green” electroanalysis.

## 1.7 Neutral Red as a near-reversible redox couple

Neutral Red (3-amine-7-dimethylamine-2-methylphenazine) is a derivative of heterocyclic phenazine, with the chemical structure shown in Figure 1.17. The presence of an electroactive imine (C=N) functional group within its structure renders NR amenable to redox reactions [220]. This capability is further enhanced by its favorable standard redox potential of -0.530 V (vs. Ag/AgCl, 3.5 M KCl) [221]. Consequently, NR functions as an efficient electron shuttle, capable of mediating electron transfer between diverse molecules or systems. This versatility enables NR to interact with a wide range of biomolecules and redox-active species, establishing it as a valuable tool in biological and electrochemical investigations.

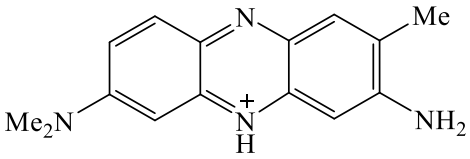


Figure 1.17 – Chemical structure of monoprotonated Neutral Red ($NRH^+$)

Neutral Red has found diverse applications across various fields. In biochemistry, it serves as a redox mediator in biosensors, facilitating electron transfer processes and energy generation for assessing microbial metabolic activity [221-223]. Additionally, it aids in detecting specific redox-active enzymes within biological samples [224-226]. Within analytical chemistry, NR functions as a redox indicator for determining endpoints in potentiometric titrations [227]. Its contributions to electrochemistry encompass studies on electrode behavior and modification [222, 228], as well as its role as a redox probe in redox flow batteries due to its reversible and rapid redox reactions [227, 229].

In aqueous solutions, NR is involved in an equilibrium between the protonated and a deprotonated form with a $pK_a$ = 6.81 [230]. The monoprotonated NR ($NRH^+$) in aqueous media over the pH range of 1.0 – 9.2 at a GCE undergoes pH dependent reduction in two stages, each involving a single electron transfer with one proton being

gained with each electron [231]. Electrochemical transformations of monoprotonated NR in aqueous media and corresponding CVs are detailed in Figures 1.18 and 1.19. The first step: ($NRH^+$) + $e^-$ ↔ radical ($NRH^\bullet$) is a reversible process (Figure 1.18). The neutral radical, which was formed at the 1st-step, could be further irreversibly reduced for pH < $pK_a$ with the possibility of further protonation: $NRH^\bullet + H^+ + e^- \rightarrow NRH_2$.

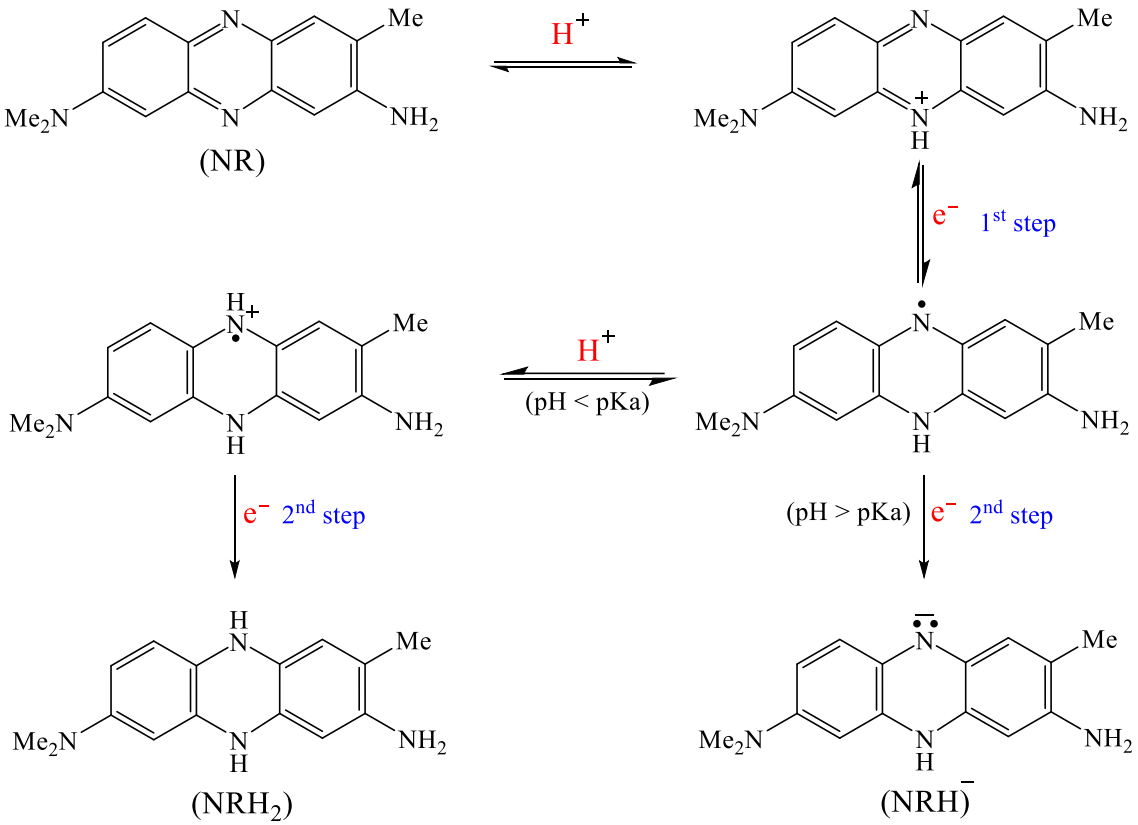


Figure 1.18 – Schematic mechanism of NR redox changes depending on pH [231]

Anık et al. [220] employed NR as a redox mediator for a preliminary qualitative assessment of bismuth film electrodes as biosensor transducers using CV. However, to the best of our knowledge, no research has been conducted to date utilizing NR as a redox probe for quantitatively evaluating the electrochemical performance of electrodes modified with “green” metals.

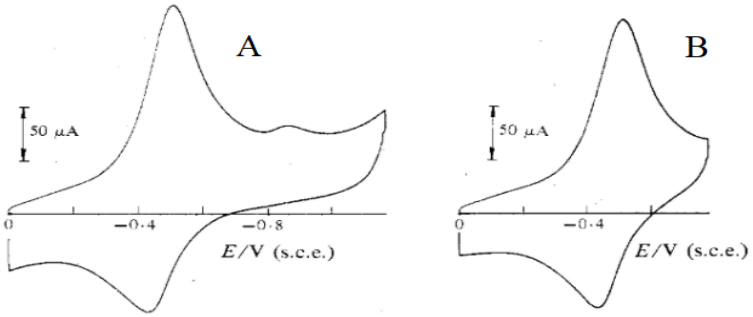


Figure 1.19 – Effect of cathodic limit on CVs of $1 \cdot 10^{-4}$ M NR, registered in phthalate buffer (pH 5.0) at GCE with υ = 100 mV/s from 0 V to -1.170 V (s.c.e) (A); -0.781 V (s.c.e) (B) [231]

Unlike the "classical" redox couples, the characteristic redox potential of NR falls in the cathodic potential region (Figure 1.19) where bismuth and antimony are not electroactive.

Therefore, it makes sense to try NR, as an alternative redox probe for the quantitative evaluation of the electrochemical performance of "green" metals (bismuth and antimony)-modified electrodes.

## 1.8 Statement of the research problem

Formaldehyde is a low-molecular-weight substance characterized by its high reactivity, toxicity, and irritant properties at ambient temperature. Extensive documentation links FA exposure to a range of adverse health effects, including poisoning, allergies, asthma, pulmonary damage and cancer. In addition, FA exhibits mutagenic and genotoxic properties.

Formaldehyde is ubiquitously found in the environment due to natural sources including biomass burning, decomposition of organic matter, volcanic eruptions and anthropogenic activities such as emissions into the atmosphere from activities of industrial facilities and fossil fuel combustion. FA is a widely produced industrial chemical, with global annual production reaching 30 million tons. It is a key component

in the production of resins for furniture, textiles, leather and building materials industries. As a preservative, it can be used in wood processing, the production of paints, cosmetics, personal hygiene products and pharmaceutical products, as it prevents mold and bacterial growth. FA has also been detected in water at wastewater treatment plants and in purified bottled drinking water, primarily due to the oxidation of organic substances during ozonation and chlorination processes. Such wide-spread use of FA in various fields creates the necessity for the development of simple and sensitive methods for its detection and control in environmental objects and pharmaceuticals. Electroanalytical approaches, due to their high sensitivity, fast response, selectivity, simplicity, low cost and miniaturization of equipment, the ability to perform measurements in real-time in small laboratories, are particularly attractive for this purpose. These methods are considered as good alternatives to expensive multi-stage, time-consuming and require careful sample preparation standard laboratory techniques like UV-Vis spectroscopy, chemiluminescence and chromatography for detecting traces of FA.

As formaldehyde in aqueous solutions is found mainly in electrochemically inactive hydrated form a frequently used signal-forming processes are the selective catalytic conversion of FA with the participation of electrode materials, mainly, noble metals and carbon-containing substrates modified with highly dispersed nanoparticles of these metals for complete conversation into its electrochemically active derivatives.

Common issues with the first approach are passivation, which hinders the effectiveness of the electrodes over time due to rapid metal surface fouling, the formation of oxide layers on the metal surface, which complicates the interpretation of voltammograms and quite complicated procedures to prepare modified electrodes, which makes it difficult to use in routine analysis.

The second approach is based on chemical reactions with acetylacetone in ammonium acetate with the formation of DDL and with amino compounds such as Girard T-reagent and hydrazine sulfate with forming electroactive adduct or

formaldehyde hydrazone. The latter method, realized with HMDE, is simpler and faster since it allows measurements at room temperature in the presence of dissolved oxygen without preliminary exposure of the analyzed solutions for the formation of FAH.

“Green” bismuth-based electrodes exhibit suitable electrochemical characteristics, such as a wide cathodic potential window, high electrocatalytic activity, the capability to adsorb organic compounds and insensitivity to dissolved oxygen, which make them a worthy alternative to toxic mercury electrodes. Notably, screen-printed carbon-containing electrodes based on carbon inks and pastes, premodified with bismuth films in a potentiostatic mode, are widely used as working ones in voltammetry owing to the simplicity of the modification procedure and their electroanalytical characteristics. SPCEs are cheap and easy to manufacture on a mass scale, provide great versatility of the modification procedures used, are characterized by a well-reproducible surface, do not require multi-stage mechanical surface regeneration during operation (unlike glassy-carbon electrodes) and can be used to create new methods for quantitative determination of FA following FAH formation using Bi/SPCEs.

Antimony, along with bismuth, is used as a modifier of carbon-containing electrodes due to its much less environmental toxicity than mercury and its electrochemical/electroanalytical characteristics. Bismuth and antimony like other modifiers contribute to changing the properties of the interface between the electrode and electrolyte, electron transfer kinetics, electroactive surface area and improving the electroanalytical characteristics of the electrode. CV and EIS are used to monitor of these changes using well-reversible redox pairs, primarily $[Fe(CN)_6]^{3-/4-}$ or $[Ru(NH_3)_6]^{3+/2+}$.

Bismuth and antimony start to oxidize at a potential of about -0.2 V in solutions with a pH of 5 – 6, which are the typical working conditions for these “classic” redox pairs. These redox pairs are unsuitable for studying the electrochemical characteristics of bismuth or antimony-based “green” metal electrodes, as their redox potentials fall within the range of metal dissolution. For this reason, the search for alternative redox pairs to

control the effectiveness of the modification procedure of SPCE surfaces with bismuth or antimony is quite relevant at this stage of the development of “green” electroanalysis.

Monoprotonated NR in aqueous media undergoes a reversible redox process in the cathodic region, in which bismuth and antimony are not electroactive. Therefore, it makes sense to try NR, as a well-known electronic mediator, in a new capacity as a redox pair for evaluating the electrochemical characteristics of SPCEs modified with bismuth or antimony.

In connection with the above, this dissertation work aims to investigate the electrochemical behavior of formaldehyde hydrazone on bismuth-modified screen-printed carbon-containing electrodes for the development of a new voltammetric method for the quantitative determination of FA in drug "Endofalk®" and technical urotropin, waste, melt, bottled waters and to study into the capabilities of NR as an alternative near-reversible redox couple for monitoring the effectiveness of electrode modification processes using “green” metals.

# CHAPTER 2 EXPERIMENTAL SECTION

## 2.1 Instrumentation and electrodes

A PC-controlled 884 Professional VA and μAutolab Type III potentiostat/galvanostat (Metrohm AG, Switzerland) complete with a magnetic stirrer and standard three-electrode cells were used for electrochemical research and EIS measurements. A sinusoidal voltage disturbance with an amplitude of 10 mV was applied in the frequency range of 0.1 − 106.0 Hz at preselected potentials of the model system according to cyclic voltammograms of Neutral Red. Fitting to electrical equivalent circuits was performed with NOVA 1.11 software.

The working electrodes used were bare and modified screen-printed carbon electrodes based on carbon-containing ink DuPont 7102 from DuPont (USA). Silver chloride reference electrode (Ag/AgCl, 3 M KCl) as reference electrode and a glassy carbon rod with a diameter of 0.2 − 0.3 cm as auxiliary electrode from Metrohm AG (Switzerland) were used in the measurements.

Screen-printed carbon-containing electrodes were laboratory-made using a TIC-50B screen printing machine (China). The carbon-containing ink was applied through a mesh stencil on textolite polymer substrate of 0.035 cm thickness (ZAO "Elektroizolit", Russia) in the form of strips measuring 0.2 × 3.8 cm and with a layer of about 40 μm thickness. The strips were heated in a drying cabinet per the regulations of the ink manufacturer and insulated with a mixture of Cementit and acetone, mixed in a ratio of 1:5 by volume. The working area of the SPCEs was 0.10 $cm^2$ (0.2 x 0.5 cm).

A computer assisted 3-channel voltammetric analyzer "El’sens - ECO" (UrFU, Russia) complete with the fluoroplast or caprolon stirrer and standard 3-electrode cells was used for ex-situ potentiostatic modification of the working SPCEs with “green” metals (Bi and Sb). Mixing solutions was carried out automatically. Silver chloride

reference electrode (Ag/AgCl, 3.5 M KCl) type ESr-10107 (Measuring Equipment LLC, Moscow) and glassy carbon rod with diameter 0.3 cm as auxiliary electrode were used.

Microscopic studies of the surface of bare and modified screen-printed carbon-containing electrodes was analyzed with a high-resolution scanning electron microscope Tescan Vega with system EDX Oxford Xplore 30 (Tescan, Czech Republic).

Spectrophotometric measurements were carried out on a spectrophotometer PE-5400 UF from OOO Ekohim (St. Petersburg, Russia). pH of the solutions was measured with an Expert-pH ionomer (Econiks-expert, Russia). The weighing of the samples and reagents was carried out using analytical balance with a discreteness of 0.0001 g CY-224C special accuracy class (Citzen, India). Ultrapure deionized water with a resistivity of 18 MΩ*cm was obtained on a device DVS-M/1HA (18)-N (Mediana filter, Russia) and used throughout the research.

## 2.2 Reagents and preparation of solutions

Acids, salts, alkalis of analytical grade purity, methanol (99.98%) and ethanol (95%) were received from Russian manufacturers and used without further purification. Neutral Red (≥ 90%), disodium salt of ethylenediaminetetraacetic acid, bismuth (III) nitrate pentahydrate ($Bi(NO_3)_3 \cdot 5H_2O$, ≥ 98%) and potassium ferricyanide/potassium ferrocyanide were supplied by Sigma-Aldrich (USA). Dimethylglyoxime (99%) was purchased from Merck (Germany). Acetaldehyde, 99% (Panreac, Spain), disodium salt of chromotropic acid (Dudley, USA) and Nafion 117, ~5%, solution in ethanol (Fluka, Switzerland) were used. Stock solutions of FA, Ni(II) and Sb(III) ions with mass concentrations of 1 g/L were purchased from “Prime Chemicals Group” (Moscow region, Mytishchi, Russia).

The bismuth (III) ion plating solutions of concentrations 1 g/L and 80 g/L were prepared by dissolving $Bi(NO_3)_3 \cdot 5H_2O$ in aqueous solution of 0.1 M $HNO_3$.

Phosphate solutions were prepared with 3.6 g $Na_2HPO_4$ and 27.2 g $KH_2PO_4$, using deionized water, in two separate volumetric flasks of 100 mL and 1000 mL, respectively. The concentration of both solutions was 0.2 M. Phosphate buffer solutions were prepared by mixing suitable phosphate solutions of $Na_2HPO_4$ and $KH_2PO_4$ in appropriate volumetric ratios. Acetate buffer solution (0.1 M, pH 4.5) was prepared by mixing acetic acid and sodium acetate. Ammonia buffer solution (pH 9.8 ± 0.2) was made by mixing ammonia solution and ammonium chloride.

A freshly prepared acidic solution of hydrazine sulfate was alkalinized to a given pH value (5.95 ± 0.10) with sodium hydroxide solution of concentration 10 M.

A 0.1 M stock solution of NR was prepared by dissolving the appropriate amount of NR in water. A 0.025 M DMG solution was prepared in 95% ethanol.

## 2.3 Preparation of “green” metals-modified screen-printed carbon-containing electrodes

The ex-situ electrodeposition of “green” metals on various substrates has become the most used electrode construction method, owing to the preparation protocol simplicity and electroanalytical performance of the electrodes prepared by this method [161]. Based on literature data, described in section 1.5 (Tables 1.2 and 1.3), well established plating conditions (chemical and instrumental) that made it possible to obtain films with significantly different morphologies were chosen for the study.

Post-modification procedures, the modified electrodes were rinsed in deionized water for 5 seconds, then transferred to the measurement cell and ready to use for analysis. After the scan, the metal films were cleaned of the residual reaction products by keeping the solution under stirring and the potential of the electrode at −1.3 V for 5 seconds for FA and at −1.25 V for 10 seconds for Ni(II) determination.

To prevent interference from the active ingredient of medicinal drug "Endofalk®" (pharmaceutical substance "Macrogol 3350"), the surface of the SPCE was covered with

a perm-selective protective Nafion coating before modification with a bismuth film according to [180]. The Nafion coating was prepared before bismuth plating by casting a 10 μL droplet of a 0.3% Nafion solution (ethanol / water in a volume ratio of 1:1) onto the surface of the screen-printed carbon-containing electrode working electrode and allowing the polymer to air dry.

## 2.4 Objects of analysis and their preparation

Samples of wastewater and snow were collected during the period of active snow melting in the Iset River and within the city industrial zone, respectively. Non-carbonated bottled water “Edelzhe” was purchased at nearby retail outlets. After collecting, samples were stored for no more than 3 days in a refrigerator at a temperature of 4 to 6 °C. The samples of wastewater and meltwater from the snow were filtered and directly applied for analysis, while the sample of bottled water was applied directly without filtration. 7 mL of the water samples were added to a voltammetric measurement cell, followed by 4 mL of 0.2 M PBS (pH 5.0 ± 0.2) and 9 mL of 0.2 M hydrazine sulfate solution (pH 5.95 ± 0.10).

For voltammetric determination, the accurate mass of the drug "Endofalk®" (10 ± 0.5 g) in its original powder form was transferred to a 100 mL volumetric flask and the volume was filled with deionized water. A 2 mL of the sample solution, 4 mL of 0.2 M PBS (pH 5.0 ± 0.2), 12 mL of 0.2 M hydrazine sulfate solution (pH 5.95 ± 0.10), and 2 mL of deionized water were added to the voltammetric cell.

Samples of technical urotropin grades C – polydisperse (with different crystal sizes) and CT – stabilized polydisperse were provided by the “Metafrax Chemicals” JSC (RF). For voltammetric determination of FA in the technical urotropin grades C and CT, the accurate mass of the samples (1.00 ± 0.01 g) in their original powder form was transferred to a 100 mL volumetric flask and the volume was filled with deionized water. A solution of technical urotropin grade CT is additionally filtered through a paper filter

(white tape) to remove the stabilizer (silica gel). A solution of 0.8 mL of the sample, 4 mL of 0.2 M PBS (pH 5.2 ± 0.1), 9 mL of 0.2 M hydrazine sulfate solution (pH 5.95 ± 0.10) and 6 mL of deionized water was added to the voltammetric cell.

To verify the accuracy of the obtained voltammetric results, a quantitative determination of the FA content in the medicinal drug "Endofalk®" was carried out by spectrophotometry at a wavelength of 567 nm according to FS 2.1.0127.18 for the pharmaceutical substance "Macrogol 3350" of the State Pharmacopoeia of the Russian Federation of the XIV edition [40]. To prepare a 10% sample solution, 0.25 mL of a 0.6% solution of chromotropic acid disodium salt was added to 1.0 g of medicinal drug "Endofalk®". Then the solution was cooled in an ice bath and 5.0 mL of concentrated sulfuric acid was added. The solution was kept for 15 minutes and slowly brought up to 10.0 mL with deionized water. FA in the drug was determined using the calibration curve method.

As for verifying the accuracy of the developed voltammetric method for the quantitative determination of FA in the specified urotropin samples, the obtained results were compared with those obtained by an independent analysis method recommended by FS 2.1.0131.18 of the State Pharmacopoeia of the Russian Federation, XIV edition [53]. According to FS 2.1.0131.18, semi-quantitative determination of FA content in the substance urotropin is carried out by visual assessment. The method is based on the formation of silver due to the interaction of silver nitrate with FA in the presence of ammonium hydroxide.

# CHAPTER 3 STUDY OF ELECTROCHEMICAL BEHAVIOR AND ELECTROANALYTICAL PERFORMANCE OF FORMALDEHYDE HYDRAZONE ON BISMUTH-MODIFIED SCREEN-PRINTED CARBON-CONTAINING ELECTRODE

## 3.1. Electrochemical behavior of formaldehyde hydrazone on bismuth-modified screen-printed carbon-containing electrode

The electrochemical behavior of FAH electroconversion process was investigated on the surfaces of bare-SPCE and those modified with bismuth and antimony using cyclic voltammetry in phosphate buffer solution containing HRZ. The Bi/SPCE and Sb/SPCE electrodes were prepared at the potentiostatic preplating conditions from 0.1 M acetate buffer solution (pH 4.5), containing 100 mg/L Bi(III) ions according to [173] or from 0.01 M HCl after adding 50 mg/L Sb(III) [153].

As illustrated in Figure 3.1, A and 3.1, C, the CVs recorded at the bare-SPCE and Sb/SPCE, respectively, exhibit no noticeable anodic or cathodic peaks, signifying the electrochemical inactivity of these electrodes towards FAH. Conversely, Bi/SPCE demonstrated a cathodic peak at -0.97 V (Figure 3.1, B). The absence of a corresponding anodic peak in the CV (Figure 3.1, B) attributable to the FA and hydrazine sulfate adduct on the bismuth surface suggests that the electrochemical reduction of FAH is an irreversible process, similar to that observed on HMDE [132]. It may be assumed that hydrogen peroxide, $H_2O_2$, formed at the electrode from dissolved oxygen oxidizes the hydrazone electroreduction product to its initial state [134]. Moreover, $H_2O_2$ formed at the electrode does not affect the FAH reduction electrode process.

The influence of the potential scan rate on the current of electrochemical reduction of 0.033 mM FA on Bi/SPCE was investigated over a range of scan rates of

0.02 – 0.50 V/s (Figure 3.2, A). The peak current is correlated linearly with the square root of the potential scan rate in this manner: $I_p$ (µA) = 21.77 $\upsilon^{½}$ (V/s)$^{½}$ – 0.60 µA (Figure 3.2, B). Furthermore, a linear relationship ($R^2$ = 0.998) was found for the plot of log $I_p$ vs. log υ with tangent of inclination angle (Slope) of 0.52 (Figure 3.2, C) is comparable to those reported in the literature (0.50) for organic molecules in which a mass transfer mechanism controls the electrochemical process [232]. These findings imply that the electrochemical process is predominantly diffusion controlled.

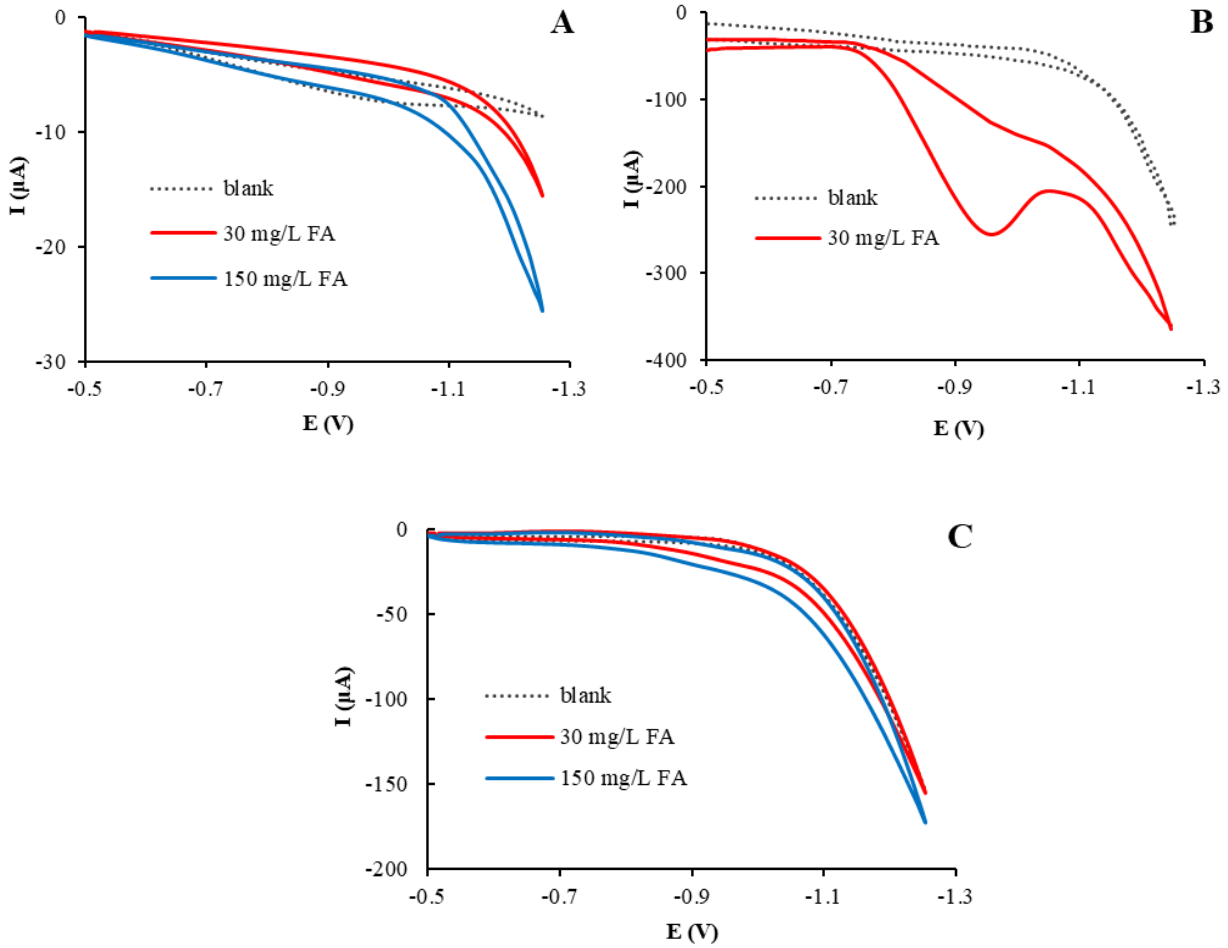


Figure 3.1 – Cyclic voltammograms registered on bare-SPCE (A), Bi/SPCE (B) and Sb/SPCE (C) in 0.04 M PBS + 0.09 M HRZ (pH 5.2 ± 0.1) without adding (blank) and after adding FA at a υ = 0.1 V/s. The deposition condition for metal films 0.1 M acetic buffer (pH 4.5) + 100 mg/L Bi(III), $E_{el}$ = -1.0 V, $t_{el}$ = 8 min (B); 0.01 M HCl + 50 mg/L Sb(III), $E_{el}$ = -0.5 V, $t_{el}$ = 5 min (C)

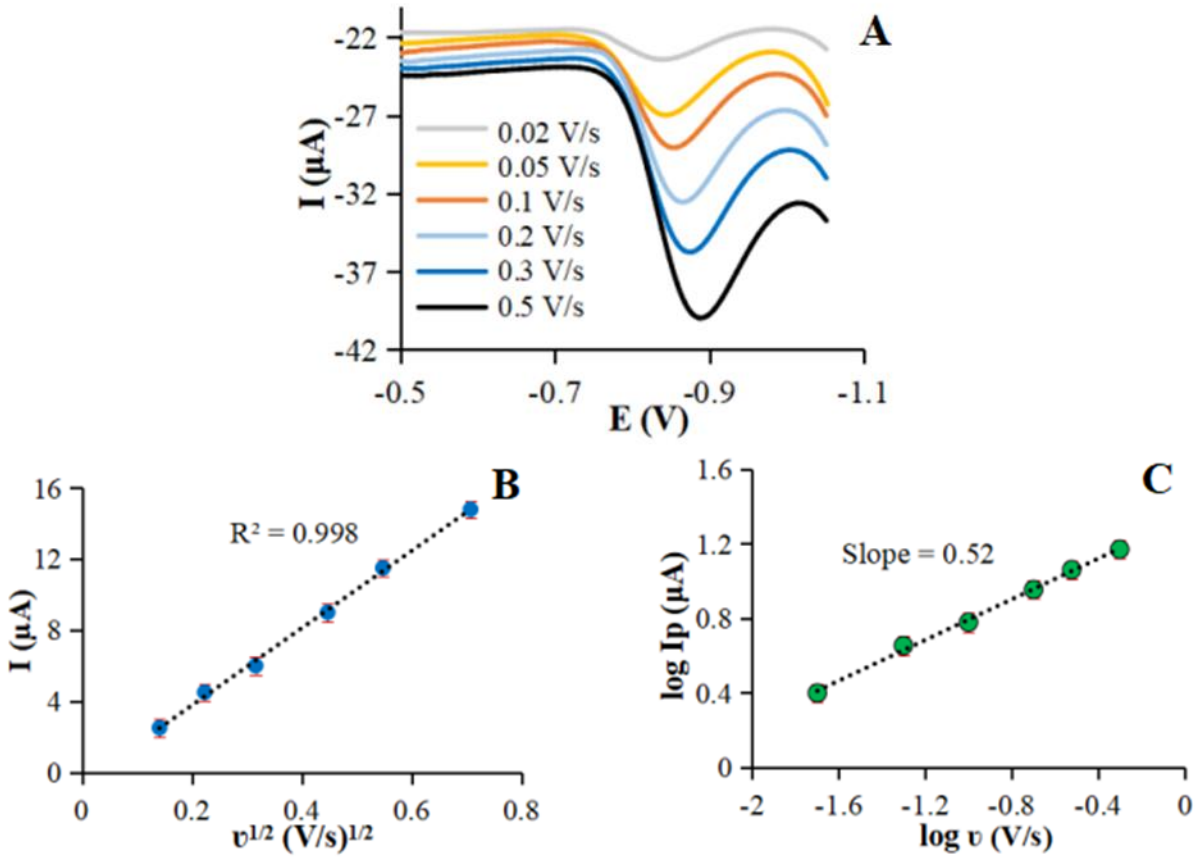


Figure 3.2 – Linear voltammograms of 1 mg/L FA (A) registered on Bi/SPCE in 0.04 M PBS + 0.09 M HRZ (pH 5.2 ± 0.1) at a υ of 0.02 – 0.5 V/s. Analysis of corresponding peak current as a function of υ (B, C). The deposition conditions of the bismuth film as in Figure 3.1, A

*Selecting the voltammetric measurement mode*

Voltammograms of FA reduction, registered at the same scan rate by linear sweep (LS), differential pulse (DP) and square wave (SqW) techniques are presented in Figure 3.3. The peak of FA in the DP technique is three times higher and more symmetrical than the other ones. Comparison of different voltammetric modes revealed that DP is the most suitable one for quantitative analysis. Therefore, further studies on FA were carried out in the DP mode.

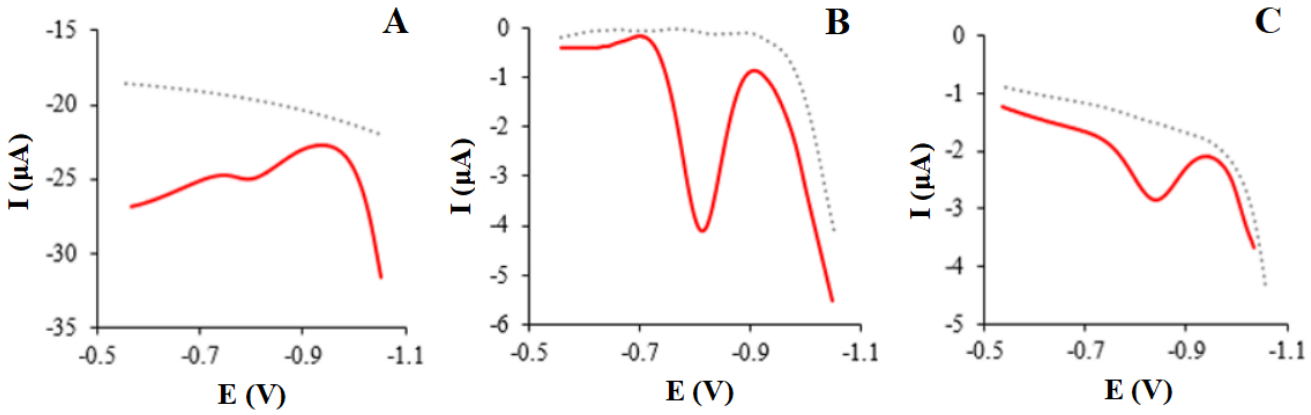


Figure 3.3 – Voltammograms of FA registered on Bi/SPCE in 0.04 M PBS + 0.09 M HRZ (pH 5.2 ± 0.1) without adding (dashed gray line) and after adding (smooth red line) 0.2 mg/L FA at a υ = 0.02 V/s by different techniques: LS (A), DP (B) and SqW (C). The deposition conditions of the bismuth film as in Figure 3.1, A

The response in the DP mode essentially depends on pulse amplitude and scan rate. The FA response in the DP mode rises linearly with the pulse amplitude in the range of 10 to 100 mV (Figure 3.4, C). The optimum pulse amplitude is 50 mV. The peak height does not reach its maximum value at pulse amplitudes less than 50 mV, reducing the sensitivity of FA determination. As the pulse amplitude increases above 50 mV, the peak shape is less symmetrical, which complicates signal processing (Figure 3.4, A).

The effect of the potential scan rate on the magnitude of the maximum of FA's reduction current was studied in the range of 0.01 − 0.1 V/s with a pulse amplitude of 50 mV. The dependence of the analytical signal on the scan rate is shown in Figure 3.4, D. As can be seen from the figure, at a scan rate of 0.02 − 0.04 V/s, the height of the FA's reduction peak reaches its maximum value. With a further increase in the scan rate, analytical signal decreases. For analytical purposes, the scan rate of 0.02 V/s was selected.

The reduction current of FA is practically independent of the accumulation time in the range from 1 to 40 s at the potentials from (-0.5) to (-0.6) V, at which the occurrence of redox processes (both the dissolution of bismuth and the reduction of FA) is excluded.

This allows us to exclude the stage of the preliminary accumulation of the analyte and to use the direct DP VA for its detection.

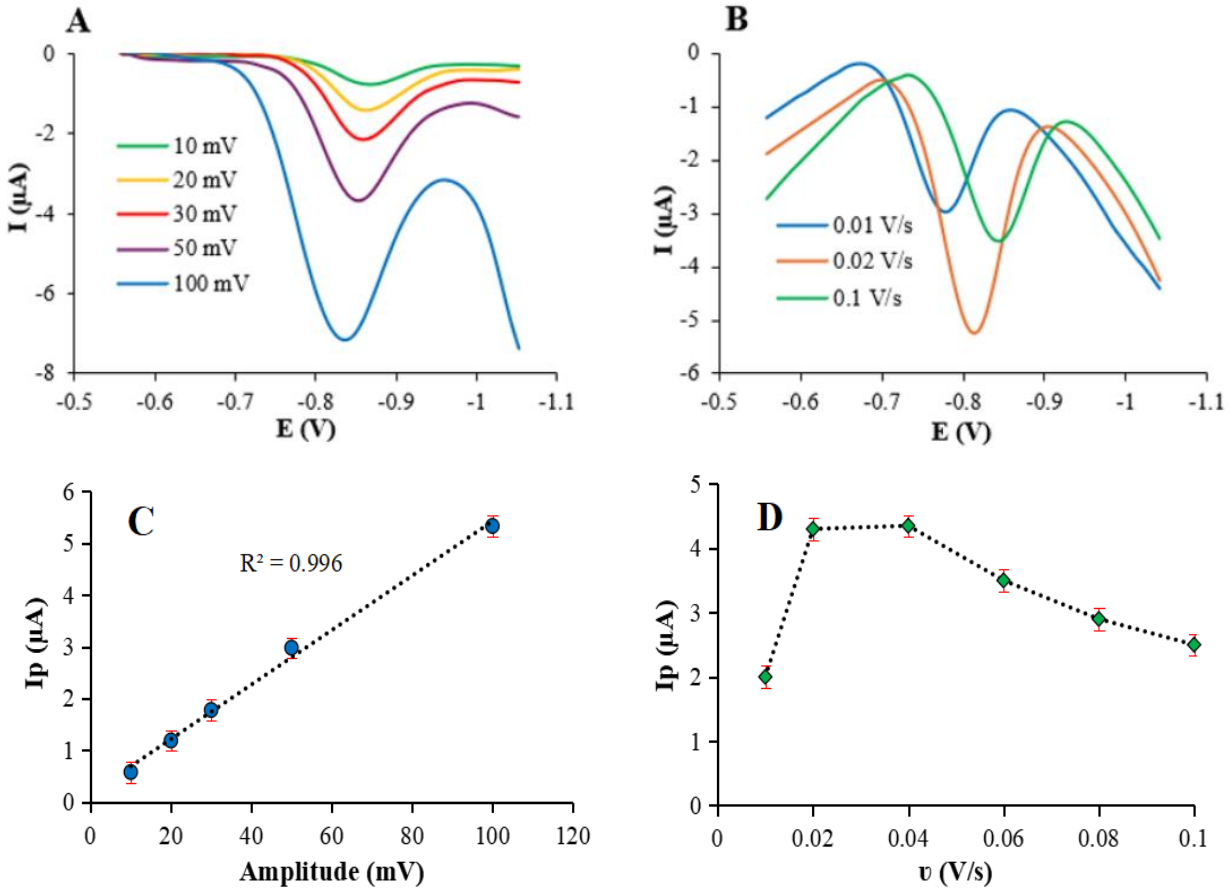


Figure 3.4 – Differential-pulse voltammograms of FA (A, B) and corresponding dependence of the peak current on: pulse amplitude (C), υ (D), registered at a υ = 0.02 V/s (A, C) and a pulse amplitude of 50 mV (B, D) on Bi/SPCE in 0.04 M PBS + 0.09 M HRZ (pH 5.2 ± 0.1) at 0.20 (A, C), 0.30 mg/L FA (B, D). Deposition conditions of the bismuth film as in Figure 3.1, A

*Effects of hydrazine sulfate concentrations and deposition conditions of the bismuth film*

The concentration of HRZ, as a reagent for the chemical reaction of FAH formation, significantly affects the FA response (Figure 3.5, A). An excess of HRZ shifts the equilibrium to the formation of an electrochemically active FAH, which increases the

yield of the reaction product [233]. The concentration of HRZ from 0.09 M to 0.15 M is sufficient to convert the main part of FA into FAH.

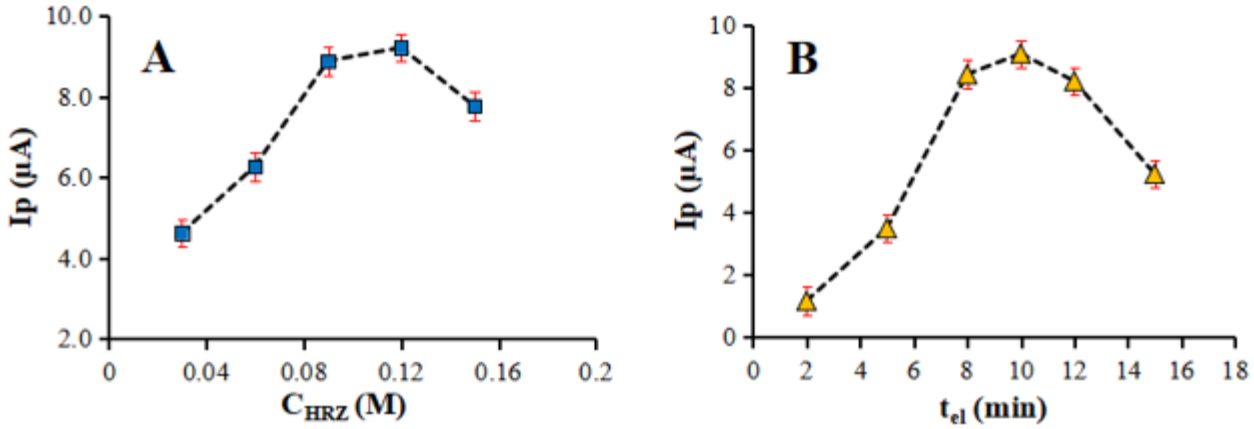


Figure 3.5 – The influence of the concentration of HRZ (A) and $t_{el}$ during bismuth film deposition on the surface of SPCE (B) on the reduction current of FA, registered on DP voltammograms at υ = 0.02 V/s and a pulse amplitude of 50 mV in 0.04 M PBS + 0.03 − 0.15 (A); 0.09 M HRZ (B) (pH 5.2 ± 0.1) + 0.6 mg/L FA. Deposition conditions of the bismuth film: 0.1 M acetate buffer (pH 4.5) + 100 mg/L Bi(III) at $E_{el}$ = -1.0 V. $t_{el}$ = 8 min (A)

Bismuth was precipitated onto the surface of the SPCE from 0.1 M acetate buffer solution at pH 4.5, containing 100 mg/L Bi(III) ions, at an electrolysis potential of -1.0 V and time of precipitation ($t_{el}$) 3 – 20 minutes while stirring the solution. This potential was chosen because at potentials more negative than –1.2 V, hydrogen generation occurs more readily than bismuth generation and the amount of plated bismuth dropped substantially [177]. The time of bismuth film deposition on the SPCE surface significantly affects the value of the reduction current of FA, which are stabilized during the electrolysis of a solution of bismuth ions for 8 – 12 minutes (Figure 3.5, B). The decrease in FA response at shorter bismuth deposition times may be due to the low degree of coverage of the SPCE surface with bismuth [161]. A further increase in the deposition time of the modifier reduces the sensitivity of the working electrode to FA

due to mechanical damage and the deterioration of adhesion of thick metal films to its surface [150]. These assumptions have been tested using SEM microscopic observations to determine the impact of deposition time on the morphology and structure of the bismuth films.

*Morphological characterization of Bi/SPCE surface*

Microscopic studies have shown that the bismuth film obtained at 3 and 5 minutes of deposition time consists of well-dispersed, firmly attached bismuth particles with an average size of 111 ± 9 μm (Figure 3.6, B) and 140 ± 11 μm (Figure 3.6, C) in length, respectively. The surface of the SPCE is shown between these crystallites. In contrast, the bismuth deposits formed at a deposition time of 10 minutes were comprised of many uniformly dispersed dendritic morphology crystals, resulting in a flat, non-porous layer with an estimated average particle size of 382 ± 25 μm (Figure 3.6, D) in length with the surface of the SPCE widely and clearly exposed. Extending the deposition time to 15 minutes results in fairly large particle sizes and lateral growth in the particle size distribution. Relatively large, broad, and evenly distributed bismuth deposits with an average particle size of 796 ± 62 μm (Figure 3.6, E) can be noticed. Data obtained from SEM and EIS [166] also point out domination of lateral growth in the bismuth film with crystalline dendritic structure prepared in acetic buffer. The bismuth deposits obtained at 20 minutes of deposition time consisted of irregular shapes and features of varying size. The surface of the electrode is mostly covered by large, elongated crystals with an average individual particle size of about 1000 – 1500 μm (Figure 3.6, F). Notably, some bismuth particles are interconnected to one another. The coating obtained is less compact and uniform with some cracks and poorer adhesion to the SPCE surface as can be seen in Figure 3.7.

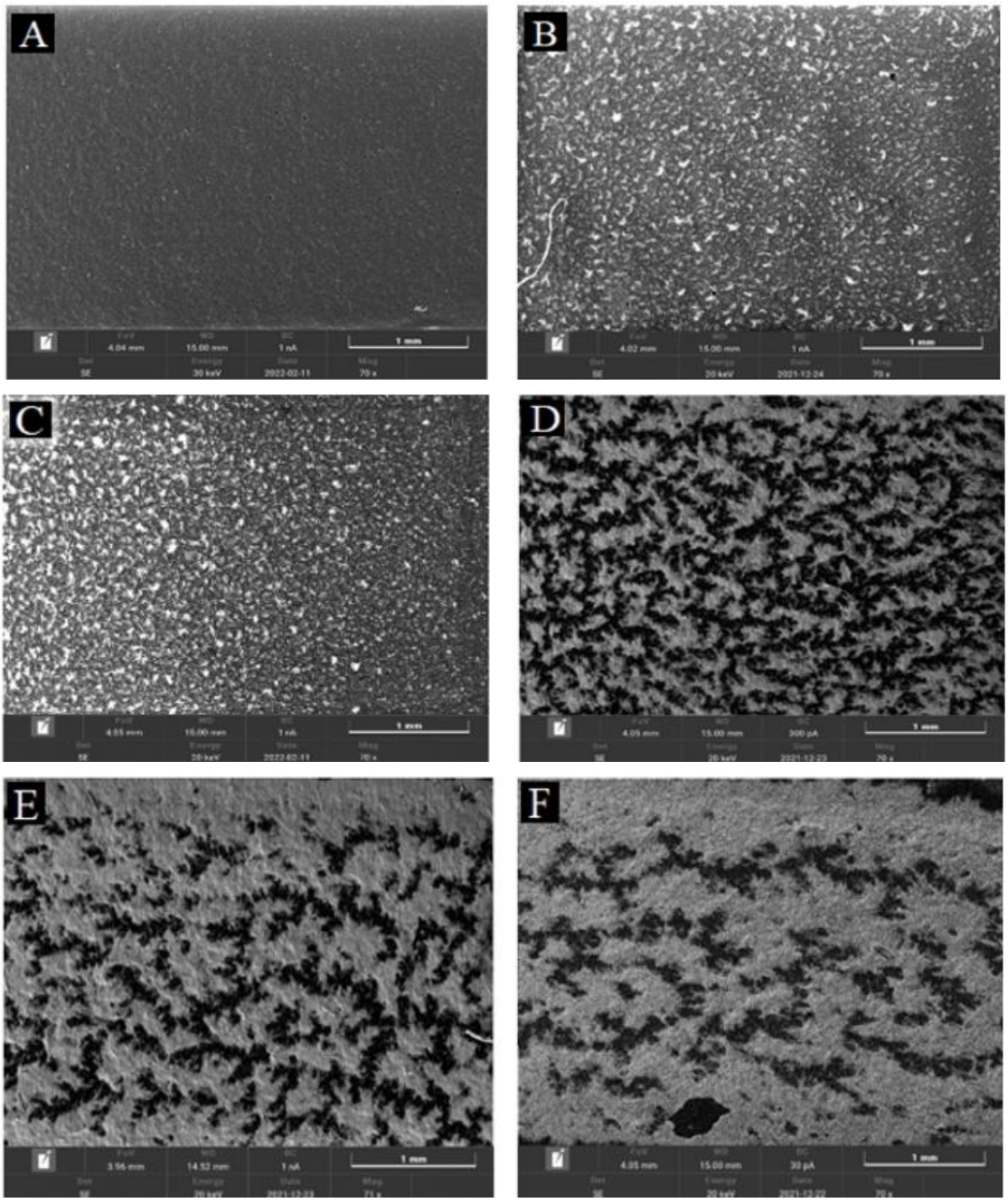


Figure 3.6 – SEM images of the SPCE surface before (A) and after bismuth film deposition by electrolysis from 0.1 M acetate buffer (pH 4.5) + 100 mg/L Bi(III) at $E_{el}$ = -1.0 V (B−F) during: 3 (B), 5 (C), 10 (D), 15 (E) and 20 min (F)

The SEM micrographs demonstrate that the morphologies of the films vary depending on the deposition time. For 3, 5, 10, 15 and 20 minutes of deposition times, the degree of surface coverage of the SPCE with bismuth was calculated as 22, 31, 49,

66 and 85%, respectively. The best analytical performance was obtained with a coating formed after 8 − 12 minutes of bismuth plating on the SPCE surface (Figure 3.5, B). This is likely due to improved surface coverage and relatively homogeneous structure of the film (Figure 3.6, D). This corresponds to the observations made based on the analysis of a large amount of experimental data [150, 161, 177, 169, 172]. For the analytical purpose, a bismuth film was deposited for 10 minutes.

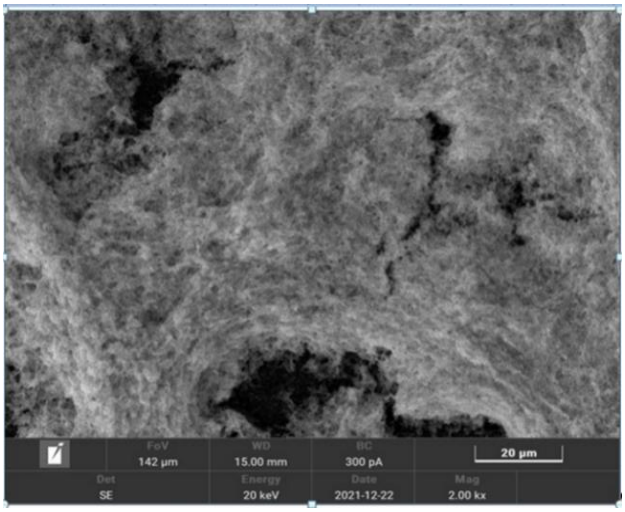


Figure 3.7 – SEM images of the SPCE surface after bismuth film deposition by electrolysis from 0.1 M acetate buffer (pH 4.5) + 100 mg/L Bi(III) at $E_{el}$ = -1.0 V during 20 min

*Effects of solution pH*

The effect of the acidity of a solution containing phosphate buffer and hydrazine sulfate on the current and reduction potential of FA was studied in the pH range 4.58–5.75 (Figure 3.8). The value of FA response depends on the acidity of the solution and reaches optimal values at pH 5.2 ± 0.1 (Figure 3.8, A). The found range of optimum pH virtually coincides with the range of pH at which the wave limiting current, or the reduction peak of FAH obtained at the dropping mercury electrode in the absence of oxygen attains a maximum [233].

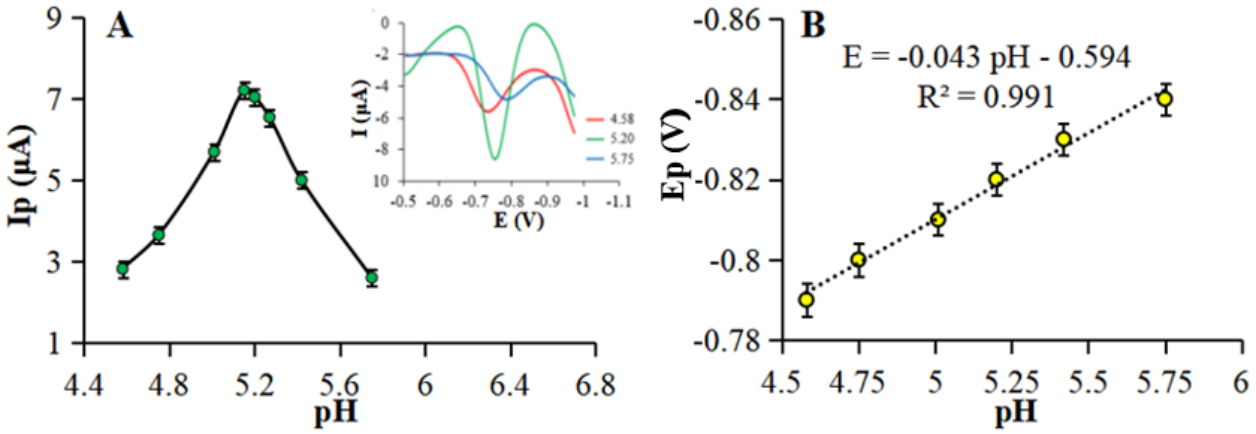


Figure 3.8 – Dependence of peak current (A) and peak potential (B) on pH for the reduction of 0.6 mg/L FA. Insert − DP voltammograms of FA registered at different pH. $t_{el}$ = 8 min. Other conditions as in Figure 3.5, B

As can be seen from Figure 3.8, B, with an increase in the pH of the solution, the maximum of the FA's reduction peak shifts towards negative potential values. The results obtained indicate the participation of hydrogen ions in the process of FA electroreduction on the surface Bi/SPCE.

Based on the research conducted the final operating conditions for recording FA voltammograms on Bi/SPCE were selected (Table 3.1).

Table 3.1 – Operating conditions for recording FA voltammograms on Bi/SPCE

| Parameter | Conditions |
|---|---|
| bismuth film deposition on the SPCE surface | 0.1 M acetic buffer (pH 4.5) + 100 mg/L Bi(III) at $E_{el}$ = -1.0 V and $t_{el}$ = 10 min |
| background electrolyte | 0.04 M phosphate buffer solution + 0.09 M hydrazine sulfate (pH 5.2 ± 0.1) |
| voltammetric technique | direct cathodic differential-pulse |
| scan range | -0.5 to -1.05 V |
| pulse amplitude | 0.05 V |
| potential scan rate | 0.02 V/s |

## 3.2. Electroanalytical performance of bismuth-modified screen-printed carbon-containing electrode towards formaldehyde

*Calibration plots, limits of detection and the quantification concentration*

Under optimal conditions, the height of FA's reduction peak current increases linearly with a concentration in the range of 0.01 − 1.0 mg/L (Figure 3.9, C), while the peak area (Q) - in a wider range of 0.01 − 5.0 mg/L (Figure 3.9, D). The $R^2$ value in the latest case is closer to 1.0. Therefore, it is preferable to use the peak area as a response for FA determination.

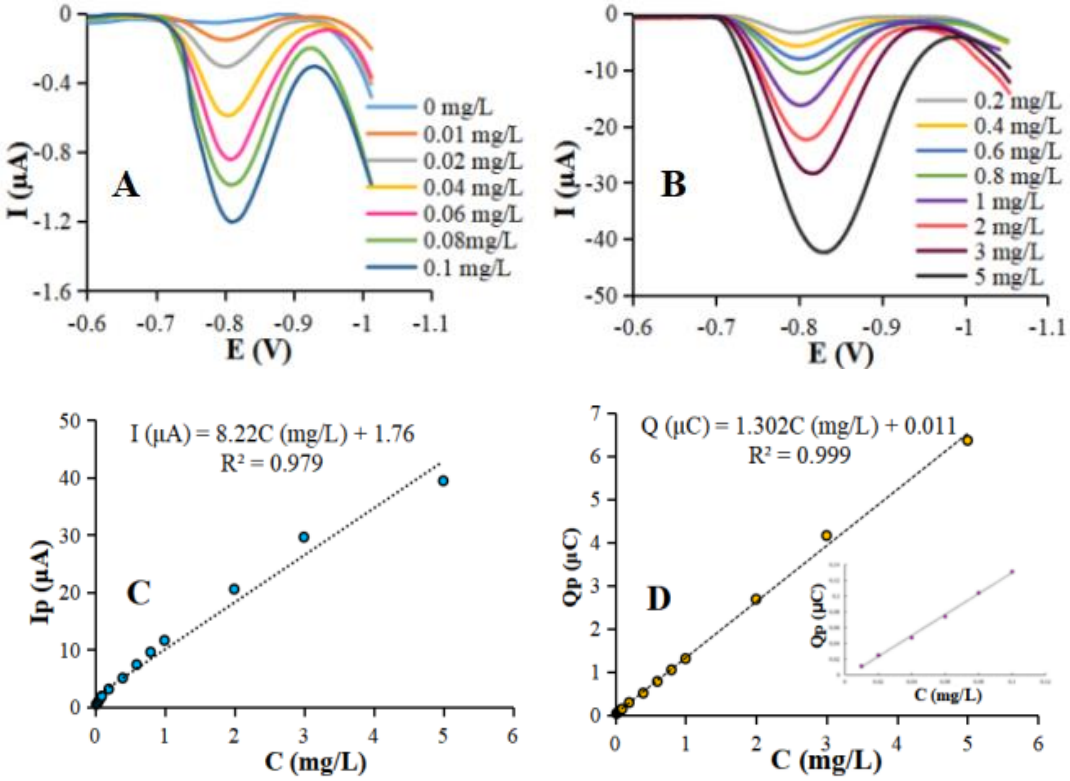


Figure 3.9 – Differential-pulse voltammograms registered at a υ = 0.02 V/s and a pulse amplitude of 50 mV on Bi/SPCE in 0.04 M PBS + 0.09 M HRZ (pH 5.2 ± 0.1) for 0 to 0.1 (A) and 0.2 to 5.0 mg/L FA (B) and the dependence of the height (C) and area of the FA reduction peak (D) on its concentration in solution. Insert D: dependence of FA response on its concentration in solution in the range of 0.0 − 0.1 mg/L. $t_{el}$ = 10 min

The LOD calculated from the regression equation Q (μC) = (1.3224 ± 0.0114) C (mg/L) – (0.0047 ± 0.0007) (μC) ($R^2$ = 0.9979) for the calibration curve in the range of 0.01 – 0.10 mg/L (Figure 3.9, D, insert) is 0.002 mg/L (0.07 μM) FA. LOD was calculated using the formula 3σ/k, where σ is the standard deviation of the free term of the linear relationship; k – sensitivity coefficient (tangent of the calibration curve slope angle) [234]. It is lower than those reported in the literature for direct electrocatalysis on solid electrodes and indirect methods with HMDE and unmodified GCE and SPCE (Table 1.1). The limit of quantification of FA is 0.01 mg/L (0.33 μM).

*Accuracy, repeatability, reproducibility, and stability of the Bi/SPCE*

Ten successive measurements were performed using the same Bi/SPCE in the low measured concentration of 0.02 mg/L FA. The mean cathodic peak response (μC) can be reported as 0.0242 ± 0.0007 (RSD = 4.1%). It indicates the good Bi/SPCE repeatability towards FAH electroreduction at trace levels. Satisfactory recoveries (n = 5, P = 0.95) were obtained in the range of 104.1 ± 4.3% for 0.02 mg/L FA (RSD = 3.6%), 99.3 ± 2.8% for 0.2 mg/L (RSD = 3.6%), 99.5 ± 1.8% for 1 mg/L FA (RSD = 1.7%), which yields the acceptable accuracy for analysis of FA.

To verify the stability of Bi/SPCE, ten successive calibration curves (with 15 responses for each one) in the range of 0.2 – 1.0 mg/L FA were registered on the same electrode under optimized conditions. RSD for the sensitivity of Bi/SPCE to FA (μC·L/mg) is only 2.7%. Such duration of stable operation is quite sufficient for an easy-to-prepare, cheap and practically disposable electrode. Similar calibration curves for 10 different electrodes with a result of RSD = 6.2% for the sensitivity of Bi/SPCEs to FA confirmed good reproducibility of these electrodes.

*Interference measurement*

An interference experiment was carried out to evaluate the selectivity of Bi/SPCE

towards FA. Since the indirect methods of FA determination are based on a functional group approach [132-134], it is expected that other aldehydes (especially those that are aliphatic and have a low molecular weight) can react with amino compounds such as Gerard's reagent and hydrazine sulfate similarly to FA. Acetaldehyde (AA), in particular, can interfere with the determination of FA [134]. After the addition of five times the amount of acetaldehyde (34 μM) to the buffer solution containing 6.7 μM FA, the peak current of acetaldehyde at -0.95 V appears clearly, while the response of FA substantially decreases (Figure 3.10).

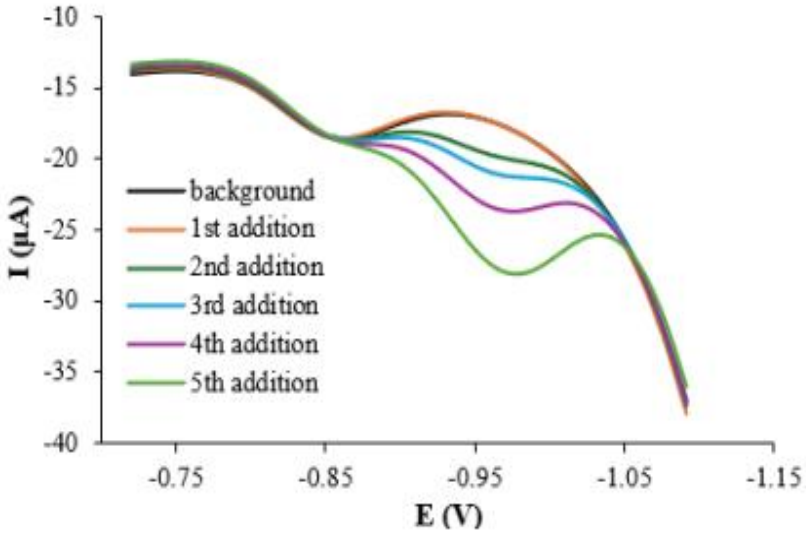


Figure 3.10 – Differential-pulse voltammograms for 6.7 μM FA registered in 0.04 M PBS + 0.09 M HRZ (pH 5.2 ± 0.1) before and after addition of 20.4, 27.2, 34, 68, and 136 μM acetaldehyde. Other conditions as in Figure 3.9

The presence of 3 times the amount of acetaldehyde, 100 times the amount of ethanol and 150 times the amount of methanol did not significantly interfere with the determination of FA. The drop in response for 6.7 μM FA does not exceed 3% in the presence of both alcohols. The results of the experiment on the effect of these chemicals on FA response at Bi/SPCE are given in Table 3.2−3.4.

Table 3.2 − Effect of acetaldehyde on FA Response

| $C_{AA}$ in the cell (μM) | $C_{AA}/C_{FA}$ | Response for 6.7 μM FA (μC)* | ΔQ, %** | Response for AA (μC)* |
|---|---|---|---|---|
| 0 | — | 0.220 | — | — |
| 20.4 | 3:1 | 0.219 | 0 | — |
| 27.2 | 4:1 | 0.153 | 30 | — |
| 34 | 5:1 | 0.099 | 55 | 0.025 |
| 68 | 10:1 | 0.071 | 68 | 0.105 |
| 136 | 20:1 | 0.021 | 90 | 0.362 |

*Note* − * Mean value from 3 measurements; ** ΔQ, % − degradation of FA Response, AA − acetaldehyde

Table 3.3 – Effect of methanol on FA Response

| $C_{methanol}$ in the cell (μM) | $C_{methanol}/C_{FA}$ | Response for 6.7 μM FA (μC)* | ΔQ, %** |
|---|---|---|---|
| 0 | — | 0.202 | — |
| 335 | 50:1 | 0.209 | 0 |
| 670 | 100:1 | 0.198 | 2 |
| 1005 | 150:1 | 0.196 | 3 |
| 1340 | 200:1 | 0.186 | 8 |

Table 3.4 – Effect of ethanol on FA Response

| $C_{ethanol}$ in the cell (μM) | $C_{ethanol}/C_{FA}$ | Response for 6.7 μM FA (μC)* | ΔQ, %** |
|---|---|---|---|
| 0 | — | 0.217 | — |
| 335 | 50:1 | 0.217 | 0 |
| 670 | 100:1 | 0.210 | 3 |
| 1005 | 150:1 | 0.202 | 7 |
| 1340 | 200:1 | 0.191 | 12 |

From these results, it can be affirmed that the sensor reported here exhibits acceptable selectivity towards these chemical species.

*Real samples analysis*

To evaluate the effectiveness of the developed methods for determining FA using Bi/SPCE in real sample analysis, filtrated wastewater, meltwater from snow collected within the industrial area of city during spring season, bottled water as well as a widely used medicinal drug "Endofalk®", technical urotropin grades C and CT as raw for pharmaceutical substance “Urotropin” were analyzed by standard addition method. The reliability of the results obtained for FA determination was assessed by the “spike-recovery” method for water samples and by comparison with the results of actual pharmacopoeial methods recommended for determining FA in the pharmaceutical substances "Macrogol 3350" [40] and “Urotropin” [53].

Differential-pulse voltammograms recorded for the samples presented well-defined reduction peaks of FA (Figure 3.11 D, E, F). The area of these peaks increased linearly with different additions from FA working solutions (Figure 3.11 A, B, C). The sensitivity of Bi/SPCE to FA in technical urotropin test solution grade CT (1.341) is close to the value obtained for pure solutions (1.302) (Figure 3.9, D). This suggests that the matrix of the samples studied does not interfere with the determination of FA. As in accordance with operating conditions, background electrolyte with (pH 5.2 ± 0.1) is used for recording FA voltammograms on Bi/SPCE (Table 3.1), the hydrolysis stability of the technical urotropin test solutions was tested (Figure 3.12). The technical urotropin test solutions are stable in measuring cell during 5 – 6 minutes, which is sufficient to carry out the analysis using the algorithm we proposed as DP voltammogram registration and Bi/SPCE surface regeneration takes 35 s.

Concentrations of FA in the water samples were determined with satisfactory results. The RSD was less than 6% (n = 3), and the recovery was in the range of 94 – 104%, which showed the sensitive and reproducible voltammetric analysis of FA traces in water samples. The results obtained are shown in Table 3.5.

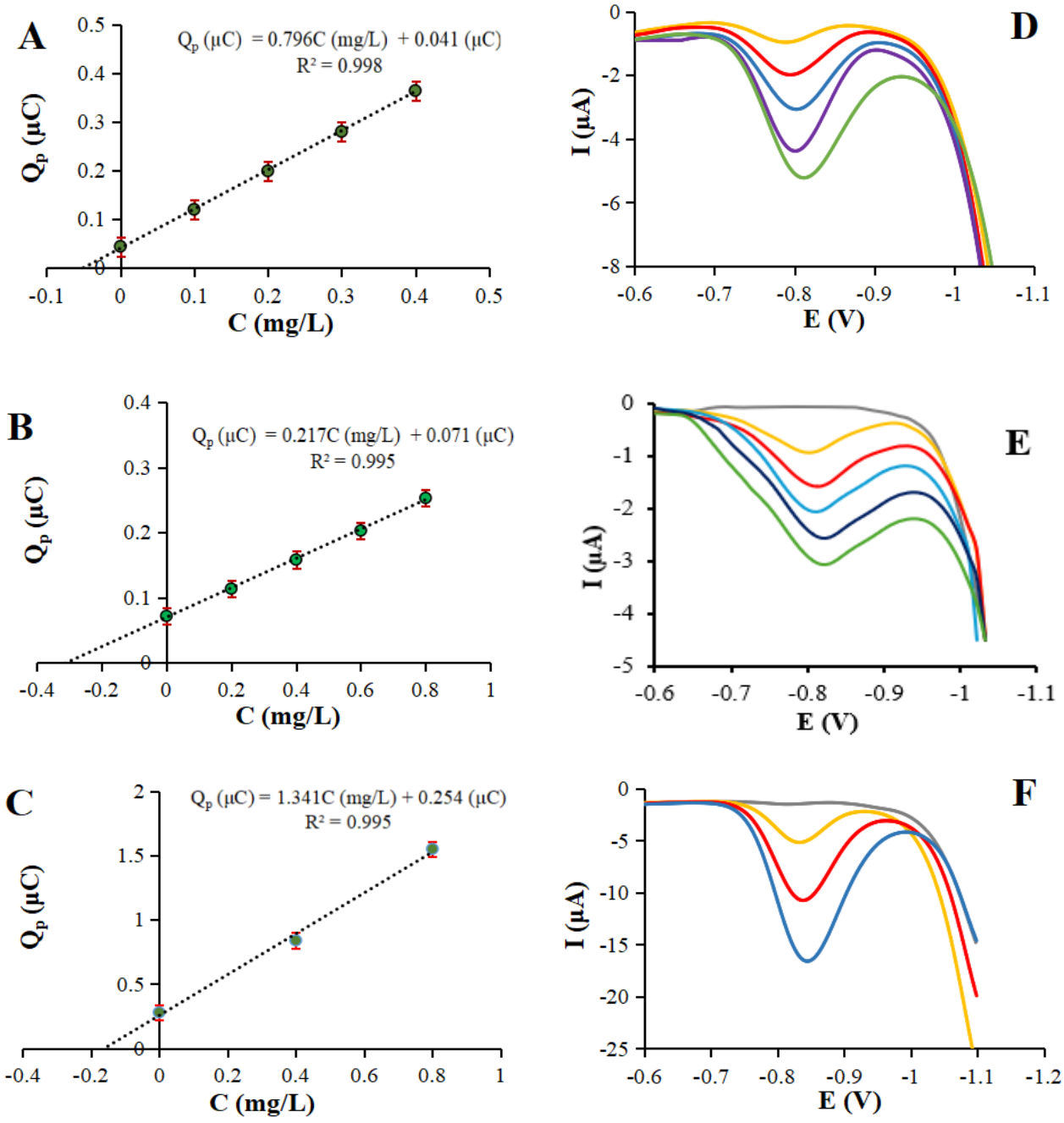


Figure 3.11 – The calibration plots of FA determination for: wastewater and addition of 0.1, 0.2, 0.3, 0.4 mg/L FA (A), solution of drug "Endofalk®" and addition of 0.2, 0.4, 0.6, 0.8 mg/L FA (B), technical urotropin test solution grade CT and addition of 0.4, 0.8 mg/L FA (C); corresponding DP voltammograms (with gray color for blank) recorded at Bi/SPCE (D, F) and Nafion coating Bi/SPCE (E) in 0.04 M PBS + 0.09 M HRZ (pH 5.2 ± 0.1). Other conditions as in Figure 3.9

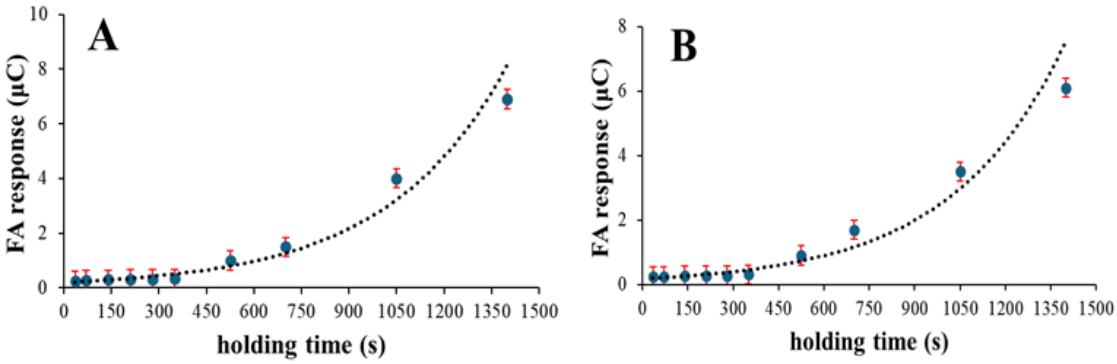


Figure 3.12 – Hydrolysis stability of the technical urotropin test solutions grade C (A) and CT (B) in the process of voltammetric measurements in 0.04 M PBS + 0.09 M HRZ (pH 5.2 ± 0.1) + 0.8 mL of 1% urotropin test solutions.

Table 3.5 – Results for FA determination in water samples (n = 3, P = 0.95)

| Samples | Added C, μg/L | Found FA | | |
|---|---|---|---|---|
| | | C ± ΔC, μg/L | RSD, % | R, % |
| Wastewater | — | 132 ± 5 | 1.6 | 97 |
| | 100 | 229 ± 14 | 2.4 | |
| Meltwater | — | 94 ± 12 | 5.4 | 94 |
| | 50 | 141 ± 10 | 2.9 | |
| Bottled water | — | 41 ± 6 | 6.0 | 104 |
| | 50 | 93 ± 8 | 3.5 | |

Table 3.6 shows a comparison of the results of FA determination in the drug "Endofalk®", obtained by the developed method and visible spectrophotometric method (Vis) according to the pharmaceutical article (F S 2.1.0127.18). The FA content found in the drug "Endofalk®" is close to the permissible content of 0.003% established for the "Macrogol 3350" substance [40].

A comparison of the results obtained by both methods using statistical *F*- and *t-criterion* values showed that the calculated *F*- and *t-criterion* values do not exceed the tabulated (theoretical) values. This confirms the absence of any significant differences between the results and precision of both methods. At the same time, performing quantitative control using the developed method, unlike Vis, does not depend on the

color of the solution, does not require cooling and keeping the test solution for 15 minutes in an ice bath for color development, as well as the use of expensive and aggressive reagents.

Table 3.6 – Determination of FA in medicinal drug "Endofalk®" (n = 6, P = 0.95)

| Found FA | | | |
|---|---|---|---|
| DP VA | | Vis | |
| Sample, % | RSD, % | Sample, % | RSD, % |
| 0.0032 ± 0.0003 | 8.4 | 0.0031 ± 0.0003 | 10.8 |
| *t-criterion* | | $t_{exp}$ = 0.85; $t_{table}$ = 2.26 (f = 10) | |
| *F-criterion* | | $F_{exp}$ = 0.63; $F_{table}$ = 4.28 ($f_1 = f_2 = 6$) | |

The results of the FA determination in the technical urotropin grades C and CT are given in Table 3.7. The results obtained for both grades are very similar. The RSD does not exceed 5% for both grades, which indicated good precision of the method developed.

Table 3.7 – Results of voltammetric determination of FA content in technical urotropin grades C and CT (n=6, P=0.95)

| Sample | Found FA | | RSD, % | Sample | Found FA | | RSD, % |
|---|---|---|---|---|---|---|---|
| Urotropin grade | Urotropin test solution, mg/L | technical Urotropin, % | | Urotropin grade | Urotropin test solution, mg/L | technical Urotropin, % | |
| C | 5.0 | 0.050 | | CT | 5.0 | 0.050 | |
| | 4.7 | 0.047 | | | 5.2 | 0.052 | |
| | 4.5 | 0.045 | | | 5.5 | 0.055 | |
| | 5.1 | 0.051 | | | 5.1 | 0.051 | |
| | 4.6 | 0.046 | | | 5.0 | 0.050 | |
| | 4.8 | 0.048 | | | 5.0 | 0.049 | |
| $\bar{C} \pm \Delta C$, % | 4.8±0.2 | 0.048±0.002 | 4.8 | $\bar{C} \pm \Delta C$, % | 5.1±0.2 | 0.051±0.002 | 4.2 |

The content of FA in technical urotropin of both grades does not go beyond the permissible values specified by the manufacturer (0.02 - 0.2% on a dry weight basis). Control of the FA content in technical urotropin is very important for the manufacturer, since it affects the quality of the produced urotropin pharmaceutical substance as an active ingredient of finished dosage forms.

The correctness of the developed methods for the quantitative determination of FA in the specified samples was assessed by comparing the obtained results with the results of independent analysis method recommended by the State Pharmacopoeia of the Russian Federation, XIV edition (FS 2.1.0131.18) [53]. According to the pharmaceutical article (F S 2.1.0131.18), semi-quantitative determination of FA content in the substance "Urotropin" is carried out by visual assessment of the color of the test sample solution. The method is based on the formation of silver as a result of the interaction of silver nitrate with FA in the presence of ammonium hydroxide. For this purpose, 2 mL of 2.5% silver ammonium nitrate solution is added to the test solution of the samples and the FA standard solution. The resulting gray color of the test solution after 5 minutes should not be more intense than the color of the comparison reference solution (RS) with 5 mg/L FA.

Figure 3.13 shows the identical colors of RS and technical urotropin test solutions, corresponding to 5 mg/L FA concentration that in terms of dry weight is about 0.05% FA for both samples.

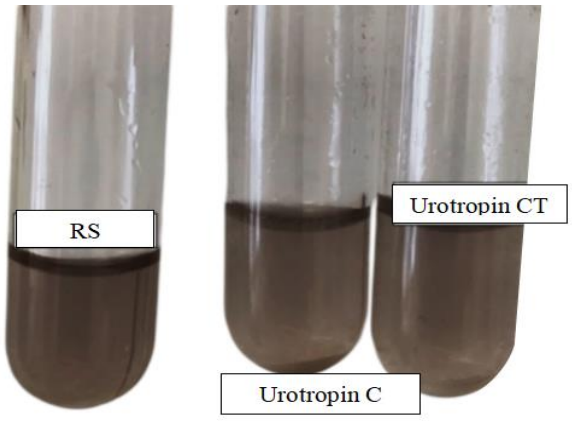


Figure 3.13 – Colors of FA reference solution (RS) and 1% test solutions of technical urotropin grades C and CT

The content of FA in urotropin test solution is 4.8 ± 0.2 mg/L for C sample and 5.1 ± 0.2 mg/L for CT sample according to the VA method (Table 3.7). In terms of dry weight, the FA content in urotropin is 0.048 ± 0.002% for C sample and 0.051 ± 0.002% for CT one. It indicates acceptable convergence of the results of both methods, developed VA and pharmacopoeial.

## Conclusions to chapter 3

The electrochemical behavior of FA in the form of its electroactive hydrazone on screen-printed carbon-containing electrodes, modified in acetic buffer with a potentiostatically preplated bismuth film, was studied. It was shown that the process of FAH electrochemical reduction is irreversible and primarily controlled by diffusion. Optimal conditions for recording FA voltammograms on Bi/SPCE were established using direct cathodic differential-pulse voltammetry in a phosphate buffer solution with a pH of 5.2 ± 0.1 and containing 0.09-0.15 M hydrazine sulfate. These conditions were selected for further research to evaluate the electroanalytical performance of Bi/SPCE towards FA.

A “green”, low-cost, very simple, reliable and fast voltammetric method for the determination of FA in the form of FAH over a sufficiently wide linear range (0.33-167 μM) was developed using Bi/SPCEs. This method demonstrated superior performance compared to existing approaches for direct electrocatalysis on solid electrodes and indirect methods with HMDE (Table 1.1), exhibiting the lowest reported detection limit (0.07 μM) and limit of quantification (0.33 μM) of FA. The simplicity of the Bi/SPCE modification process and its exceptional electroanalytical capabilities make it a promising tool for FA analysis. The proposed voltammetric method offered a simple determination of FA in pharmaceutical formulations and environmental objects with satisfactory recoveries and accuracy.

# CHAPTER 4 STUDY OF "GREEN" METALS-MODIFIED SCREEN-PRINTED CARBON-CONTAINING ELECTRODES WITH PHYSICOCHEMICAL METHODS

## 4.1 Morphological characterization of the "green" metals-modified electrodes

*Morphological characterization of Bi/SPCEs*

Based on systematic study on the influence of plating conditions on the surface morphology of bismuth film electrodes, from the available electrodeposition conditions listed in Table 1.2, we selected those that have been proposed for: the determination of Ni(II) [173] and Co(II) [150] by cathodic adsorptive stripping voltammetry using dimethylglyoxime as complexing agent, the determination of glutathione and folic acid [161] by SqW cathodic stripping voltammetry and the electrochemical study of the bismuth electrodes using standard redox mediators $[Fe(CN)_6]^{3-/4-}$ or $[Ru(NH_3)_6]^{3+/2+}$ [169]. These conditions were chosen to obtain Bi/SPCEs with expectedly different surface morphologies (Table 4.1).

Table 4.1 – Selected conditions for potentiostatic preplating of the bismuth films

| Electrode | Plating solution | Deposition conditions | | Reference |
|---|---|---|---|---|
| | | $E_{el}$, V | $t_{el}$, s | |
| Bi/SPCE-1 | 0.1 M acetic buffer (pH 4.5) + 50 mg/L NaBr + 50 mg/L Bi(III) | -0.3 | 60 | [169] |
| Bi/SPCE-2 | 0.1 M acetic buffer (pH 4.5) + 100 mg/L Bi(III) | -1.0 | 600 | [173] |
| Bi/SPCE-3 | 0.1 M acetic buffer (pH 4.5) + 200 mg/L Bi(III) + 1 mM EDTA | -0.9 | 600 | [161] |
| Bi/SPCE-4 | 1 M HCl + 0.5 M NaBr + 4 g/L Bi(III), without stirring | -0.28 | 20 | [150] |

The morphology of the Bi/SPCEs surface was determined using SEM. Figure 4.1 displays typical SEM images that illustrate how different bismuth plating conditions affect the morphology of the films. Bi/SPCE-1 film (Figure 4.1, B) is characterized by the formation of randomly distributed insufficient amounts of bismuth grains with an average size of 10 ± 2 μm and surface coverage of about 10%. At a scale of 50 μm, particles of the metal are easily distinguishable. In this case, the surface of the substrate is almost entirely exposed. This is mainly attributed to the limited amount of bismuth in the plating solution combined with its low electrolysis potential (Table 4.1).

The micrograph for Bi/SPCE-2 (Figure 4.1, C) shows the formation of evenly distributed dendritic morphology bismuth crystals with an average particle size of 374 ± 38 μm in length, with the SPCE surface partially exposed. These bismuth particles cover around 49% of the substrate surface. For Bi/SPCE-3 (Figure 4.1, D), most of the substrate surface is covered by relatively large and uniformly distributed flake-like dendritic structures of bismuth deposits with an average grain size of 1000 ± 192 μm. Some of the bismuth particles are linked to each other. The added complexing ligand EDTA to the plating solution contributed to the enhancement of particle size growth mainly laterally, which led to greater surface coverage, approximately 73%. In both cases (C, D), lateral growth for the bismuth films with crystalline dendritic structure is dominant, which is typical for acetic buffer as a plating solution [161].

On the other hand, bismuth film on Bi/SPCE-4 surface (Figure 4.1, E) consists of many fine, well-dispersed bismuth crystals with an average particle size of 95 ± 20 μm and surface coverage of about 52%. The dominance of vertical particle growth leads to a decrease in the average size of the particles and the acquisition of the highest roughness. This result is similar to the report provided by Królicka et al. [150], which proves that bromide ions play a great role in the growth of particles perpendicular to the substrate surface.

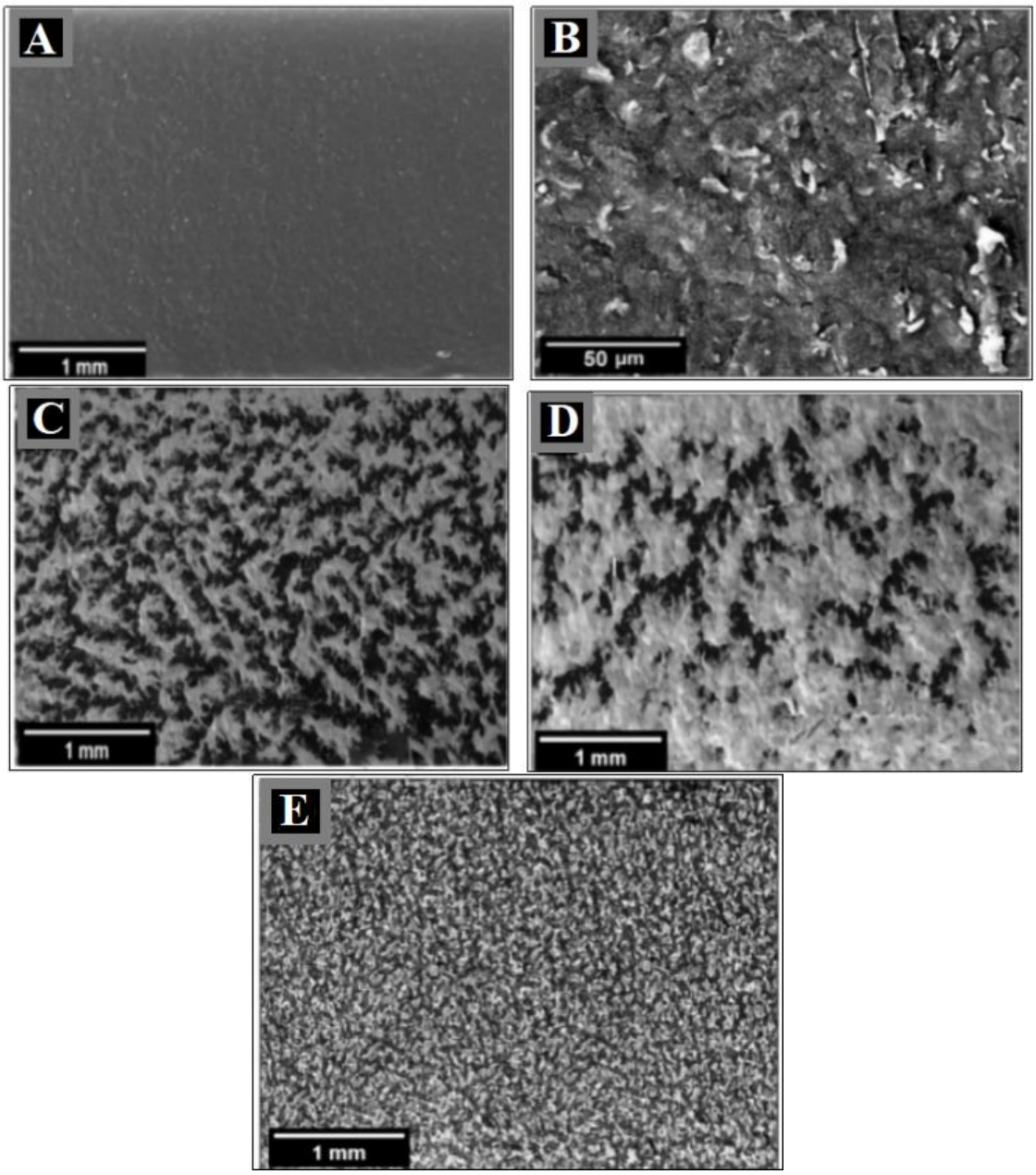


Figure 4.1 – SEM images of SPCE surfaces before (A) and after modification with bismuth: Bi/SPCE-1 (B), Bi/SPCE-2 (C), Bi/SPCE-3 (D) and Bi/SPCE-4 (E)

*Morphological characterization of Sb/SPCEs*

Systematic studies on the influence of plating conditions on the surface morphology of antimony film electrodes in contrast to bismuth films electrodes were not conducted. From the available plating conditions (Table 1.2), we chose plating

conditions that have been proposed for the determination of Ni(II) [153, 193], Pb(II) and Cd(II) [192] by cathodic adsorptive stripping voltammetry using dimethylglyoxime [153, 193] and pyrogallol red [192] as complexing agents. These conditions were chosen to obtain Sb/SPCEs with significantly different surface morphologies (Table 4.2).

Table 4.2 – Conditions for potentiostatic preplating of the antimony films

| Electrode | Plating solution | Deposition conditions | | Reference |
|---|---|---|---|---|
| | | $E_{el}$, V | $t_{el}$, s | |
| Sb/SPCE-1 | 0.01 M HCl + 50 mg/L Sb(III) | -0.5 | 300 | [153] |
| Sb/SPCE-2 | 0.5 M HCl + 100 mg/L Sb(III) | -1.2 | 50 | [192] |
| Sb/SPCE-3 | 0.01 M HCl + 10 mg/L Sb(III) | -1.0 | 120 | [193] |

As per reference [153], the antimony film on the surface of ex-situ prepared Sb/SPCE consist of randomly dispersed and firmly fixed antimony particles ranging in size from 0.5 to 2 μm and does not completely cover the carbon surface. With the electroplating conditions used in [193] microscopic examination of the surface of electroplated antimony films electrodes by SEM revealed a low coverage of their surface with antimony, characterized by scarce and widely dispersed antimony particles. SEM images for Sb/SPCEs surface (Figure 4.2) show the effect of the different plating conditions on the morphology of the films.

Scanning electron microscopy image of bare-SPCE (Figure 4.2, A) displays a rough electrode surface predominantly composed of inhomogeneous carbon substrate. Dispersed bright tinges are shown at the edges of the graphite particles, possibly due to more secondary electrons emitted from them. Sb/SPCE-1 film (Figure 4.2, B) is characterized mainly by the formation fairly evenly distributed tiny Sb particles with average size of 0.6 ± 0.1 μm. Most of the Sb nucleation is favored at the elevated sites of the rough electrode surface, most probably due to relatively high electric field at the elevated sites in comparison to at the smooth sites. In addition to this, few scarcely

distributed irregularly shaped bigger Sb particles with average size 4 ± 1μm were observed. The total surface SPCE covered by Sb was calculated to be 12%.

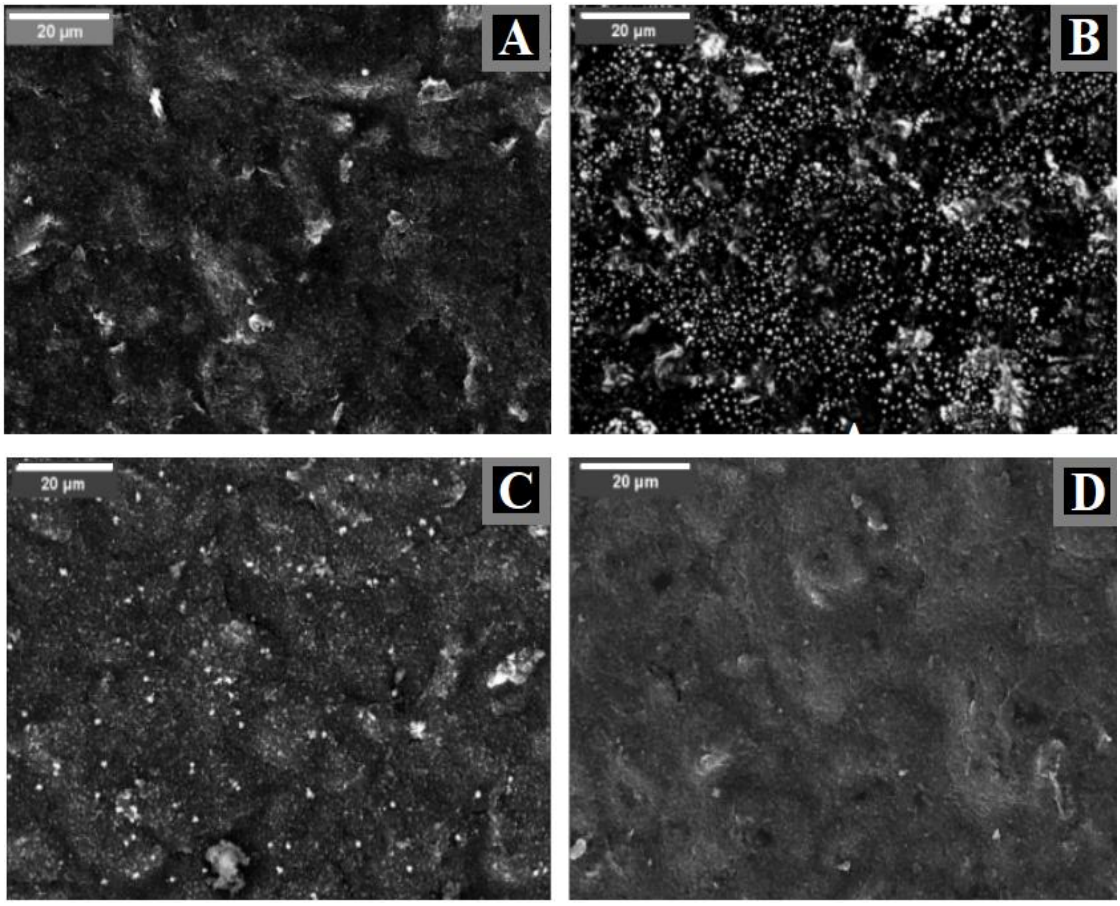


Figure 4.2 – SEM images of SPCE surfaces before (A) and after modification with antimony: Sb/SPCE-1 (B), Sb/SPCE-2 (C), Sb/SPCE-3 (D)

The micrograph for Sb/SPCE-2 (Figure 4.2, C) showed the formation of evenly dispersed fine Sb grains with an average particle size of 1 ± 0.3 μm in diameter, with the electrode surface clearly exposed. These Sb particles cover about 4% of the substrate surface. As for Sb/SPCE-3 (Figure 4.2, D), due to the small amount of Sb(III) in the plating solution (Table 4.2), extremely small particles are formed that are invisible in the SEM images, even with the highest possible resolution for the microscope we used. Despite this, ImageJ software analysis estimates the surface coverage by Sb particles to be around 1%. These results indicate the dependence of antimony morphology on the

chosen plating conditions (Sb(III) concentration, pH of the plating solution, deposition potential, and deposition time).

## 4.2 Neutral Red as a redox probe for evaluation of electrochemical performance of "green" metals-modified electrodes

*Electrochemical behavior of NR at bare and "green" metals-modified electrodes*

It is known that the monoprotonated NR ($NRH^+$) in an aqueous medium in the pH range of 1.0 – 9.2 undergoes reduction on a GCE in two stages, each of which involves a single electron transfer with one proton being gained with each electron and the 1st-stage: NR protonated form ($NRH^+$) ↔ radical ($NRH^{\bullet}$) is a reversible one [231]. As can be seen from Figures 4.3 and Figure 4.4, NR behaves in a similar way at bare-SPCE (Figure 4.3, A), Bi/SPCE-2 (Figure 4.4, A) and Sb/SPCE-1 (Figure 4.4, C) in the 0.05 M PBS + 0.1 M $NaNO_3$ solution. This solution is often used as a background electrolyte in the study of NR redox transformations [235]. Two single-electron peaks of NR reduction were recorded at -0.51 V and -0.88 V on bare-SPCE, at -0.53 V and -0.81 V on Bi/SPCE-2 and, at -0.53 V and -0.82 V on Sb/SPCE-1.

The CVs registered from -1.2 V to +1.2 V at Bi/SPCE-2 and Sb/SPCE-1 in a 0.05 M PBS + 0.1 M $NaNO_3$ solution (Figure 4.3, B, C) showed a large and broad oxidation peak up to 2200 µA for Bi/SPCE-2 and 435 µA for Sb/SPCE-1, corresponding to the dissolution of their previously deposited films in the potential range of −0.3 V to +1.2 V and −0.4 V to +1.2 V for Bi/SPCE-2 and Sb/SPCE-1, respectively. As shown in Figure 4.3, A, the characteristic potential range of $[Fe(CN)_6]^{3-/4-}$ activity lies in the positive potential range where it is completely masked by the oxidation currents of both Bi/SPCE and Sb/SPCE films. Therefore, we infer that $[Fe(CN)_6]^{3-/4-}$ is inconvenient to use as a redox probe for characterizing bismuth- and antimony-modified SPCEs. In contrast, NR

in the protonated form undergoes redox transformations in the negative potential range where neither bismuth nor antimony exhibit electroactivity (Figure 4.3, A and 4.4, A, C).

For bare-SPCE (Figure 4.3, A), the value of the potential difference between the peaks for the oxidation/reduction currents (ΔE) of the $[Fe(CN)_6]^{3-/4-}$ pair is 0.92 V, while for the NR it is about 0.07 V. This is attributed to the strong electron transfer ability of NR as a redox mediator [228].

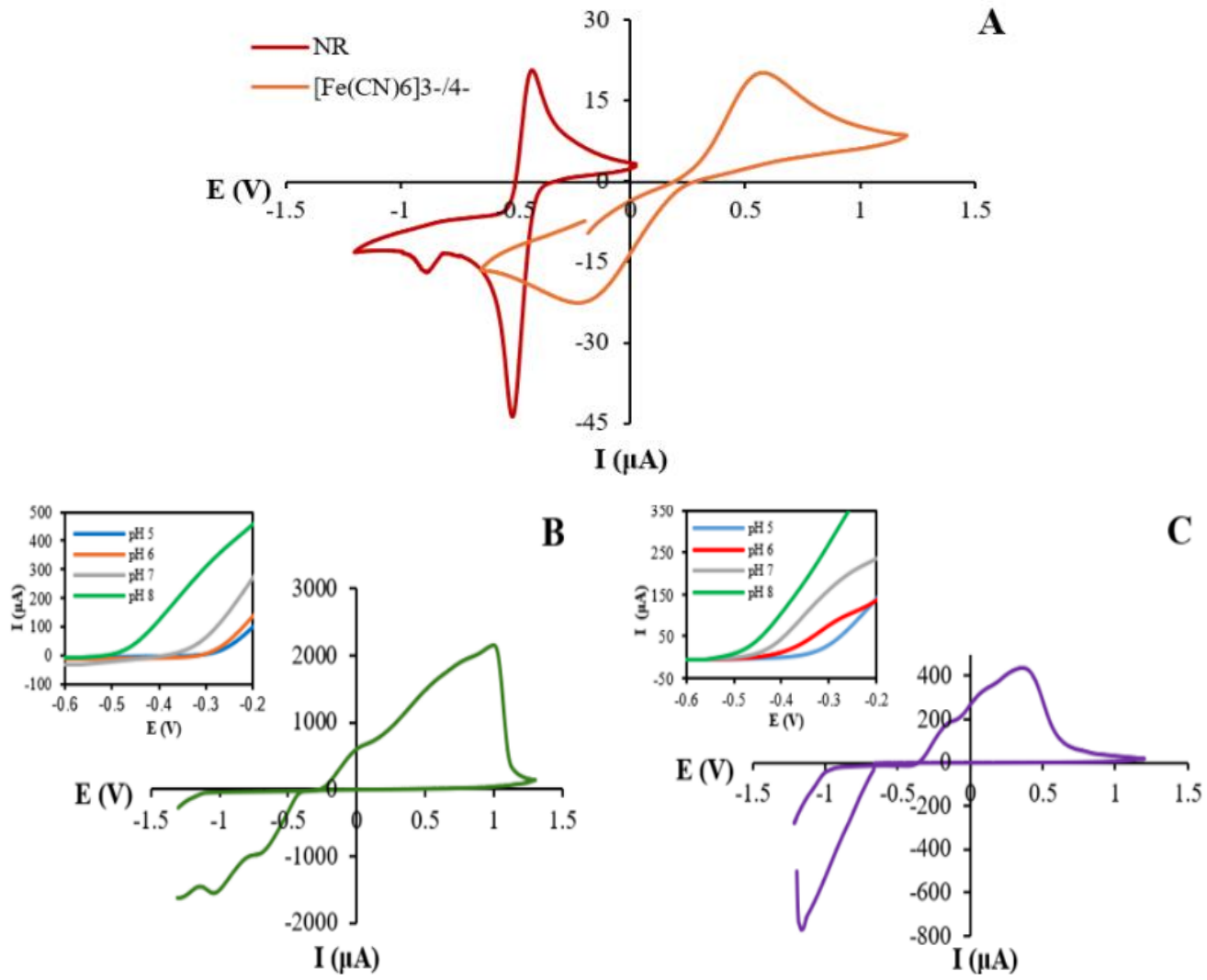


Figure 4.3 – Cyclic voltammograms registered in 0.05 M PBS + 0.1 M $NaNO_3$ (pH 5.0 ± 0.5) with υ = 0.1 V/s on: bare-SPCE after addition of 2 mM $[Fe(CN)_6]^{3-/4-}$ or 2 mM NR (A); Bi/SPCE-2 (B) and Sb/SPCE-1 (C) without NR. (Inserts B and C: the effect of the pH of the solution on the beginning of the metal dissolution process)

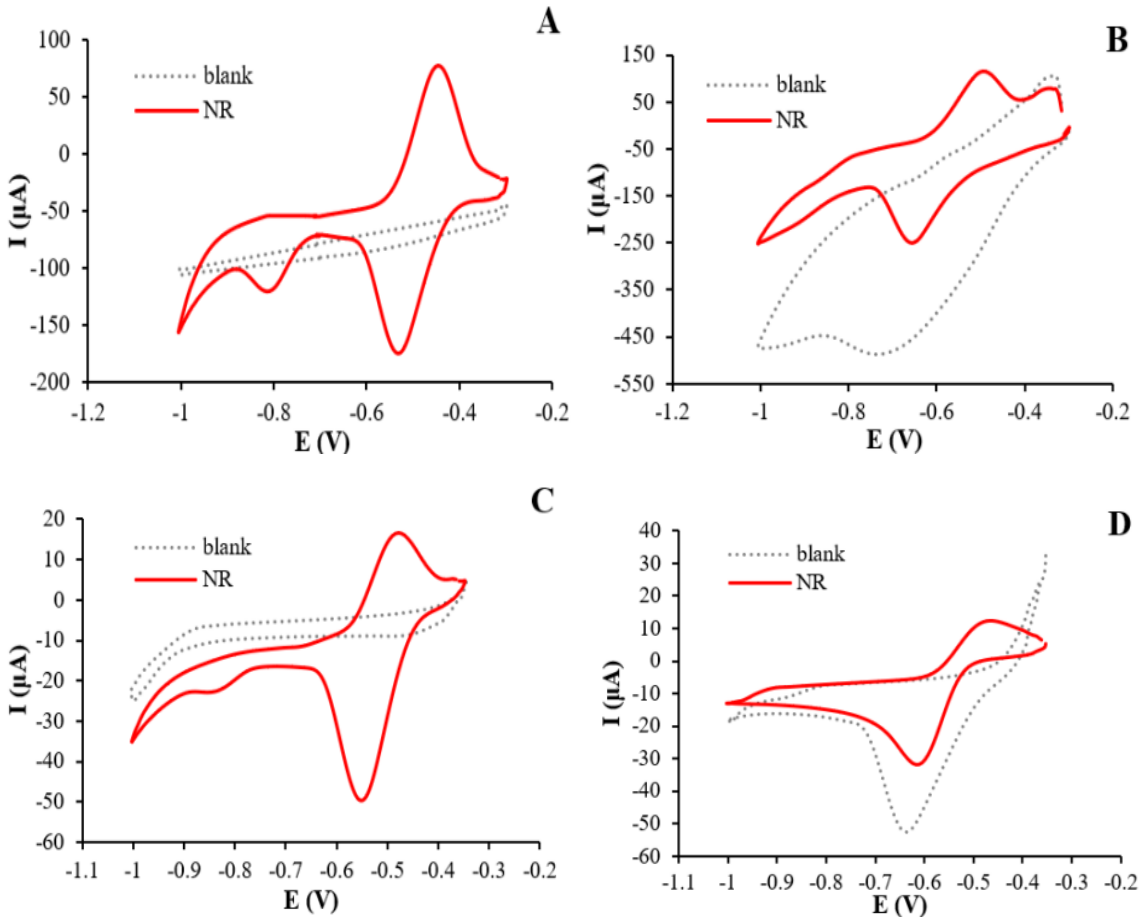


Figure 4.4 – Cyclic voltammograms registered in 0.05 M PBS + 0.1 M $NaNO_3$ with a υ = 0.1 V/s at Bi/SPCE-2 (A, B), Sb/SPCE-1 (C, D) without and with addition of 0.5 mM NR. Buffer solution pH 5 (A, C) and 7.0 (B, D**)**

The effect of pH of solution on the dissolution of bismuth and antimony films from their corresponding electrode surface in the potential range of -0.6 to -0.2 V is shown in Figure 4.3, B, C (insets). As can be visually perceived, a rise in pH of the electrolyte solution resulted in a shift of the potential for bismuth and antimony dissolution toward more negative values. The produced Bi(III) and Sb(III) ions are easily hydrolyzed at higher pHs which facilitates the oxidation process and leads to shift of the anodic potential to a more negative range with increasing pH [203, 236, 237].

Therefore, we can observe the reduction current of bismuth and antimony ions from the near-electrode layer in neutral PBS in the absence of NR (Figure 4.4, B, D,

blank). Therefore, the optimal pH value in this study was chosen as 5.5 ± 0.5. At pH 5 – 6, bismuth and antimony practically do not dissolve at a potential of about -0.3 V as demonstrated in Figure 4.3, B, C (insets).

*Evaluation of mass transfer conditions for Neutral Red at bare-SPCE, Bi/SPCEs and Sb/SPCEs*

The influence of the potential scan rate on the cathodic currents of 0.05 mM NR on bare-SPCE, Bi/SPCEs and Sb/SPCEs was investigated using CV over a range of scan rates of 0.02 – 0.50 V/s, as given in Figure 4.5, (A-C).

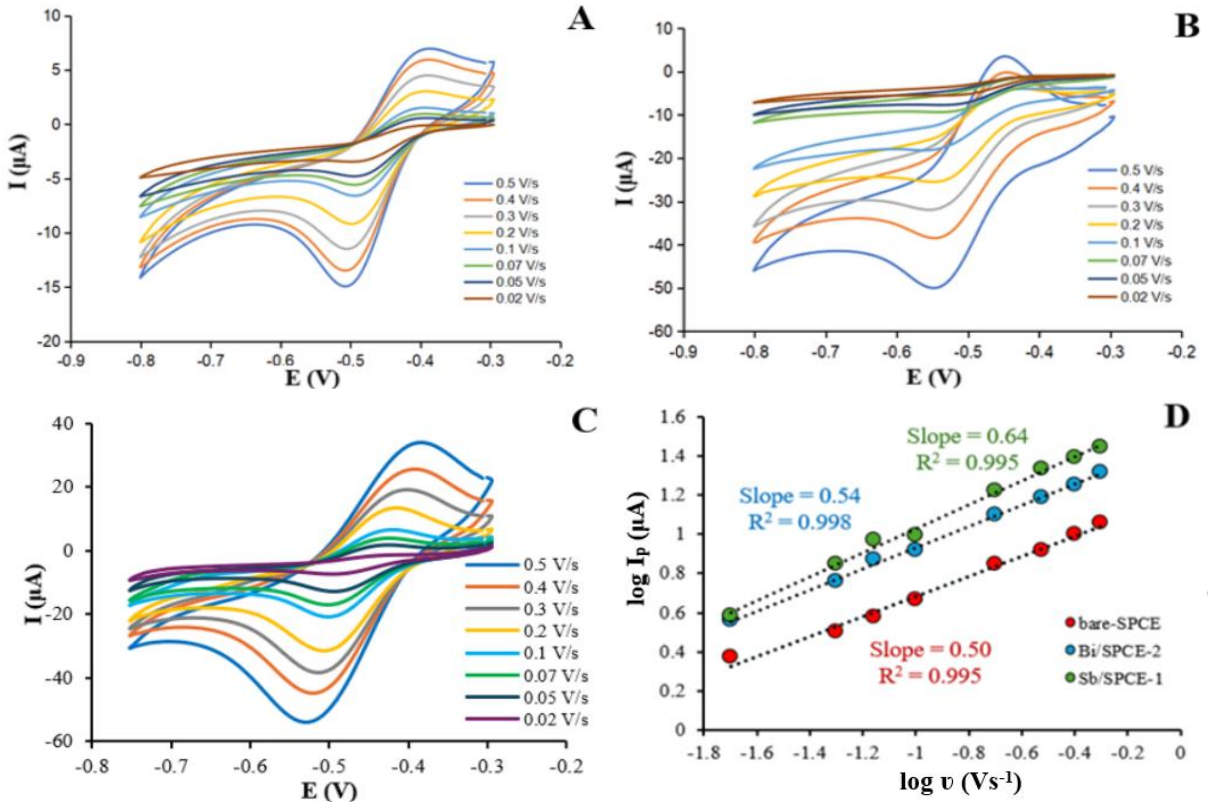


Figure 4.5 – Cyclic voltammograms of NR registered on bare-SPCE (A), Bi/SPCE-2 (B) and Sb/SPCE-1 (C) in 0.05 M PBS + 0.1 M $NaNO_3$ + 0.05 mM NR (pH 5.0) at a υ = 0.02 – 0.5 V/s. Analysis of corresponding cathodic peak currents as a function of scan rate (D, E)

It was observed that the peak heights of NR increased, and the peak potential shifted to more negative values with increasing scan rates. The peak current is linearly correlated to the square root of the potential scan rate, as follows: For bare-SPCE: $I_p$ (μA) = 16.47 $\upsilon^{½}$ $(V/s)^{½}$ – 0.20 μA, $R^2$ = 0.997 (Figure 4.5, E, red curve); for Bi/SPCE-2: $I_p$ (μA) = 29.82 $\upsilon^{½}$ $(V/s)^{½}$ – 0.81 μA, $R^2$ = 0.998 (Figure 4.5E, blue curve) and for Sb/SPCE-1: $I_p$ (μA) = 45.47 $\upsilon^{½}$ $(V/s)^{½}$ – 3.09 μA, $R^2$ = 0.987 (Figure 4.5, E, green curve). A linear relationship between the log $I_p$ vs. log υ with a slope value of 0.50 and $R^2$ = 0.995 was obtained for bare-SPCE (Figure 4.5, D, red curve). These results suggest that the electrochemical process at bare-SPCE is diffusion-controlled, as for the glassy carbon electrode [231]. Nevertheless, for Bi/SPCE-2 and Sb/SPCE-1 straight lines with slope values of 0.54, $R^2$ = 0.998 (Figure 4.5, D, blue curve) and 0.64, $R^2$ = 0.995 (Figure 4.5, D, green curve) were received, indicating diffusion processes accompanied by adsorption [238]. From the slopes, it can be noted that Sb/SPCE is more susceptible to NR adsorption than Bi/SPCE-2.

*Electrochemical Characterization and Electrochemical Impedance Spectroscopy Study*

Cyclic voltammetry and EIS, employing NR as a redox probe, were used to study the electrochemical characteristics of bare-SPCE and Bi/SPCEs. CVs and Nyquist plots obtained for these electrodes are displayed in Figures 4.6.

Every Nyquist curve was recorded at a working potential, which was chosen based on the corresponding CV voltammogram. As the electrochemical process at bare and bismuth-modified SPCEs is mainly controlled by diffusion, the electroactive surface areas of the investigated electrodes were calculated based on the CV data (Figure 4.6, A) using the Randles-Sevcik equation (4.1) for reversible systems:

$$I_p = (\pm\ 2.69 \times 10^5) \cdot n^{3/2} \cdot A \cdot D^{1/2} \cdot C \cdot v^{1/2}, \qquad (4.1)$$

where $A$ – electroactive area ($cm^2$); $I_p$ – the anodic or cathodic peak current; D – the diffusion coefficient of the electroactive species in solution (2.28 x $10^{-6}$ $cm^2/s$ for NR) [227]; $\upsilon$ – the potential scan rate (0.1 V/s); C – the concentration of the redox system in the background electrolyte (0.05 M); $n$ – the number of electrons involved in the redox process ($n$ = 1). The values of the cathodic currents were used for $A$ calculation.

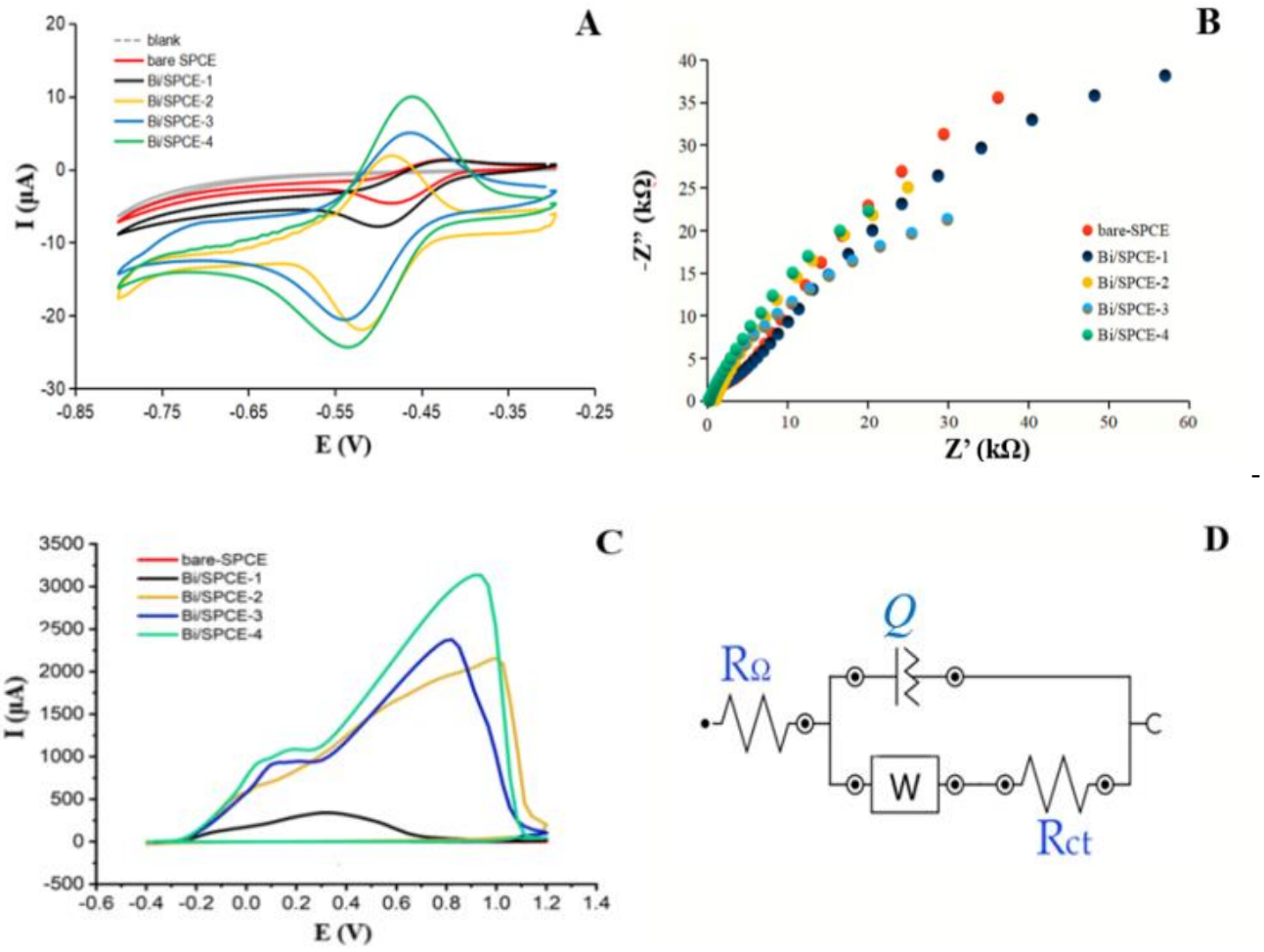


Figure 4.6 – Cyclic voltammograms (A), Nyquist curves (B), Bismuth oxidation voltammograms (C), with (A, B) and without (C) 0.05 mM NR recorded in 0.05 M PBS + 0.1 M $NaNO_3$ (pH 5.0) at $\upsilon$ = 0.10 V/s on bare-SPCE and Bi/SPCEs; Randles equivalent electrical circuit (D) [239]

Results of processing the CV and EIS data received are summarized in Table 4.3. For all electrodes (Table 4.3), the potential difference between the oxidation and

reduction peaks for NR does not exceed 0.08 V and reduction/oxidation peak currents ratio – 2.0. These observations indicate a quasi-reversible behavior of NR at the interface of bare and modified SPCEs. As for Bi/SPCEs-2, 3, 4, the $I_{pc}/I_{pa}$ ratio is closer to 1. Considering this fact and the observed peak separation of 0.03 – 0.08 V, which is characteristic of a one-electron transfer process, allows us to assume the near-reversible nature for the processes at these electrodes.

The modification of SPCEs with bismuth significantly increased the electroactive surface area of Bi/SPCEs by a factor of approximately 1.4 – 3.7 in comparison to the bare-SPCE. Bi/SPCE-4 exhibited the highest *A* value in comparison to the other electrodes, as expected from the SEM image of bismuth film (Figure 4.1, E). In this case, the film consists of many fine and well-dispersed bismuth crystals formed during the vertical growth of particles. Figure 4.6, C compares the cyclic voltammetry curves of bismuth dissolution registered from -0.4 V to +1.2 V at Bi/SPCEs in 0.05 M PBS + 0.1 M $NaNO_3$ solution at 0.1 V/s. In comparison to Bi/SPCE-1, Bi/SPCE-2, 3, 4 showed a higher integrated area.

Table 4.3 – Electrochemical characterization of electrodes studied in 0.05 M + 0.1 M $NaNO_3$ + 0.05 mM NR (pH 5.5)

| Electrode | $I_{pc}$, μA | $I_{pa}$, μA | $I_{pc}$ / $I_{pa}$ | ΔE, V | *A*, $cm^2$ | $C_s$, $mF/cm^2$ | $R_s$, Ω | $R_{ct}$, Ω | W, μS | *Q*, μS | n | $Bi_{cov}$, % |
|---|---|---|---|---|---|---|---|---|---|---|---|---|
| bare-SPCE | -4.3 | 2.4 | 1.8 | 0.06 | 0.67 | 0.2 | 310 | 3900 | 16.8 | 2.59 | 0.75 | - |
| Bi/SPCE-1 | -6.1 | 3.2 | 1.9 | 0.08 | 0.95 | 14.0 | 334 | 3300 | 18.7 | 2.13 | 0.78 | 10 |
| Bi/SPCE-2 | -12.2 | 9.5 | 1.3 | 0.03 | 1.90 | 104.4 | 253 | 80 | 25.3 | 2.17 | 0.95 | 49 |
| Bi/SPCE-3 | -11.9 | 9.4 | 1.3 | 0.08 | 1.86 | 100.0 | 268 | 8 | 23.9 | 2.58 | 0.94 | 73 |
| Bi/SPCE-4 | -15.9 | 15.7 | 1.0 | 0.07 | 2.48 | 131.3 | 267 | 70 | 27.0 | 19.6 | 0.81 | 52 |

*Note* – ΔE – potential peak separation; *A* – electroactive area; $C_s$ – specific areal capacitance; $R_s$ – solution resistance; $R_{ct}$ – charge transfer resistance; W – Warburg diffusion element; *Q* – constant phase element; n – exponent determining the nature of the frequency dependence of impedance; $Bi_{cov}$ – degree of substrate coverage by bismuth

The specific areal capacitance ($C_s$) values for Bi/SPCEs were calculated from the CV curves using equation 4.2 [241].

$$Cs = \frac{\int I(V)dV}{Ag\upsilon\Delta V} \quad (4.2)$$

where ∫ I(V)dV – the integrated area of the CV curve; $A_g$ – the electrode's geometric area ($cm^2$); υ – scan rate (V/s); ΔV – the potential window (V).

As can be seen from Table 4.3, $C_s$ – values for Bi/SPCEs correlate well with their electroactive/specific electroactive surface area. The obtained result is confirmed by the conclusions of several studies that increase in electrochemical capacity result in enhanced specific surface area [240, 241]. Quite good convergence of the results of assessing the electroactive area of Bi/SPCEs with independent methods confirms the effectiveness of NR in the evaluation of electrochemical performance of bismuth-modified electrodes.

As conductive material, SPCE covered by a metal film is under investigation, the most likely model to describe the surface phenomena in the bismuth-NR system, in our opinion, is the Randles EEC, proposed in [215] for copper-bismuth-film in-situ formed on the glassy carbon electrode surface (Figure 4.6, D). It describes a mixed kinetic- and diffusion-controlled process that corresponds to the diffusion process, accompanied by adsorption, in the system under study.

Randles EEC consists of the uncompensated resistance with a parallel combination of charge transfer resistance, a constant phase element and diffusion, which is represented by the Warburg diffusion element. A majority of the $R_Ω$ is due to the solution resistance. The $R_{ct}$ represents the difficulty of electron transfer of NR redox probe between the solution and the electrode, thus giving information on the electrode surface. The diffusion resembles the mass transfer of the species from or to the electrode's surface during the EIS measurements. Element *Q* models non-ideal capacitor, which probably arises for at least two reasons: first, due to non-uniformity of the interface electrode-electrolyte. The bismuth film surface has a complex porous structure,

and in the case of bare-SPCE, fractal particles, presumably of carbon nanomaterial, protrude above the surface of the bulk of the carbon ink (Figure 4.1, B, bismuth uncoated surface). It should be noted that the greatest vertical growth of bismuth particles is observed on Bi/SPCE-4 (Figure 4.1, E). This is probably why the electroactive surface area, specific capacitance and *Q* values for this film are the highest (Table 4.3). Second, due to the looseness of the top layer of the electrode, diffusion processes can probably be distorted. The calculated exponential factor lies in the range 1> n >0.5 (Table 4.3), which according to [242], can confirm this assumption. It is not excluded that the distortion of diffusion may be associated with the adsorption of NR on the surface of bare SPCE and Bi/SPCEs under conditions of mixed mass transfer kinetics.

The highest $R_{ct}$ values were obtained at bare-SPCE and Bi/SPCE-1 with a low degree (10%) of substrate coverage by bismuth as shown in Table 4.3. The lowest $R_{ct}$ value (8 Ω) was measured at Bi/SPCE-3 with the highest degree (73%) of $Bi_{cov}$. This result can be explained by the very good electrical conductivity of metallic bismuth. In this case, the contribution of the substrate surface not covered with metal to the total $R_{ct}$ value is minimal. The data obtained are consistent with the well-known fact that EIS can provide information about surface coverage with metal films [161].

In a similar way to Bi/SPCEs, CV and EIS measurements, with NR as a redox probe, were used to study the electrochemical characteristics of bare-SPCE and Sb/SPCEs. The CVs and Nyquist plots acquired for these electrodes are demonstrated in Figure 4.7. Each Nyquist curve was recorded at a working potential, which was chosen based on the corresponding CV voltammogram.

As mentioned above in section 4.2, the electrochemical process of NR at bare- and antimony-modified SPCEs is mainly controlled by diffusion, subsequently, the electroactive surface areas of the investigated electrodes were calculated based on the CV data (Figure 4.7, A) using the Randles-Ševćik equation (4.1) for reversible systems.

The values of the cathodic currents (Figure 4.7, A) were used for *A* calculation. The data obtained from the CVs are presented in Table 4.4.

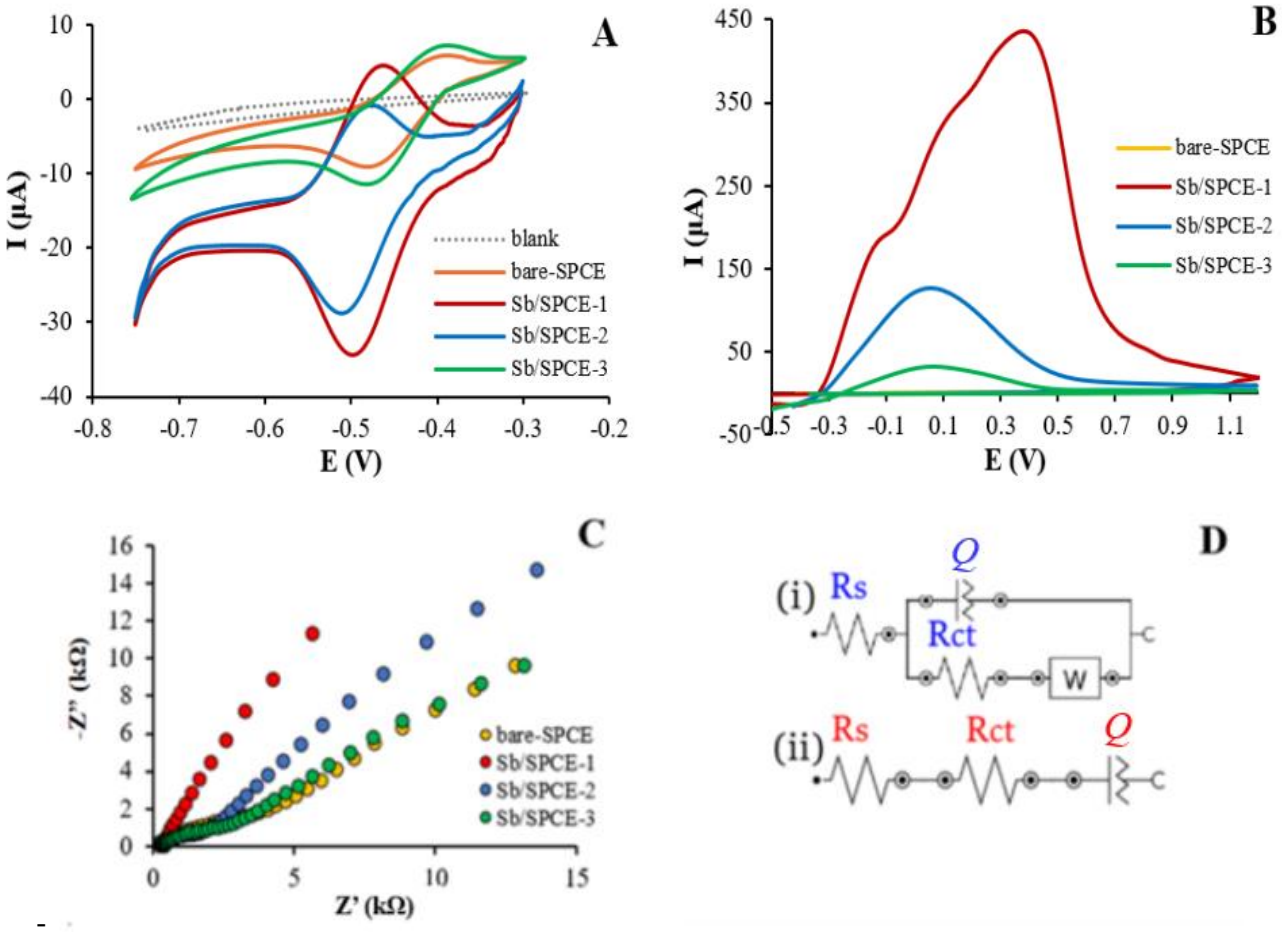


Figure 4.7 – Cyclic voltammograms (A, B), Nyquist curves (C), recorded in 0.05 M PBS + 0.1 M $NaNO_3$ (pH 5.5) without (B) and with addition of 0.05 mM NR on bare-SPCE and Sb/SPCEs (A and C). Randles equivalent electrical circuits for bare-SPCE, Sb/SPCE-2 and Sb/SPCE-3 (D, i). Modernized model of an ideally polarizable electrode with a distributed double-layer capacitance for Sb/SPCE-1 (D, ii). υ: 0.30 (A) and 0.1 V/s (B) [243]

For all electrodes (Table 4.4), the potential difference between the peaks for the oxidation/reduction current does not exceed 0.08 V and $I_{pc}/I_{pa}$ is close to 2.5. This fact indicates quasi-reversible behavior of NR at the interface of bare- and antimony-

modified SPCEs. As for Sb/SPCEs-1, 2 $I_{pc}/I_{pa}$ = 1.6 and peak separation of 0.04 – 0.05 V for a one-electron transfer, point to the near-reversible nature of the processes.

The modification of SPCEs with antimony increased the *A* of Sb/SPCEs by a factor of 2.4 and 1.7 than the bare-SPCE for Sb/SPCE-1 and Sb/SPCE-2, respectively. Sb/SPCE-1 exhibited the highest *A* value in comparison to the other electrodes, as expected from the SEM image of an antimony film (Figure 4.2, B). As for Sb/SPCE-3, practically, there is no profit in *A* value in comparison to bare-SPCE because the surface of the substrate is almost entirely exposed.

Figure 4.7, B compares the cyclic voltammetry curves of antimony dissolution registered from -0.4 V to +1.2 V at Sb/SPCEs in 0.05 M PBS + 0.1 M $NaNO_3$ solution at a scan rate of 0.1 V/s. Sb/SPCE-1 showed a higher integrated area. The specific areal capacitance values for Sb/SPCEs were calculated from the CV curves using equation (4.2) [241].

As can be seen from Table 4.4, $C_s$ – values for Sb/SPCEs correlate well with their electroactive/specific electroactive surface area. Quite good convergence of the results of assessing the *A* of Sb/SPCEs using Randles-Ševćik equation with independent method confirms the effectiveness of NR in the evaluation of electrochemical performance of antimony-modified electrodes.

Table 4.4 – Electrochemical characterization of electrodes studied in 0.05 M PBS + 0.1 M $NaNO_3$ + 0.05 mM NR (pH 5.0)

| Electrode | $I_{pc}$, μA | $I_{pa}$, μA | $I_{pc}$ / $I_{pa}$ | ΔE, V | *A*, $cm^2$ | $C_s$, $mF/cm^2$ | $R_s$, Ω | $R_{ct}$, Ω | W, μS | *Q*, μS | n | $Sb_{cov}$, % |
|---|---|---|---|---|---|---|---|---|---|---|---|---|
| bare-SPCE | -7.9 | 3.1 | 2.5 | 0.08 | 0.71 | 0.1 | 285 | 4380 | 85.9 | 5.68 | 0.6 | - |
| Sb/SPCE-1 | -18.7 | 12.1 | 1.6 | 0.04 | 1.68 | 17.8 | 289 | 6 | - | 126 | 0.8 | 12 |
| Sb/SPCE-2 | -13.1 | 8.0 | 1.6 | 0.05 | 1.18 | 4.3 | 261 | 1160 | 75.0 | 16.6 | 0.7 | 4 |
| Sb/SPCE-3 | -8.3 | 3.5 | 2.4 | 0.07 | 0.74 | 1.1 | 309 | 2780 | 81.8 | 11.3 | 0.6 | 1 |

*Note* – $Sb_{cov}$ – degree of substrate coverage by antimony

According to research [64], the most probable model for describing surface phenomena in the metal-NR system is the generalized Randles EEC (Figure 4.7, D, i). It describes a mixed kinetic- and diffusion-controlled process that corresponds to the diffusion process, accompanied by adsorption, in the system under study (Sb/SPCE-2, 3 – NR). EEC consists of $R_\Omega$ with a parallel combination of the $R_{ct}$, *Q* and W. Majority of the $R_\Omega$ is due to the solution resistance. The $R_{ct}$ represents the difficulty of electron transfer of NR redox probe between the solution and the electrode, thus giving information on the electrode surface. *Q* models non-ideal capacitance. The diffusion resembles the mass transfer of the species from or to the electrode's surface during the EIS measurements. The results of impedance spectra processing with generalized Randles EEC for bare-SPCE, Sb/SPCE-2 and Sb/SPCE-3 are calculated and presented in Table 4.4.

To describe the Nyquist diagrams obtained on Sb/SPCE-1, we used a modernized circuit of an ideally polarizable electrode with a distributed double-layer capacitance (Figure 4.7, D, ii) [243]. In the system under study, there is also uncompensated resistance with a series combination of charge transfer resistance. Due to the heterogeneity of the electroactive surface of the electrode, as well as considering the diffusion part of the double electrical layer, the simplest way to model these changes relative to an ideally polarized electrode is to represent double layer capacitance ($C_{dl}$) as a constant-phase element of the capacitive type. Thus, as in the case of the generalized Randles equivalent electrical circuit, the element *Q* models a non-ideal capacitor.

According to the SEM data (Figure 4.2, B), Sb/SPCE-1 surface differs significantly from other electrodes in the largest substrate surface area coated with metallic antimony in the form of evenly distributed finely dispersed antimony particles. This is probably why the electroactive surface area, specific capacitance and *Q* values for this film are the highest (Table 4.4). The calculated exponential factor for Sb/SPCE-1, n = 0.8 (Table 4.4), corresponds to the values given in Stoynov et al. [242].

## Conclusions to chapter 4

The crucial role of plating conditions (metal ions concentration, potential, additives) in shaping the morphology of bismuth and antimony on SPCEs is assessed on specific examples on the same carbon-containing substrate. These factors influenced “green” metals films size, shape and surface coverage, ultimately impacting their performance. Sb/SPCEs generally form smaller particles with lower coverage than Bi/SPCEs.

Neutral Red showed its suitability to evaluate the electrochemical performance of screen-printed carbon-containing electrodes modified with bismuth or antimony under different deposition conditions. EIS with NR as a redox probe allows to assess the degree of substrate coverage by metal. CV experiments showed an increase in the *A* of Bi/SPCEs and Sb/SPCEs compared to the bare-SPCE, depending on surface morphology. The calculated *A* of the electrodes obtained under various conditions of deposition of metal films largely corresponds to micrographs of the Bi/SPCEs and Sb/SPCEs surface. The obtained SEM, CV and EIS data are in good agreement.

# CHAPTER 5 ELECTROANALYTICAL PERFORMANCE OF "GREEN" METALS-MODIFIED SCREEN-PRINTED CARBON-CONTAINING ELECTRODES

## 5.1 Electroanalytical performance of the bismuth-modified screen-printed carbon-containing electrodes towards nickel (II) and formaldehyde

The electroanalytical performance of the SPCEs modified with the "green" metals was assessed using model analytes with known protocols for their determinations. Ni(II) ions and FA were used as model analytes to determine the electroanalytical performance of the SPCEs modified with bismuth under different electrodeposition conditions (Table 4.1). Ni(II) ions were determined by adsorptive stripping voltammetry using dimethylglyoxime as a complexing agent [171-173]. FA was completely converted to an electrochemically active derivative FAH in the presence of HRZ. The area of FAH reduction current was used as the FA response [244].

A comparison of the characteristics of Ni(II) and FA calibration curves was carried out with three separately prepared Bi/SPCEs for every type of bismuth film. The results obtained and corresponding DP voltammograms of Ni(II) and FA are shown in Tables 5.1–5.2 and Figures 5.1–5.2, respectively.

As can be seen from Figure 5.1, for Bi/SPCE-2 (B), Bi/SPCE-3 (C) and Bi/SPCE-4 (D) the area of reduction current for Ni(II)-dimethylglyoxymate (response) linearly depends on its concentration in the solution in the range of 5 – 20 μg/L. The $R^2$ value is closer to the value of 1 (Table 5.1). Recoveries for 5 μg/L Ni(II) are about 100% on Bi/SPCE-2 (B), Bi/SPCE-3 (C) and Bi/SPCE-4 (D) (Table 5.1).

The sensitivity of Bi/SPCEs-2, 3, 4 towards Ni(II) is characterized by good reproducibility for three separately prepared ones for every film (RSD of 1.6% for Bi/SPCE-2, 3.5% for Bi/SPCE-3 and 7.7% for Bi/SPCE-4).

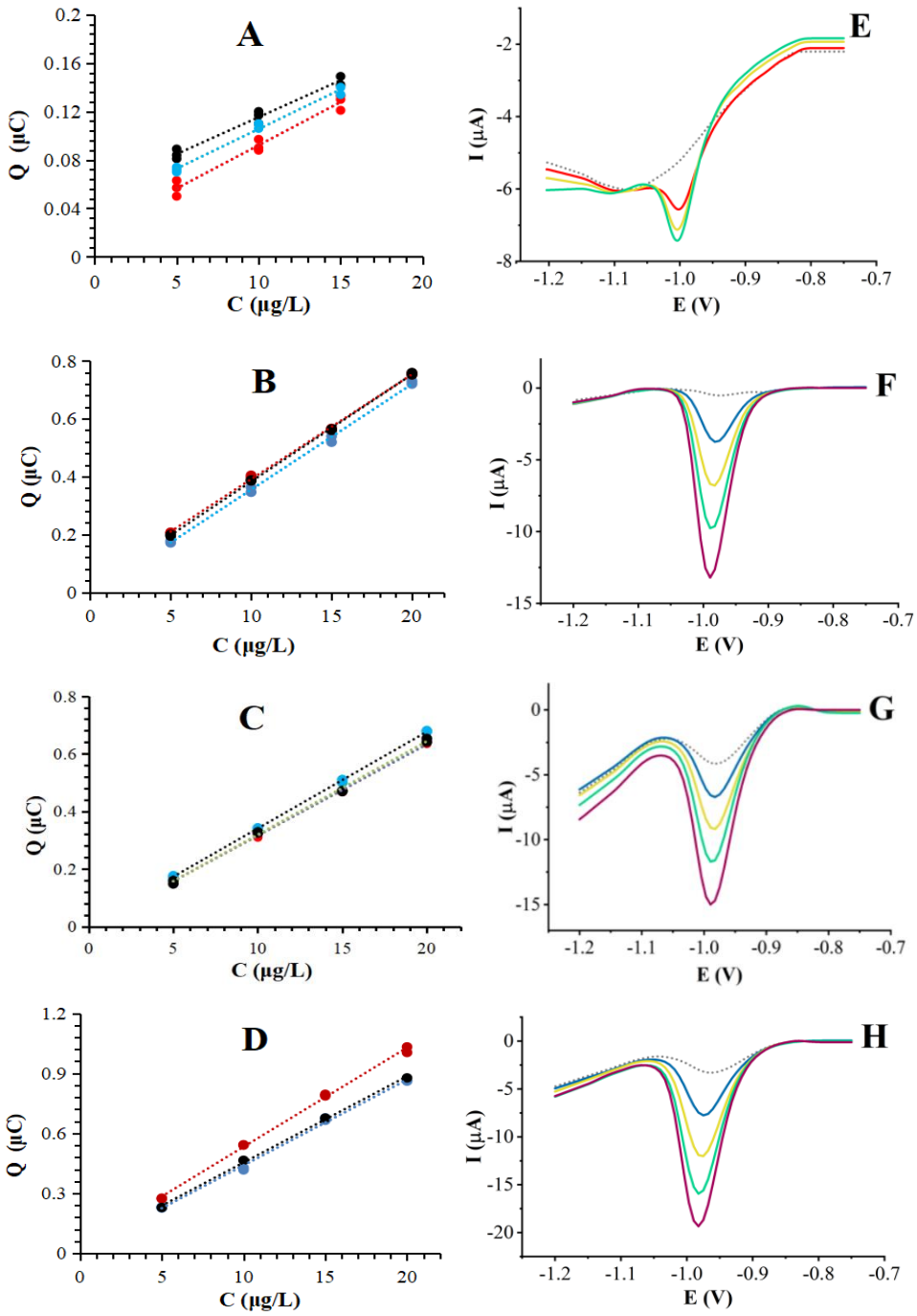


Figure 5.1 – The calibration plots of Ni(II) determination over a concentration range of 0 to 15 μg/L at Bi/SPCE-1 (A) and 0 to 20 μg/L at Bi/SPCE-2 (B), Bi/SPCE-3 (C) and Bi/SPCE-4 (D) with a step of 5 μg/L and corresponding DP voltammograms of Ni(II) (E–H) registered in ammonia buffer (pH 9.5 ± 0.5) + 0.25 mM DMG. DP voltammogram parameters: pulse step 0.006 V, pulse amplitude 0.05 V, $\upsilon$ = 0.06 V/s. Analysis conditions: $E_{acc}$ = -0.75 V, $t_{acc}$ = 30 s

Table 5.1 – Comparison of electroanalytical performance of SPCEs modified with bismuth under different plating conditions towards Ni(II) ions with the "Spiked-recovery method" in ammonia buffer (pH 9.5 ± 0.5) + 0.25 mM DMG. Analysis conditions: $E_{acc}$ = -0.75 V, $t_{acc}$ = 30 s (n = 3, P = 0.95)

| Electrode | Linear range, µg/L | Regression equation Q (µC) = kC (µg/L) + b (µC) | $R^2$ | R, % for 5µg/L of Ni(II) | RSD, % |
|---|---|---|---|---|---|
| Bi/SPCE-1 | 5 – 15 | Q = 0.007 C + 0.022 | 0.977 | 217 ± 107 | 8.7 |
| | | Q = 0.006 C + 0.052 | 0.986 | | |
| | | Q = 0.007 C + 0.033 | 0.989 | | |
| Bi/SPCE-2 | 5 – 20 | Q = 0.037 C + 0.012 | 0.999 | 101 ± 6 | 2.4 |
| | | Q = 0.036 C + 0.028 | 0.999 | | |
| | | Q = 0.036 C – 0.011 | 0.998 | | |
| Bi/SPCE-3 | 5 – 20 | Q = 0.032 C – 0.005 | 0.998 | 101 ± 14 | 5.6 |
| | | Q = 0.032 C – 0.001 | 0.999 | | |
| | | Q = 0.034 C + 0.005 | 0.999 | | |
| Bi/SPCE-4 | 5 – 20 | Q = 0.049 C + 0.037 | 0.998 | 101 ± 9 | 3.7 |
| | | Q = 0.043 C + 0.012 | 0.997 | | |
| | | Q = 0.043 C + 0.023 | 0.999 | | |

In the case of using Bi/SPCE-1 (Figure 5.1, A), the linearity of the calibration plot narrows and the recovery of 217 ± 107% indicates a significant systematic overstatement of the analysis results due to the absence of a direct proportional dependence of the response on the concentration of Ni(II) ions in the solution. The electrode shows the lowest sensitivity towards Ni(II) ions, with a calibration plot slope about 4 – 7 times less compared to the other Bi/SPCEs (Table 5.1). In addition, the shape of the curves is asymmetrical (Figure 5.1, E) and inappropriate for use as a response. This electrode is unsuitable for analytical purposes. Obviously, this may be explained by the very small amount of bismuth on the Bi/SPCE-1 surface (Figure 4.1, B).

Similar experiments were performed for FA in 0.04 M PBS + 0.09 M HRZ (pH 5.2 ± 0.1) with successively increased concentrations of FA in the range of 0.2 – 1.0 mg/L at a step of 0.2 mg/L. The DP voltammograms obtained for FA on Bi/SPCE-2 (B), Bi/SPCE-3 (C) and Bi/SPCE-4 (D) showed good linear relationship between the added FA concentrations and the response, as shown in Figure 5.2, (B–D). The $R^2$ value is closer to the value of 1 (Table 5.2).

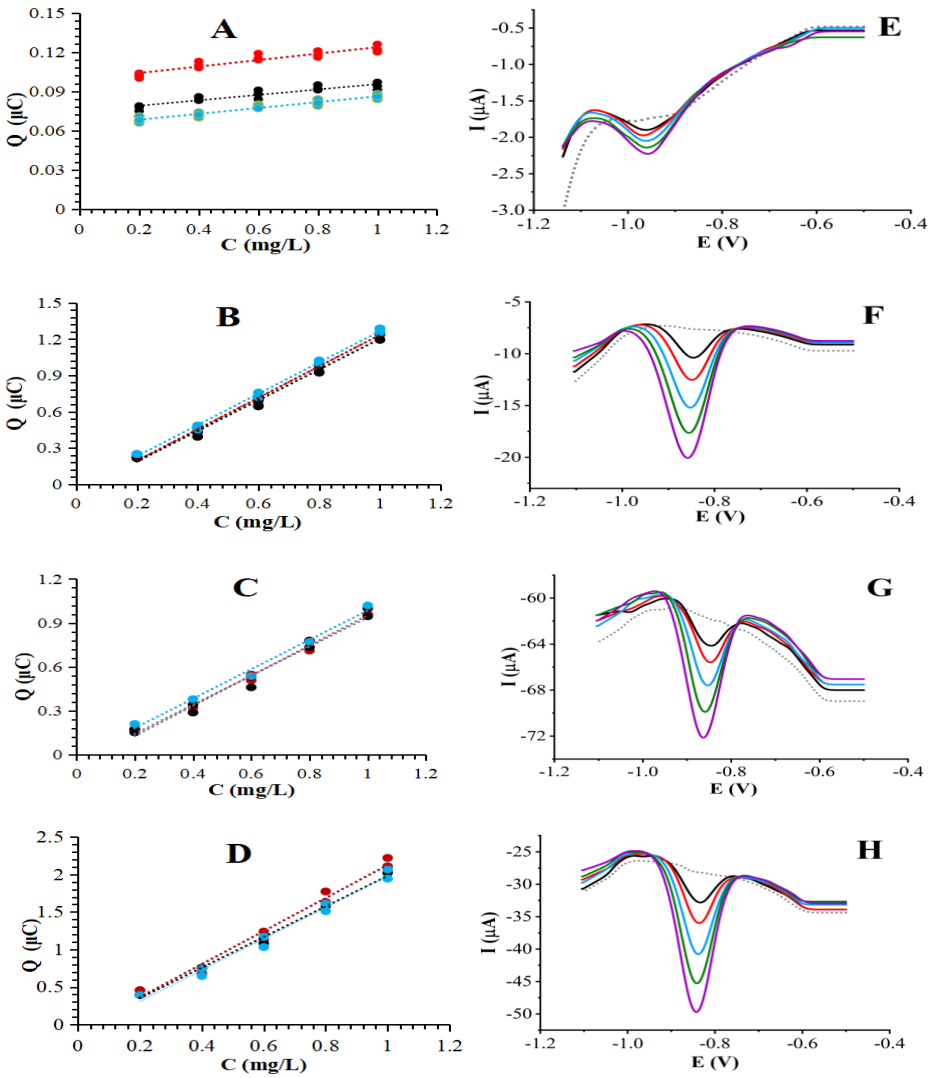


Figure 5.2 – The calibration plots of FA determination over a concentration range of 0 to 1.0 mg/L with a step of 0.2 mg/L at Bi/SPCE-1 (A), Bi/SPCE-2 (B), Bi/SPCE-3 (C) and Bi/SPCE-4 (D) and corresponding DP voltammograms of FA (E–H) registered in 0.04 M PBS + 0.09 M HRZ (pH 5.2 ± 0.1). DP voltammogram parameters: pulse amplitude 0.05 V, pulse step 0.002 V, $\upsilon$ = 0.02 V/s. Analysis conditions: $E_{acc}$ = -0.5 V, $t_{acc}$ = 5 s

Table 5.2 – Comparison of electroanalytical performance of Bi/SPCEs towards FA received under different plating conditions with "Spiked-recovery method" in solution of 0.04 M PBS + 0.09 M HRZ (pH 5.2 ± 0.1) + 0.2 – 1 mg/L FA with 0.2 mg/L step (n = 3, P = 0.95). Analysis conditions: $E_{acc}$ = -0.5 V, $t_{acc}$ = 5 s

| Electrode | Regression equation Q (μC) = kC (μg/L) + b (μC) | $R^2$ | R, % for 0.2 mg/L of FA | RSD, % |
|---|---|---|---|---|
| Bi/SPCE-1 | Q = 0.026 C + 0.098 | 0.836 | 1760 ± 530 | 12.1 |
| | Q = 0.022 C + 0.074 | 0.821 | | |
| | Q = 0.022 C + 0.064 | 0.883 | | |
| Bi/SPCE-2 | Q = 1.30 C – 0.066 | 0.991 | 98 ± 14 | 5.7 |
| | Q = 1.29 C – 0.028 | 0.997 | | |
| | Q = 1.27 C – 0.068 | 0.992 | | |
| Bi/SPCE-3 | Q = 1.04 C – 0.073 | 0.983 | 93 ± 5 | 2.1 |
| | Q = 1.03 C – 0.078 | 0.983 | | |
| | Q = 1.01 C – 0.019 | 0.989 | | |
| Bi/SPCE-4 | Q = 2.20 C – 0.074 | 0.983 | 98 ± 9 | 3.9 |
| | Q = 2.04 C – 0.056 | 0.994 | | |
| | Q = 2.03 C – 0.064 | 0.985 | | |

Recoveries for 0.2 mg/L FA (Table 5.2) are approaching 100% on Bi/SPCE-2 (B), Bi/SPCE-3 (C) and Bi/SPCE-4 (D). The sensitivity of Bi/SPCEs-2, 3, 4 to FA has quite an acceptable reproducibility for three separately prepared ones for every film (RSD of 1.2% for Bi/SPCE-2, 1.6% for Bi/SPCE-3 and 4.6% for Bi/SPCE-4). As for Bi/SPCE-1, the $R^2$ value of the calibration plot is significantly reduced (Table 5.2). It demonstrates the lowest sensitivity towards FA (Table 5.2), an asymmetrical response shape (Figure 5.2, E) and an overestimated recovery value of 1760% (Table 5.2) for 0.2 mg/L FA due to lack of a direct proportional dependence of the response on the concentration of FA in the solution. These characteristics indicate the unsuitability of Bi/SPCE-1 for analytical purposes.

Data for comparing the surface characteristics of Bi/SPCEs with their sensitivity towards Ni(II) and FA are shown in Table 5.3. The conditions for obtaining experimental

data are presented in the corresponding sections. It is evident that Bi/SPCE-1 with low bismuth coverage (10%) (Figure 4.1, B) yields the worst electroanalytical results, including the lowest sensitivity to Ni(II) ions and FA and differs the lowest value of the roughness factor (RF, equal to the ratio of the electroactive surface area to the geometric one (Table 5.3). The increase in RF for Bi/SPCE-1 is only 30% compared to bare-SPCE, while for the rest of Bi/SPCEs, it increases by 3 – 4 times. The sensitivity of Bi/SPCE-1 to Ni(II) is reduced by about 5 – 6 times compared to other electrodes. The sensitivity of Bi/SPCE-1 to FA is also reduced by approximately 4 – 5 times compared to Bi/SPCE-2, Bi/SPCE-3 and by an order of magnitude compared to Bi/SPCE-4 (Table 5.3). The formed bismuth structures with low coverage of substrate surface possessed low adsorptive properties since adsorption of nickel dimethylglyoximate occurs preferentially on the metal rather than on the carbon containing substrate.

In contrast, Bi/SPCE-4 is characterized by the highest sensitivity to both Ni(II) ions and FA (Table 5.3) as for NR reduction current (Table 4.3) and therefore the highest RF. This feature can be explained by the fact that the electrode surface is half covered with several tiny, well-dispersed bismuth crystals (Figure 4.1, E). Obviously, in this case, an optimal combination of two factors is achieved: the degree of dispersion of bismuth particles and the area of coverage of the substrate surface with metal.

Table 5.3 – Comparison of morphological, electrochemical and electroanalytical characterization of Bi/SPCEs (n = 3, P = 0.95)

| Electrode | Particle size, μm | $Bi_{cov}$, % | RF | Sensitivity towards Ni(II), μC·L/μg | Sensitivity towards FA, μC·L/mg |
|---|---|---|---|---|---|
| bare-SPCE | – | – | 6.4 ± 0.6 | – | – |
| Bi/SPCE-1 | 10 ± 2 | 10 | 8.2 ± 2.8 | 0.007 ± 0.001 | 0.023 ± 0.007 |
| Bi/SPCE-2 | 374 ± 38 | 49 | 18.6 ± 1.0 | 0.036 ± 0.001 | 1.29 ± 0.04 |
| Bi/SPCE-3 | 1000 ± 192 | 73 | 17.4 ± 3.1 | 0.033 ± 0.003 | 1.02 ± 0.04 |
| Bi/SPCE-4 | 95 ± 20 | 52 | 25.4 ± 1.5 | 0.045 ± 0.009 | 2.09 ± 0.24 |

The sensitivity of Bi/SPCE-1 to Ni(II) is reduced by about 5 – 6 times compared to other electrodes. The sensitivity of Bi/SPCE-1 to FA is also reduced by approximately 4 – 5 times compared to Bi/SPCE-2, Bi/SPCE-3 and by an order of magnitude compared to Bi/SPCE-4 (Table 5.3).

Comparison of average values of RF and sensitivity to both model analytes for Bi/SPCEs with two-tailed Pearson's criterion showed a high degree of correlation between their electrochemical and electroanalytical characteristics, with $R^2$ values of 0.981 for Ni(II) and 0.998 for FA (n = 4, P = 0.95, $R_{crit}$ = 0.900) [245]. This corresponds to the general conclusion, based on the accumulated enormous experimental experience, that it is desirable to obtain a highly developed bismuth surface for satisfactory analytical performance [161].

## 5.2 Electroanalytical performance of the antimony-modified screen-printed carbon-containing electrodes towards nickel (II)

Since FAH is not electroactive on the surface of Sb/SPCE (Figure 3.1, C), Ni(II) ions were used as model analyte to assess the electroanalytical performance of the SPCEs modified with antimony under different plating conditions (Table 4.2). The protocols of Ni(II) ions determination by cathodic adsorptive stripping voltammetry using DMG as a complexing agent at antimony-modified electrodes are described in [153, 192, 193].

Characteristics of Ni(II) calibration curves for every type of Sb/SPCEs and corresponding DP voltammograms of Ni(II) ions are shown in Figure 5.3 and Table 5.4. As can be seen from Table 5.4, for Sb/SPCE-1 the area of reduction current for Ni(II)-DMG (the response) linearly depends on its concentration in the solution in the range of 5 – 50 μg/L, the $R^2$ value is closer to the value of 1 and recovery for 5 μg/L Ni(II) is about 100%. The LOD calculated from the regression equation Q (μC) = (0.0161 ± 0.0002) C (μg/L) – (0.0059 ± 0.0026) (μC) ($R^2$ = 0.9981) for the calibration curve

(Figure 5.3, A) in the range of 5 – 25 µg/L Ni(II) is 0.5 µg/L Ni(II) ions. It is lower than those reported in [153] as 0.9 µg/L for commercial SPCE provided by DropSens (Spain) with ex-situ preplating antimony film under identical conditions.

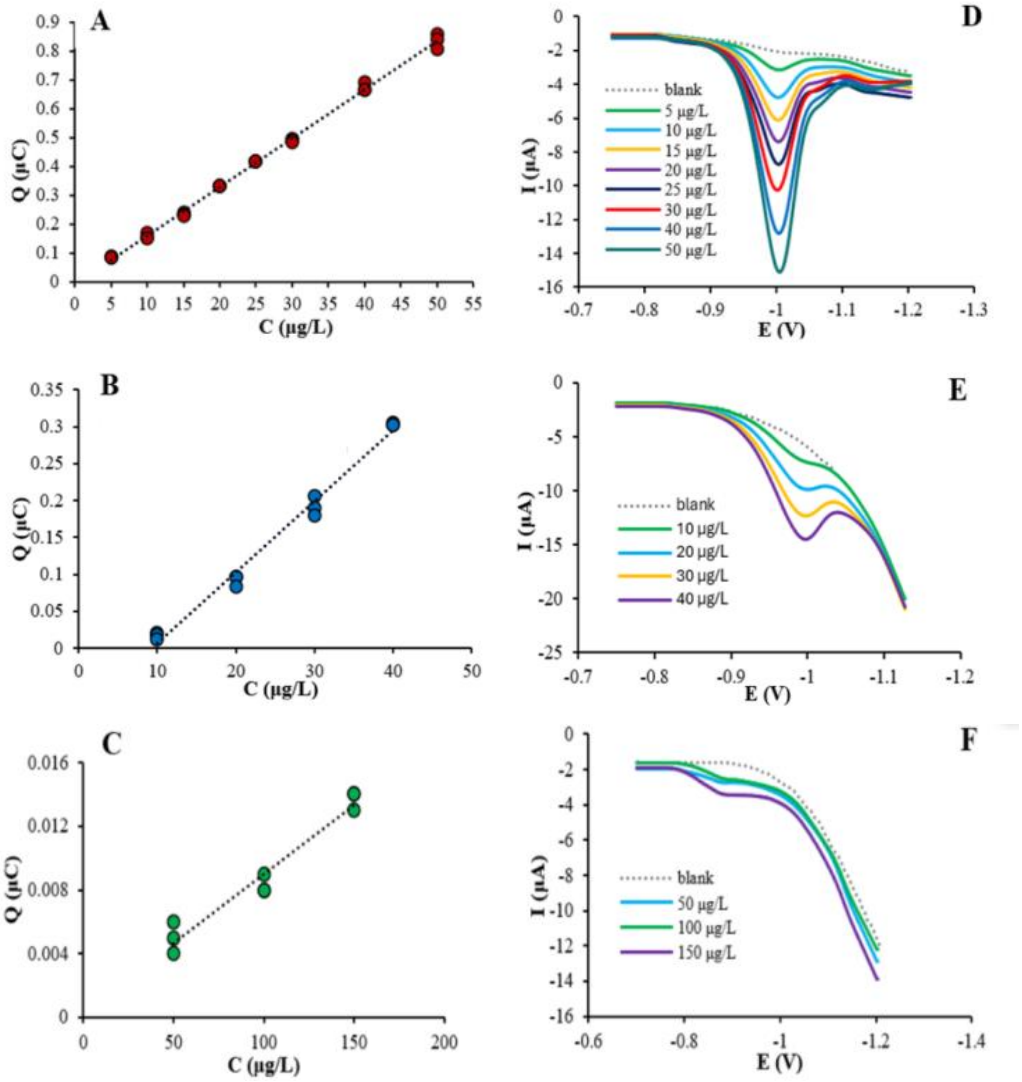


Figure 5.3 – The calibration plots of Ni(II) determination over a concentration range of 0 to 50 µg/L at Sb/SPCE-1 with a step of 5 µg/L (A), 0 to 40 µg/L at –Sb/SPCE-2 with a step of 10 µg/L (B), 0 to 150 µg/L at Sb/SPCE-3 with a step of 50 µg/L (C); Corresponding DP voltammograms of Ni(II) registered on Sb/SPCE-1 (D), Sb/SPCE-2 (E) and Sb/SPCE-3 (F) in ammonia buffer (pH 9.5 ± 0.5) + 0.25 mM DMG; DP voltammogram parameters: pulse step 0.006 V, pulse amplitude 0.05 V, $\upsilon$ = 0.06 V/s. Analysis conditions: $E_{acc}$ = -0.75 V, $t_{acc}$ = 30 s

In the case of using Sb/SPCE-2 (Figure 5.3, B), the linearity of the calibration plot narrows up to 10 – 40 μg/L Ni(II). The electrode shows a significant lowering in sensitivity towards Ni(II) ions, recoveries for 10 μg/L Ni(II) ions amount to 7.5% (Table 5.4) and indicate a significant systematic underestimation of the analysis results due to the absence of a direct proportional dependence of the response on the concentration of Ni(II) ions in the solution, which makes it inconvenient for analytical purposes.

Table 5.4 – Comparison of electroanalytical performance of SPCEs modified with antimony under different plating conditions towards Ni(II) ions with the "Spiked-recovery method" in ammonia buffer (pH 9.5 ± 0.5) + 0.25 mM DMG (n = 3, P = 0.95). Analysis conditions: $E_{acc}$ = -0.75 V, $t_{acc}$ = 30 s

| Electrode | Linear range, μg/L | Regression equation Q (μC) = kC (μg/L) + b (μC) | $R^2$ | R, % for Ni(II) * | RSD, % |
|---|---|---|---|---|---|
| Sb/SPCE-1 | 5 – 50 | Q = 0.017 C – 0.009 | 0.998 | 96 ± 0.4 | 3.2 |
| Sb/SPCE-2 | 10 – 40 | Q = 0.010 C – 0.089 | 0.989 | 7.5 ± 1.7 | 9.1 |
| Sb/SPCE-3 | 50 – 150 | Q = 0.0001 C – 0.0001 | 0.974 | 110 ± 33 | 21 |

*Note* – *$C_{Ni(II)}$ = 5 μg/L – on Sb/SPCE-1; $C_{Ni(II)}$ = 10 μg/L – on Sb/SPCE-2; $C_{Ni(II)}$ = 50 μg/L – on Sb/SPCE-3

The Sb/SPCE-3 (Table 5.4) shows the lowest sensitivity towards Ni(II) ions. The $R^2$ value of the calibration plot reduced significantly up to 0.974. The slope of the calibration plot for Ni(II) ion determination with Sb/SPCE-3 (0.0001 μC·L/μg) is two orders of magnitude less compared to the other Sb/SPCEs (Table 5.4). The negligible responses of Ni(II) ions (Figure 5.3, F) are unsuitable for analytical purposes. This may be explained by the very small amount of antimony on the Sb/SPCE-3 surface (Figure 4.2, D) as indicated by the low current of dissolving antimony from the Sb/SPCE-3 surface (Figure 4.7, B). Data for comparing the surface characteristics of Sb/SPCEs with their sensitivity towards Ni(II) are shown in Table 5.5. The conditions for obtaining experimental data are presented in the corresponding sections.

As we can see, the worst electroanalytical characteristics, including the lowest sensitivity towards Ni(II) ions, are obtained on Sb/SPCE-3 with a least degree of antimony coverage (Figure 4.2, D). The results we obtained for Sb/SPCE-3 are close to the data [193] for GCE with antimony film preplating under identical conditions. In this case, no responses of nickel-dimethylglyoximate could be registered. According to the authors the formed structure with low coverage of GCE surface with antimony possessed low adsorptive properties since adsorption occurs preferentially on the metal (Sb) rather than on the carbon substrate. At the same time, Sb/SPCE-1 is characterized by the greatest sensitivity towards Ni(II) (Table 5.5). It demonstrates the highest peak current value for NR reduction (Table 4.4) and therefore the highest roughness factors. This result can be explained by the formation of the finely dispersed antimony particles (Figure 4.2, B), combined with the largest area of metal coverage of the substrate in comparison with other electrodes (Table 4.4). On the contrary, Sb/SPCE-3, characterized by a practically bare surface, is distinguished by the lowest RF value.

Table 5.5 – Comparison of morphological, electrochemical and electroanalytical characterization of Sb/SPCEs

| Electrode | Particle size, μm | $Sb_{cov}$, % | RF | Sensitivity towards Ni(II), μC·L/μg |
|---|---|---|---|---|
| bare-SPCE | – | – | 7.1 | – |
| Sb/SPCE-1 | 0.63 ± 0.08 | 12 | 16.8 | 0.017 ± 0.001 |
| Sb/SPCE-2 | 0.96 ± 0.25 | 4 | 11.8 | 0.010 ± 0.0003 |
| Sb/SPCE-3 | ND | 1 | 7.4 | 0.0001 ± 0.00003 |

*Note* – ND – not determined

As for FA, as we have shown earlier, the process of electrochemical reduction of FAH does not occur on the surface of bare-SPCE, as well as on Sb/SPCEs with a degree of metal coverage of the substrate ≤ 12%. Unfortunately, for thicker antimony films it is not possible to obtain a strong adhesion of the metal to the carbon-containing substrate.

Comparison of average values of RF and sensitivity to model analyte for Sb/SPCEs with two-tailed Pearson's criterion showed a high degree of correlation between their electrochemical and electroanalytical characteristics with $R^2$ values of 0.994 for Ni(II) ions (n = 3, P = 0.95, $R_{crit}$ = 0.988) [244].

## Conclusions to chapter 5

The electroanalytical performance of the SPCEs modified with the “green” metals under different plating conditions to obtain films with significantly different morphologies was assessed using model analytes with known protocols for their determinations on the electrodes under study.

A comparison of roughness factor and sensitivity of “green” metals-modified SPCEs towards model analytes (Ni(II) ions and FA) using a two-tailed Pearson's criterion showed a high degree of correlation between their electrochemical and electroanalytical characteristics. In turn, RF magnitude is determined by a combination of two factors: the area of metal coverage of the substrate and the dispersion of metal particles.

# CONCLUSION

The following results were obtained in the course of the work:

1. The operating conditions for the formation of the electroactive form of FA (FAH) in a phosphate buffer solution (pH 5.2 ± 0.1) in the presence of 0.09 – 0.15 M hydrazine sulfate were selected. It has been established that on the bismuth surface the process of electrochemical reduction of FAH is irreversible and is controlled mainly by diffusion.

2. The SEM method showed that the morphology of the bismuth film preliminarily deposited on the surface of SPCE from 0.1 M acetate buffer solution (pH 4.5) at an electrolysis potential of -1.0 V depends significantly on the metal deposition time. Maximum current value of FA was obtained for bismuth-modified SPCE with a coating formed after 8 – 12 minutes of bismuth plating on SPCE surface as a consequence of the improved surface coverage and relatively arranged homogeneous structure of the film. It was shown that FA response does not depend on the accumulation time for 1 – 40 s at a potential of -0.5 V, at which no redox process occurs in the system under study. Under experimental operating conditions (pulse amplitude of 50 mV, scan rate of 0.02 V/s) using the direct voltammetric method with differential pulse potential scan, the reduction peak area of FA on Bi/SPCE increases linearly with a concentration in the range of 0.01 – 5.0 mg/L (0.33 – 167 μM) of model solutions. The Limit of detection and quantification of FA are 0.002 mg/L (0.07 μM) and 0.01 mg/L (0.33 μM), respectively.

3. It was demonstrated that NR in the protonated form performs quasi-reversible single-electron redox transformations at bare-SPCE, Bi/SPCEs and Sb/SPCEs in phosphate buffer solutions (pH 5.5 ± 0.5) in the potential range of -0.3 to -0.8 V, where the bismuth and antimony are not electroactive. The analysis of the data obtained by the CV method allows us to conclude that the process of NR reduction is controlled by

diffusion on bare-SPCE, while on Bi/SPCEs and Sb/SPCEs the diffusion process is accompanied by adsorption.

4. The surface morphology of Bi/SPCEs and Sb/SPCEs was characterized by SEM and EIS methods. It has been established that EIS data obtained with NR as redox pair can provide information about surface coverage with metal films. Analysis of CV experiments with NR showed an improvement in the electrochemical performances of SPCEs modified with “green” metals in comparison to the bare-SPCE. The calculated electroactive surface area of the electrodes obtained under various conditions of deposition of metal films largely corresponds to micrographs of the Bi/SPCEs and Sb/SPCEs surfaces. The highest *A* values were received for the films with a fairly high degree of coverage by the metals and consist of many fine and more or less evenly distributed metals. Quite good convergence of SEM, CV and EIS data confirms the effectiveness of NR as a redox pair for evaluating the electrochemical performance of “green” metals-modified electrodes.

5. A comparison of roughness factor and sensitivity of “green” metals-modified SPCEs towards model analytes (Ni(II) ions and FA) using a two-tailed Pearson's criterion showed a high degree of correlation between their electrochemical and electroanalytical characteristics.

6. A voltammetric method using Bi/SPCE was developed for the determination of formaldehyde in medicinal drug ("Endofalk®"), technical urotropin, waste, melt and bottled waters. The method exhibited acceptable selectivity towards acetaldehyde and demonstrated satisfactory recovery and precision.

**Prospects for further development of the research topic** lie in expanding the range of objects for determining trace amounts of FA on Bi/SPCE using the developed environmentally friendly, fast, easy-to-use, cheap voltammetric methods with high electroanalytical performance.

Pioneering studies conducted on the possibility of using NR as an alternative redox pair for quantitative assessment of changes in charge transfer resistance at the interface between carbon-containing ink and modifier, the area of the electroactive surface, the degree of reversibility of the processes of oxidation/reduction of the electroactive substance at the SPCE before and after modification may turn out to be very useful in the development of not only new varieties of electrodes based on “green” metals, but also for different types of modified electrodes in cases where the redox processes of traditional redox pair and modifier occur in a close range of anodic potentials.

The high degree of correlation between the electrochemical and electroanalytical characteristics of the electrodes revealed in the work will make it possible to choose the most effective strategy for their modification for the purpose of application in analytical practice.

# LIST OF SYMBOLS AND ABBREVIATIONS

Bi/SPCE – bismuth-modified screen-printed carbon-containing electrode;

CV – cyclic voltammetry;

DP VA – differential pulse voltammetry;

$E_{acc}$ – accumulation potential;

$E_{pa}$ – anodic peak potential;

$E_{pc}$ – cathodic peak potential;

EDTA – disodium salt of ethylenediaminetetraacetic acid;

$E_{el}$ – electrodeposition potential;

EIS – electrochemical impedance spectroscopy;

FA – formaldehyde;

FAH – formaldehyde hydrazone;

GCE – glass-carbon electrode;

HMDE – hanging mercury drop electrode;

HRZ – Hydrazine sulfate;

$I_p$ – peak current;

$I_{pa}$ – anodic peak current;

$I_{pc}$ – cathodic peak current;

NR – Neutral Red;

PBS – phosphate buffer solution;

Q – peak area;

R –recovery, %;

$R^2$ – correlation coefficient;

RSD – relative standard deviation, %;

Sb/SPCE – antimony-modified screen-printed carbon-containing electrode;

SEM – scanning electron microscopy;

SPCE – screen-printed carbon-containing electrode;

$t_{acc}$ – accumulation time;

$t_{el}$ – electrodeposition time;

VA – voltammetry;

$\upsilon$ – potential scan rate.

# LIST OF REFERENCES

1. World Health Organization. WHO guidelines for indoor air quality: selected pollutants. – Geneva: World Health Organization, 2010. – 484 p.

2. Sangthong, W. Computational study of the carbonylene reaction of encapsulated formaldehyde in Na-FAU zeolite / W. Sangthong, M. Probst, J. Limtrakul // Journal of Molecular Structure. – 2005. – Vol. 748. – № 1-3. – P. 119-127.

3. Barakoti, K. K. Formaldehyde Analysis in Non-Aqueous Methanol Solutions by Infrared Spectroscopy and Electrospray Ionization / K. K. Barakoti, P. Subedi, F. Chalyavi, S. Gutierrez-Portocarrero, M. J. Tucker, M. A. Alpuche-Aviles // Frontiers in Chemistry. – 2021. – Vol. 9. – Article 678112.

4. Subasi, N. T. Formaldehyde Advantages and Disadvantages: Usage Areas and Harmful Effects on Human Beings / N. T. Subasi // Biochemical Toxicology - Heavy Metals and Nanomaterials / G. O. Muharrem Ince, Olcay Kaplan Ince, ed. – London: IntechOpen, 2020. – P. 101-110.

5. Nielsen, G. D. Recent trend in risk assessment of formaldehyde exposures from indoor air / G. D. Nielsen, S. T. Larsen, P. Wolkoff // Archives of Toxicology. – 2013. – Vol. 87. – № 1. – P. 73-98.

6. Swenberg, J. A. Formaldehyde carcinogenicity research: 30 years and counting for mode of action, epidemiology, and cancer risk assessment / J. A. Swenberg, B. C. Moeller, K. Lu, J. E. Rager, R. Fry, T. B. Starr // Toxicologic Pathology. – 2013. – Vol. 41. – № 2. – P. 181-189.

7. Khoshakhlagh, A. H. Inhalational exposure to formaldehyde, carcinogenic, and non-carcinogenic risk assessment: A systematic review / A. H. Khoshakhlagh, M. Mohammadzadeh, S. S. Manafi, F. Yousefian, A. Gruszecka-Kosowska // Environmental Pollution. – 2023. – Vol. 331. – Article 121854.

8. Kootenaei, A. S. B36 borophene as an electronic sensor for formaldehyde: Quantum chemical analysis / A. S. Kootenaei, G. Ansari // Physics Letters, Section A.

– 2016. – Vol. 380. – № 34. – P. 2664-2668.

9. Tang, X. Formaldehyde in China: Production, consumption, exposure levels, and health effects / X. Tang, Y. Bai, A. Duong, M. T. Smith, L. Li, L. Zhang // Environment International. – 2009. – Vol. 35. – № 8. – P. 1210-1224.

10. Gelbke, H. P. Derivation of safe exposure levels for potential migration of formaldehyde into food / H. P. Gelbke, H. Buist, R. Eisert, E. Leibold, J. H. Sherman // Food and Chemical Toxicology. – 2019. – Vol. 132. – Article 110598.

11. Ahmed, H. O. Preliminary study: Formaldehyde exposure in laboratories of Sharjah university in UAE / H. O. Ahmed // Indian journal of occupational and environmental medicine. – 2011. – Vol. 15. – № 1. – P. 33-37.

12. Agency for Toxic Substances and Disease Registry (ATSDR). Formaldehyde (HCHO) CAS 50-00-0; UN 1198, UN 2209 (formalin) / CDC. – 2014. – Vol. 2209. – P. 1-24.

13. Amiri, A. Formaldehyde exposure during pregnancy / A. Amiri, E. Pryor, M. Rice, C. A. Downs, A. Turner-Henson, M. V. Fanucchi // MCN. The American journal of maternal child nursing. – 2015. – Vol. 40. – № 3. – P. 180-185.

14. Kim, S. H. Effect of Lead on Human Middle Ear Epithelial Cells / S. H. Kim, S. H. Shin, Y. Y. Go, S. Chae, J. Song // BioMed Research International. – 2018. – Vol. 2018. – Article 5058729.

15. Denda, T. Thin films exhibiting multicolor changes induced by formaldehyde-responsive release of anionic dyes / T. Denda, R. Mizutani, M. Iijima, H. Nakahashi, H. Yamamoto, Y. Kanekiyo // Talanta. – 2015. – Vol. 144. – P. 816-822.

16. Hao, J. N. A dual-emitting 4d-4f nanocrystalline metal-organic framework as a self-calibrating luminescent sensor for indoor formaldehyde pollution / J. N. Hao, B. Yan // Nanoscale. – 2016. – Vol. 8. – № 23. – P. 12047-12053.

17. Wang, X. Colorimetric sensor strips for formaldehyde assay utilizing fluoral-p decorated polyacrylonitrile nanofibrous membranes / X. Wang, Y. Si, X. Mao, Y. Li, J. Yu, H. Wang, B. Ding // Analyst. – 2013. – Vol. 138. – № 17. – P. 5129-5136.

18. WHO Guidelines for Indoor Air Quality: Selected Pollutants. – Geneva: World Health Organization, 2010. – 378 p.

19. SanPin RF. Hygienic standards and requirements for ensuring the safety and (or) harmlessness of environmental factors for humans. SanPiN 1.2.3685-21. – 2021.

20. WHO Guidelines for drinking-water quality Volume 2, 2nd ed. Health criteria and other supporting information. Geneva: World Health Organization, 1996. – 842 p.

21. Khalikov, I. S. Formaldehyde in atmospheric air: sources of entry and removal routes / I. S. Khalikov // Environmental Chemistry. – 2019. – Vol. 28. – № 6. – P. 307–317.

22. Parrish, D. D. Primary and secondary sources of formaldehyde in urban atmospheres: Houston Texas region / D. D. Parrish, T. B. Ryerson, J. Mellqvist, J. Johansson, A. Fried, D. Richter, J. G. Walega, R. A. Washenfelder, J. A. de Gouw, J. Peischl, K. C. Aikin, S. A. McKeen, G. J. Frost, F. C. Fehsenfeld, S. C. Herndon // Atmospheric Chemistry and Physics. – 2012. – Vol. 12. – № 7. – P. 3273-3288.

23. Salthammer, T. Formaldehyde in the Indoor Environment / T. Salthammer, S. Mentese, R. Marutzky // Chemical Reviews. – 2010. – Vol. 110. – № 4. – P. 2536-2572.

24. Viskari, E. L. Seasonal and diurnal variation in formaldehyde and acetaldehyde concentrations along a highway in Eastern Finland / E. L. Viskari, M. Vartiainen, P. Pasanen // Atmospheric Environment. – 2000. – Vol. 34. – № 6. – P. 917-923.

25. Malik, M. I. Methanol to Formaldehyde: An Overview of Surface Studies and Performance of an Iron Molybdate Catalyst / M. I. Malik, N. Abatzoglou, I. E. Achouri. – 2021. – Vol. 11. – № 8. – P. 1210-1224.

26. Delbono, V. Novel Method of Analysis for the Determination of Residual Formaldehyde by High-Performance Liquid Chromatography / V. Delbono, C. P. Larch, K. C. Newlands, S. Rhydderch, T. C. Baddeley, J. M. D. Storey // International Journal of Analytical Chemistry. – 2022. – Vol. 2022. – Article 9171836.

27. Kumari, P. K. Alternative to artificial preservatives / P. K. Kumari, S. Akhila, Y. S. Rao, B. R. Devi // Systematic Reviews in Pharmacy. – 2019. – Vol. 10. – № 1. – P. 99-102.

28. Yu, Y. Cu(I)-MOF: Naked-eye colorimetric sensor for humidity and formaldehyde in single-crystal-to-single-crystal fashion / Y. Yu, X. M. Zhang, J. P. Ma, Q. K Liu, P. Wang, Y. B. Dong // Chemical Communications. – 2014. – Vol. 50. – № 12. – P. 1444-1446.

29. Borkar, T. G. Techniques Employed in Production of Traditional Vaccines Commonly Used by Military Forces: A Review / T. G. Borkar, V. Goenka // Journal of Archives in Military Medicine. – 2019. – Vol. 7. – № 1-2. – Article 96149.

30. Schiller, L. R. Osmotic effects of polyethylene glycol / L. R. Schiller, M. Emmett, C. A. Santa Ana, J. S. Fordtran // Gastroenterology. – 1988. – Vol. 94. – № 4. – P. 933-941.

31. Pelham, R. W. Clinical trial: single- and multiple-dose pharmacokinetics of polyethylene glycol (PEG-3350) in healthy young and elderly subjects / R. W. Pelham, L. C. Nix, R. E. Chavira, M. V. B. Cleveland, P. Stetson // Alimentary Pharmacology & Therapeutics. – 2008. – Vol. 28. – № 2. – P. 256-265.

32. Ichijima, R. Efficacy of macrogol 4000 plus electrolytes in bowel preparation for colonoscopy in patients with chronic constipation. / R. Ichijima, S. Suzuki, M. Esaki, T. Sugita, K. Ogura, C. Kusano, H. Ikehara, T. Gotoda // BMC gastroenterology. – 2021. – Vol. 21. – № 1. – 387 p.

33. Ma, G. The safety and effects of high- and low-volume polyethylene glycol bowel preparation methods before colonoscopy on bowel cleanliness: a systematic review and meta-analysis / G. Ma, X. Fang // Journal of Gastrointestinal Oncology. – 2023. – Vol. 14. – № 4. – P. 1759-1769.

34. Bouhnik, Y. Prospective, randomized, parallel-group trial to evaluate the effects of lactulose and polyethylene glycol-4000 on colonic flora in chronic idiopathic constipation / Y. Bouhnik, C. Neut, L. Raskine, C. Michel, M. Riottot, C. Andrieux, F. Guillemot, F. Dyard, B. Flourié // Alimentary Pharmacology & Therapeutics. – 2004. – Vol. 19. – № 8. – P. 889-899.

35. Cleveland, M. B. New polyethylene glycol laxative for treatment of

constipation in adults: a randomized, double-blind, placebo-controlled study. / M. B. Cleveland, D. P. Flavin, R. A. Ruben, R. M. Epstein, G. E. Clark // Southern Medical Journal. – 2001. – Vol. 94. – № 5. – P. 478-481.

36. Kryuk, T. V. Promising Inhibitors of Poly(ethylene glycol) Oxidation in Aqueous Solutions / T. V. Kryuk, V. M. Mikhal'chuk, L. V. Petrenko, O. A. Nelepova, A. N. Nikolaevskii // Pharmaceutical Chemistry Journal. – 2002. – Vol. 36. – № 1. – P. 32-35.

37. Waterman, K. C. N-Methylation and N-Formylation of a Secondary Amine Drug (Varenicline) in an Osmotic Tablet / K. C. Waterman, W. B. Arikpo, M. B. Fergione, T. W. Graul, B. A. Johnson, B. C. MacDonald, M. C. Roy, R. J. Timpano // Journal of Pharmaceutical Sciences. – 2008. – Vol. 97. – № 4. – P. 1499-1507.

38. Moskovchenko, D. Concentrations of major and trace elements within the snowpack of tyumen, russia / D. Moskovchenko, R. Pozhitkov, A. Zakharchenko, A. Tigeev // Minerals. – 2021. – Vol. 11. – № 7. – 709 p.

39. Huang, T. C. Analytical method development, validation, and out-of-specification investigations for polyethylene glycol / T. C. Huang, G. Chu, S. Singh // Journal of Pharmaceutical and Biomedical Analysis. – 2023. – Vol. 235. – Article 115613.

40. State Pharmacopoeia of the Russian Federation Volume 3. – XIV ed. – Moscow: Medicine, 2018. – 4284 p. [Russian]

41. The Merck Index - An Encyclopedia of Chemicals, Drugs, and Biologicals. Cambridge: Royal Society of Chemistry, 2013. – 1108 p.

42. Altinoz, M. A. Methenamine's journey of 160 years: Repurposal of an old urinary antiseptic for treatment and hypoxic radiosensitization of cancers and glioblastoma / M. A. Altinoz, A. Ozpinar, J. L. Perez, İ. Elmaci / Clinical and Experimental Pharmacology and Physiology. – 2019. – Vol. 46. – № 5. – P. 407-412.

43. Lo, T. S. Methenamine:a forgotten drug for preventing recurrent urinary tract infection in a multidrug resistance era/ T. S. Lo, K. D. P. Hammer, M. Zegarra, W. C. S. Cho // Expert Review of Anti-infective Therapy. – 2014. – Vol.12. – № 5. – P. 549-554.

44. Swift, L. P. Activation of adriamycin by the pH-dependent formaldehyde-

releasing prodrug hexamethylenetetramine / L. P. Swift, S. M. Cutts, A. Rephaeli, A. Nudelman, D. R. Phillips // Molecular Cancer Therapeutics. – 2003. – Vol. 2. – № 2. – P. 189-198.

45. Masunaga, S. I. Usefulness of hexamethylenetetramine in combination with chemotherapy using free and pegylated liposomal doxorubicin in vivo, referring to the effect on quiescent cells / S. I. Masunaga, K. Kono, J. Nakamura, K. Tano, H. Yoshida, M. Watanabe, G. Kashino, M. Suzuki, Y. Kinashi, Y. Liu, K. Ono // Oncology Reports. – 2009. – Vol.21. – №.5. – P..1307-1312.

46. Sweetman, S. C. The Complete Drug Reference. Martindale, 37th ed. London: Pharmaceutical Press, 2011. – 325 p.

47. Scott, C. R. The antibacterial activity of a series of quaternaries prepared from hexamethylenetetramine and halohydrocarbons / C. R. Scott, P. A. Wolf // Applied Microbiology. – 1962. – Vol. 10. – №. 3. – P. 211-216.

48. Restani, P, Oral toxicity of formaldehyde and its derivatives / P. Restani, C. L. Gali // Critical Reviews in Toxicology. – 1991. – Vol. 21. – №. 5. – P. 315-328.

49. Tachev, A. Rapid spectrophotometric method for determination of hexamethylenetetramine (urotropine) in foot care products/ A. Tachev, V. Christova-Bagdassarian, N. Vasileva, A. Dimitrova, M. Atanassova // Journal of Chemical Technology and Metallurgy. –2013. – Vol. 48. – №.3. –P. 254-258.

50. Yu, Y. Cu(I)-MOF: naked-eye colorimetric sensor for humidity and formaldehyde in single-crystal-to-single-crystal fashion/ Y. Yu, X. M. Zhang, J. P. Ma, Q. K. Liu, P. Wang, Y. B. Dong // Chemical Communication. – 2014. – Vol. 50, – P. 1444-1446.

51. Hauksson, I. D. Contact Allergy to Formaldehyde. Diagnosis and Clinical Relevance Volume 19. – Lund: Lund University,2014.

52. Sokolova, T. V. Advances in Medical Mycology: Prevention of foot mycosis / T. V. Sokolova, T. A. Malyarchuk // Epidemiology and Vaccinal Prevention. – 2015. – Vol. 14. – № 1. – P. 44-47. [Russian]

53. State Pharmacopoeia of the Russian Federation Volume 3. – XIV ed. – Moscow: Medicine, 2018. – P. 4351-4352. [Russian]

54. Can, Z. S. Formaldehyde formation during ozonation of drinking water / Z. S. Can, M. Gurol // Ozone: Science and Engineering. – 2003. – Vol. 25. – № 1. – P. 41-51.

55. Nishikawa, S. Assessment of indirect inhalation exposure to formaldehyde evaporated from water / S. Nishikawa, Y. Matsui, T. Matsushita, N. Shirasaki // Regulatory Toxicology and Pharmacology. – 2019. – Vol. 106. – P. 43-49.

56. Nachaki, E. O. Nickel-Palladium-Based Electrochemical Sensor for Quantitative Detection of Formaldehyde / E. O. Nachaki, P. M. Ndangili, N. M. Naumih, E. Masika // ChemistrySelect. – 2018. – Vol. 3. – № 2. – P. 384-392.

57. Krasner, S. W. The occurrence of disinfection by-products in US drinking water / S. W. Krasner, M. J. McGuire, J. G. Jacangelo, N. L. Patania, K. M. Reagan, E. M. Aieta // Journal of the American Water Works Association. – 1989. – Vol. 81. – P. 41-53.

58. He, J. Trace carbonyl analysis in water samples by integrating magnetic molecular imprinting and capillary electrophoresis / J. He, J. Liu, Y. Liu, Z. Liyin, X. Wu, G. Song, Y. Hou, R. Wang, W. Zhao, H. Sun // RSC Advances. – 2021. – Vol. 11. – № 52. – P. 32841-32851.

59. Tsai C. F. Determination of low-molecule-weight aldehydes in packed drinking water by high performance liquid chromatography / C. F. Tsai, H. W. Shiau, S. C. Lee, S.

60. Yasri, N. G. Spectrophotometric determination of formaldehyde based on the telomerization reaction of tryptamine / N. G. Yasri, H. Seddik, M. A. Mosallb. – 2011. – Vol. 8. – № 4. – P. 487-494.

61. Anastasio, C. Light absorption by soluble chemical species in Arctic and Antarctic snow / C. Anastasio, T. Robles // Journal of Geophysical Research Atmospheres. – 2007. – Vol. 112. – № 24. – P. 1-14.

62. Barret, M. Formaldehyde in the Alaskan Arctic snowpack: Partitioning and physical processes involved in air-snow exchanges / M. Barret, F. Domine, S. Houdier, J. Gallet, P. Weibring, J. Walega, A. Fried, D. Richter // Journal of Geophysical

Research Atmospheres. – 2011. – Vol. 116. – № 18. – P. 1-12.

63. Shevchenko, V. P. Impact of snow deposition on major and trace element concentrations and elementary fluxes in surface waters of the Western Siberian Lowland across a 1700’km latitudinal gradient / V. P. Shevchenko, O. S. Pokrovsky, S. N. Vorobyev, I. V. Krickov, R. M. Manasypov, N. V. Politova, S. G. Kopysov, O. M. Dara, Y. Auda, L. S. Shirokova, L. G. Kolesnichenko, V. A. Zemtsov, S. N. Kirpotin // Hydrology and Earth System Sciences. – 2017. – Vol. 21. – № 11. – P. 5725-5746.

64. Yuan, D. Characteristic contaminants in snowpack and snowmelt surface runoff from different functional areas in Beijing, China / D. Yuan, Y. Liu, X. Guo, J. Liu // Environmental Science and Pollution Research. – 2018. – Vol. 25. – № 36. – P. 36256-36266.

65. Meyer, T. Measuring the release of organic contaminants from melting snow under controlled conditions / T. Meyer, Y. D. Lei, F. Wania // Environmental Science and Technology. – 2006. – Vol. 40. – № 10. – P. 3320-3326.

66. Wang, X. L. Headspace-gas chromatography method for determination of formaldehyde content in wastewater / X. L. Wang, L. Zhang // IOP Conference Series: Earth and Environmental Science. – 2021. – Vol. 647. – Article 012155.

67. Yuan, C. UV–vis spectroscopic detection of formaldehyde and its analogs: A convenient and sensitive methodology / C. Yuan, J. Pu, D. Fu, Y. Min, L. Wang, J. Liu // Journal of Hazardous Materials. – 2022. – Vol. 438. – Article 129457.

68. Akshath, U. S. Detection of formaldehyde in food samples by enhanced chemiluminescence / U. S. Akshath, L. S. Selvakumar, M. S. Thakur // Analytical Methods. – 2012. – Vol. 4. – № 3. – P. 699-704.

69. Teixeira, L. S. Determination of formaldehyde in Brazilian alcohol fuels by flow-injection solid phase spectrophotometry / L. S. Teixeira, E. S. Leao, A. F. Dantas, H. L. C. Pinheiro, A. C. S. Costa, J. B. de Andrade // Talanta. – 2004. – Vol. 64. – № 3. – P. 711-715.

70. Pickard, A. D. The determination of traces of formaldehyde / A. D. Pickard, E. R. Clark // Talanta. – 1984. – Vol. 31. – P. 763-771.

71. Hladovai, M. Review of Spectrophotometric Methods for Determination of Formaldehyde / M. Hladovai, J. Martikai, P. Rantuch, A. Necas // Research Papers Faculty of Materials Science and Technology Slovak University of Technology. – 2019. – Vol. 27. – № 44. – P. 105-120.

72. Sawicki, E. Spectrophotometric Determination of Formaldehyde and Formaldehyde-Releasing Compounds with Chromotropic Acid, 6-Amino-1-naphthol-3-sulfonic Acid (J Acid), and 6-Anilino-1-napthol-3-sulfonic Acid (Phenyl J Acid) / E. Sawicki, T. R. Hauser, S. Mcpherson // Analytical Chemistry. – 1962. – Vol. 34. – № 11. – P. 1460-1464.

73. Solovyova, T. V. Guide to methods for determining harmful substances in atmospheric air / T. V. Solovyova, V. A. Khrustaleva. – Moscow: Medicine, 1974. – P. 210-213. [Russian]

74. Birkeland1, M. J. Determination of native (wood derived) formaldehyde by the desiccator method in particleboards generated during panel production / M. J. Birkeland1, L. Lorenz, J. M. Wescott, C. R. Frihart // Holzforschung. – 2010. – Vol. 64. – P. 429-433.

75. Fagnani, E. Chromotropic Acid- 22 Formaldehyde Reaction in Strongly Acidic Media. The Role of Dissolved Oxygen and Replacement of Concentrated Sulphuric Acid / E. Fagnani, C. B. Melios, L. Pezza, H. R. Pezza // Talanta. – 2003. – Vol. 60. – № 1. – P. 171-176.

76. Gasparini, F. A simple and green analytical method for the determination of formaldehyde / F. Gasparini, P. L. Weinert, L. S. Lima, L. Pezza, H. R. Pezza // Journal of the Brazilian Chemical Society. – 2008. – Vol. 19. – № 8. – P. 1531-1537.

77. Pinto, G. F. Indirect determination of formaldehyde by square-wave voltammetry based on the electrochemical oxidation of 3,5–diacetyl–1,4–dihydrolutidine using an unmodified glassy-carbon electrode / G. F. Pinto, D. P. Rocha, E. M. Richter, R. A. A. Muñoz, S. G. Silva // Talanta. – 2019. – Vol. 198. – P. 237-241.

78. Kaysina, O. V. Detrmination of formaldehyde with acetylacetonereagent / O. V. Kaysina, I.A. Krylova, O. A. Chumicheva // Nanotechnology. – 1986. – P. 43-44. [Russian]

79. Motyka, K. Flow-injection chemiluminescence determination of formaldehyde in water / K. Motyka, A. Onjia, P. Mikuska, Z. Vecera // Talanta. – 2007. – Vol. 71. – № 2. – P. 900-905.

80. Khataee, A. A simple and sensitive flow injection method based on the catalytic activity of CdS quantum dots in an acidic permanganate chemiluminescence system for determination of formaldehyde in water and waste water / A. Khataee, R. Lotfi, A. Hasanzadeha, M. Iranifam // Photochemical & Photobiological Sciences. – 2016. – Vol. 15. – P. 496-505.

81. Sumner, A. L. Atmospheric chemistry of formaldehyde in the Arctic troposphere at Polar Sunrise, and the influence of the snowpack / A. L. Sumner, P. B. Shepson, A. M. Grannas, J. W. Bottenheim, K. G. Anlauf, D. Worthy, W. H. Schroeder, A. Steffen, F. Dominé, S. Perrier, S. Houdier // Atmospheric Environment. – 2002. – Vol. 36. – No 15-16. – P. 2553-2562.

82. Lipskerov, F. A. Approaches to Formaldehyde Measurement: From Liquid Biological Samples to Cells and Organisms / F. A. Lipskerov, E. V. Sheshukova, T. V. Komarova // International Journal of Molecular Sciences. – 2022. – Vol. 23. – № 12. – Article 6642.

83. Gryllaki-Berger, M. A comparative study of formaldehyde detection using chromotropic acid, acetylacetone and HPLC in cosmetics and household cleaning products / M. Gryllaki-Berger, C. Mugny, D. Perrenoud, A. Pannatier, E. Frenk // Contact Dermatitis. – 1992. – Vol. 26. – № 3. – P. 149-154.

84. Sebaei, A. S. Determination of formaldehyde by HPLC with stable precolumn derivatization in egyptian dairy products / A. S. Sebaei, A. M. Gomaa, A. A. El-Zwahry, E. A. Emara // International Journal of Analytical Chemistry. – 2018. – Article 2757941.

85. Malinauskiene, L. A Formaldehyde may be found in cosmetic products even when unlabelled / L. Malinauskiene, A. Blaziene, A. Chomiciene, M. Isaksson // Open Medicine (Poland). – 2015. – Vol. 10. – № 1. – P. 323-328.

86. Nikitina O. Bi-enzyme biosensor based on NAD+ - and glutathione-dependent

recombinant formaldehyde dehydrogenase and diaphorase for formaldehyde assay / O. Nikitina, S. Shleev, G. Gayda, O. Demkiv, M. Gonchar, L. Gorton, E. Csöregi, M. Nistor // Sensors & Actuators, B: Chemical. – 2000. – Vol. 125. – № 1. – P. 1-9.

87. Vastarella, W. Protein-based biosensors using nanomaterials? / W. Vastarella, R.Talanta Nicastri // Physical Chemistry. – 2005. – Vol. 66. – № 3. – P. 627-632.

88. Daoudy, B. D. A. D. A Robust Static Headspace GC-FID Method to Detect and Quantify Formaldehyde Impurity in Pharmaceutical Excipients / B. D. A. D. Daoudy, M. A. Al-Khayat, F. Karabet, M. A. Al-Mardini // Journal of Analytical Methods in Chemistry. – Vol. 2018. – № 1. – Article 4526396.

89. Ott, M. Distillation of formaldehyde containing mixtures: laboratory experiments, equilibrium stage modeling and simulation / M. Ott, H. Schoenmakers, H. Hasse // Chem. Engineering and Processing. – 2005. – Vol. 44. – № 6. – P. 687-694.

90. Kellogg, D. W. Analysis of rumen fluid volatile fatty acids by chromatography with Porapak QS1 / D. W. Kellogg // Journal Dairy Science. – 1973. – Vol. 52. – № 10. – P. 1690-1692.

91. Dyuldina, E. V. Surface phenomena and disperse systems: Textbook / E. V. Dyuldina, S. P. Klochkovsky, M. V. Shubina. – Magnitogorsk: MSTU, 2007. – 119 p. [Russian]

92. Vyakhirev, D. A. Handbook of Gas Chromatography / D. A. Vyakhirev, A. F. Shushunova. – Moscow: Higher School, 1996. – 302 p. [Russian]

93. Skubnevskaya, G. I. Pollution of the atmosphere with formaldehyde / G. I. Skubnevskaya, G. G. Dultseva. – Novosibirsk: Institute of Chemical Kinetics and Combustion, 1994. – 70 p. [Russian]

94. Yue, X. F. An air-driving FI device with merging zones technique for the determination of formaldehyde in beers / X. F. Yue, Y. N. Zhang, Z. Q. Zhang // Food Chemistry. – 2007. – Vol. 102. – № 1. – P. 90–94.

95. Yue, X. F. Simultaneous determintion of formaldehyde and methanol by flow injection catalytic spectrometry / X. F. Yue, Z. Q. Zhang // Journal of Analytical Chemistry. – 2007. – Vol. 62. – № 10. – P. 992-996.

96. Pentin, Y. A. V. Physical research methods in chemistry / Y. A. Pentin, L. V. Vilkov. – Moscow: Mir, 2003. – 683 p. [Russian]

97. Tretyakov, V. F. Methods of formaldehyde analysis / V. F. Tretyakov, R. M. Talyshinsky, A. M. Ilolov, I. A. Golubeva, N. I. Kovaleva, N. A. Frantsuzova, M. S. Yakimova // Bulletin of MITHT. – 2008. – Vol. 3. – №. 6. [Russian]

98. Li, Z. Analysis of aldehydes in excipients used in liquid/semi-solid formulations by gas chromatography–negative chemical ionization mass spectrometry / Z. Li, B. M. Kozlowski, E. P. Chang // Journal of Chromatography A. – 2007. – Vol. 1160. – № 1-2. – P. 299-305.

99. Sax's Dangerous Properties of Industrial Materials. 11th ed. / R. J. Lewis (ed). // Wiley & Sons, Inc. New Jersey, 2004. – 1940 p.

100. International Program on Chemical Safety/European Commission; International Chemical Safety Card (ICSC) on Hexamethylenetetramine (100-97-0), 2002. Available from https://www.inchem.org/pages/icsc.html

101. Dreyfors, J. M. Hexamethylenetetramine: a review / J. M. Dreyfors, S. B. Jones, Y. Sayed // American Industrial Hygiene Association Journal. – 1989. – Vol. 50. – № 11. – P. 579-85.

102. Wang, S. Determination of formaldehyde in pharmaceutical product of urotropin / S. Wang, X. Chen, Y. Xing, R. Li, R. Pang, Z. Zhang // Chinese Journal of Pharmaceutical Analysis. – 2010. – Vol. 30. – № 9. – P. 1774-1776.

103. Devi, P. Ruthenium-Induced Decomposition of Hexamethylenetetramine as a Tool for the Acid-Free Sommelet Reaction in Aqueous Medium / P. Devi, V. D. Ghule, S. Muthaiah // Journal of Orgaanic Chemistry. – 2024. – Vol. 89. – № 7. – P. 4366–4374.

104. Jeffreys, G.V., Davis, G.A. Coalescence of droplets and dispersions // In the book – Recent advances in liquid extraction. Moscow: Chemistry, 2003. – P. 255 – 356. [Russian]

105. Marutzky R. Release of Formaldehyde by Wood Products // In the book – Wood adhesives: Chemistry and Technology,Volume 2. – California:VSP; 1989. – 329 p.

106. Zhao, H. Determination of degree of substitution of formyl groups in

polyaldehyde dextran by the hydroxylamine hydrochloride method / H. Zhao, N. D. Heindel // Pharmaceutical research. – 1991. – Vol. 8. – № 3. – P. 400-402.

107. Bryant, W. M. D. Improved Hydroxylamine Method for the Determination of Aldehydes and Ketones. Displacement of Oxime Equilibria by Means of Pyridine / W. M. D. Bryant, D. M. Smith // Journal of the American Chemical Society. – 1935. – Vol. 57. – № 1. – P. 57-61.

108. Wang, J. Electrochemical detection for microscale analytical systems: A review / J. Wang // Talanta. – 2002. – Vol. 56. – № 2. – P. 223-231.

109. Bard, A. J. Electrical methods: Fundamentals and Applications, 2nd ed / A. J. Bard, L. R. Faulkner. – New York: John Wiley & Sons, 2001. – 850 p.

110. Ngamchana, S. Sub-millimolar determination of formalin by pulsed amperometric detection / S. Ngamchana, W. Surareungchai // Analytica Chimica Acta. – 2004. – Vol. 510. – № 2. – P. 195-201.

111. Mahmoudian, M. R. Voltammetric sensing of formaldehyde by using a nanocomposite prepared by reductive deposition of palladium and platinum on polypyrrole-coated nitrogen-doped reduced graphene oxide / M. R. Mahmoudian, W. J. Basirun, P. M. Woi, H. Hazarkhani, Y. B. Alias // Microchimica Acta. – 2019. – Vol. 186. – № 6. – 369 p.

112. Kong, L. B. Electrooxidation of Formaldehyde on Silver / Ordered Mesoporous Carbon Composite Electrode in Alkaline Solutions / L. B. Kong, R. T. Wang, X. W. Wang, Z. S. Yang, Y. C. Luo, L. Kang // International Journal of Applied Physics and Mathematics. – 2011. – Vol. 1. – № 1. – P. 5-9.

113. Zhao, C. Determination of formaldehyde by staircase voltammetry based on its electrocatalytic oxidation at a nickel electrode / C. Zhao, M. Li, K. Jiao // Journal of Analytical Chemistry. – 2006. – Vol. 61. – № 12. – P. 1204-1208.

114. Trafela, Š. Formation of a Ni(OH)2/NiOOH active redox couple on nickel nanowires for formaldehyde detection in alkaline media / Š. Trafela, J. Zavašnik, S. Šturm, K. Ž. Rožman // Electrochimica Acta. – 2019. – Vol. 309. – P. 346-353.

115. Kongkaew, S. A preparation of homogeneous distribution of palladium nanoparticle on poly (acrylic acid)-functionalized graphene oxide modified electrode for formalin oxidation / S. Kongkaew, P. Kanatharana, P. Thavarungkul, W. Limbut // Electrochimica Acta. – 2017. – Vol. 247. – P. 229-240.

116. Norkus, E. Polarographic Determination of Formaldehyde According to the Anodic Oxidation Wave in Alkaline Solutions / E. Norkus, A. Vaskelis, R. Pauliukaite // Electroanalysis. – 1999. – Vol. 11. – № 6. – P. 447-449.

117. Dvorak, P. A new electroanalytical methodology for the determination of formaldehyde in wood-based products / P. Dvorak, R. M. Ramos, V. Vyskocil, J. A. Rodrigues // Talanta. – 2020. – Vol. 217. – Article 121068.

118. Nellaiappan, S. In-situ preparation of Au(111) oriented nanoparticles trapped carbon nanofiber-chitosan modified electrode for enhanced bifunctional electrocatalysis and sensing of formaldehyde and hydrogen peroxide in neutral pH solution / S. Nellaiappan, A. S. Kumar, S. Nisha, K. C. Pillai // Electrochim Acta. – 2017. – Vol. 249. – P. 227-240.

119. Xi, H. T. Electrochemical determination of formaldehyde via reduced AuNPs@PPy composites modified electrode / H. T. Xi, X. G. Chen, Y. Cao, J. J. Xu, C. Z. Ye, D. W. Deng, J. S. Zhang, G. H. Huang // Microchemical Journal. – 2020. – Vol. 156. – Article 104846.

120. Chou, C. H. Effective analysis of gaseous formaldehyde based on a platinum-deposited screen-printed edge band ultramicroelectrode coated with Nafion as solid polymer electrolyte / C. H. Chou, J. L. Chang, J. M. Zen // Sens. Actuators B. – 2010. – Vol. 147. – № 2. – P. 669-675.

121. Chen, Y. A. Electrocatalytic oxidation of formaldehyde on direct electrodeposited graphene-platinum nanoparticles composites electrode / Y. A. Chen, X. H. Liu, W. Zhang, Y. Zhang, L. J. Li, Z. Z. Cao, H. Wang, G. Jia, Y. F. Gao, J. R. Liu // Analalytical Methods. – 2013. – Vol. 5. – № 16. – P. 3915-3919.

122. Zhang, J. Electrocatalytic oxidation of formaldehyde and formic acid at Pd

nanoparticles modified glassy carbon electrode / J. Zhang, L. Z. Shangguan, C. Dong // Micro & Nano Letters. – 2013. – Vol. 8. – № 10. – P. 704-708.

123. Zhang, Y. A novel electrochemical sensor for formaldehyde based on palladium nanowire arrays electrode in alkaline media / Y. Zhang, M. Zhang, Z. Q. Cai, M. Q. Chen, F. L. Cheng // Electrochimica Acta. – 2012. – Vol. 68. – P. 172-177.

124. Sun, X. Noble-Metal-Based Catalysts on a Scale from Nanoparticles to Subnanoclusters and Single Atoms for Formaldehyde Oxidation at Room Temperature: A Review / X. Sun, Y. Wang, J. Cui, Y. Li, J. Lin // ACS Applied Nano Materials. – 2024. – Vol. 7. – № 4. – P. 3546-3563.

125. Cuenya, B. R. Synthesis and catalytic properties of metal nanoparticles: Size, shape, support, composition, and oxidation state effects / B. R. Cuenya // Thin Solid Films. – 2010. – Vol. 518. – № 12. – P. 3127-3150.

126. Baez-Gaxiola, M. R. Gold cluster based electrocatalytic sensors for the detection of formaldehyde / M. R. Baez-Gaxiola, C. Fernández-Sánchez, E. Mendoza // Analytical Methods. – 2015. – Vol. 7. – № 2. – P. 538-542.

127. Skvortsova, L. I. Voltammetry of formaldehyde at mechanically renewable solid electrodes / L. I. Skvortsova, T. P. Aleksandrova // Journal of Analytical Chemistry. – 2004. – Vol. 59. – P. 847-853.

128. Aini, B. N. Development of formaldehyde biosensor for determination of formalin in fish samples; malabar red snapper (lutjanus malabaricus) and longtail tuna (Thunnus tonggol) / B. N. Aini, S. Siddiquee, K. Ampon // Biosensors. – 2016. – Vol. 6. – № 3. – 32 p.

129. Marzuki, N. I. Development of electrochemical biosensor for formaldehyde determination based on immobilized enzyme / N. I. Marzuki, F. A. Bakar, A. B. Salleh, L. YookHeng, N. A. Yusof, S. Siddiquee // International Journal of Electrochemical Scie

130. Kryukova, T. A. Polarographic analysis / T. A. Kryukova, S. I. Sinyakova, T. V. Aref'eva. – Moscow: Goshimizdat, 1959. – P. 289-304. [Russian]

131. Mayranovsky, S. G. Polarography in organic chemistry / S. G. Mayranovsky,

Y. P. Stradin, V. D. Bezugly. – Leningrad: Chemistry, 1975. – 351 p. [Russian]

132. Chan, W. H. Adsorption voltammetric determination of μg/L levels formaldehyde via in situ derivatization with Girard's reagent T / W. H. Chan, T. Y. Xie // Analytica Chimica Acta. – 1997. – Vol. 339. – № 1-2. – P. 173-179.

133. Chan, W. H. Differential-pulse Polarographic Micro-determination of Formaldehyde / W. H. Chan, W. C. Chung, P. X. Cai // Analyst. – 1995. – Vol. 120. – № 8. – P. 2233-2236.

134. Dedov, A. G. Indirect determination of formaldehyde by alternating-current voltammetry at a hanging mercury drop in the presence of oxygen / A. G. Dedov, N. K. Zaitsev, P. M. Zaitsev, A. V. Pavlyuk, S. G. Suslov // Journal of Analytical Chemistry. – 2000. – Vol. 55. – № 6. – P. 583-585.

135. Wang, J. Palladium-doped Screen-printed Electrodes for Monitoring Formaldehyde / J. Wang, M. Pedrero, X. Cai // Analyst. – 1995. – Vol. 120. – № 6. – P. 1969-1972.

136. Trivedi, D. The electrochemical determination of formaldehyde in aqueous media using nickel modified electrodes / D. Trivedi, J. Crosse, J. Tanti, A. J. Cass, K. E. Toghill // Sensors and Actuators, B: Chemical. – 2018. – Vol. 270. – P. 298-303.

137. Daemi, S. An efficient platform for the electrooxidation of formaldehyde based on amorphous NiWO4 nanoparticles modified electrode for fuel cells / S. Daemi, M. Moalem-Banhangi, S. Ghasemi, A. A. Ashkarran // Journal of Electroanalytical Chemistry. – 2019. – Vol. 848. – Article 113270.

138. Zarei, E. Highly sensitive electrocatalytic determination of formaldehyde using a Ni/Ionic liquid modified carbon nanotube paste electrode / E. Zarei, M. R. Jamali, F. Ahmadi // Bulletin of Chemical Reaction Engineering and Catalysis. – 2018. – Vol. 13. – № 3. – P. 529-542.

139. Nag, S. A simple nano cerium oxide modified graphite electrode for electrochemical detection of formaldehyde in mushroom / S. Nag, S. Pradhan, H. Naskar, R. B. Roy, B. Tudu, P. Pramanik, R. Bandyopadhyay // IEEE Sensors Journal. –

2021. – Vol. 21. – № 10. – P. 12019-12026.

140. Dong, Q. Co-Based Transition Metal Hydroxide Nanosheet Arrays on Carbon Cloth for Sensing Glucose and Formaldehyde / Q. Dong, L. Yang, Z. He, Y. Zhang, X. Tang, J. Tang, K. Huang, Z. Zou, X. Xiong // ACS Applied Nano Materials. – 2021. – Vol. 4. – № 5. – P. 5076-5083.

141. Zhang, S. Fabrication of CuO/Cu/TiO2 nanotube arrays modified electrode for detection of formaldehyde / S. Zhang, X. Wen, M. Long, J. Xi, J. Hu, A. Tang // Journal of Alloys and Compounds. – 2020. – Vol. 829. – Article 154568.

142. Hajilari, F. Application of Cu/porous silicon nanocomposite screen printed sensor for the determination of formaldehyde / F. Hajilari, K. Farhadi, H. Eskandari, F. Allahnouri // Electrochimica Acta. – 2020. – Vol. 355. – Article 136751.

143. Philip, A. S. Electrochemical Sensing of Formaldehyde in Fish Samples Using a Polydopamine-Modified Stainless Steel Electrode / A. S. Philip, S. Rison, A. R. Cherian, K. B. Akshaya, L. George, A. Varghese // ECS Journal of Solid State Science and Technology. – 2021. – Vol. 10. – № 6. – Article 067003.

144. Su, L. Electrochemical Sensor with Bimetallic Pt–Ag Nanoparticle as Catalyst for the Measurement of Dissolved Formaldehyde / L. Su, Y. Cheng, J. Shi, X. Wang, P. Xu, Y. Chen, Y. Zhang, S. Zhang, L. Xinxin // Journal of The Electrochemical Society. – 2022. – Vol. 169. – № 4. – Article 047507.

145. Xu, S. Efficient formaldehyde sensor based on PtPd nanoparticles-loaded nafion-modified electrodes / S. Xu, L. Jiang, X. Huang, W. Ju, Y. Liang, Z. Tao, Y. Yang, B. Zhu, G. Wei // Nanotechnology. – 2024. – Vol. 35. – Article ID 025704.

146. Alves, G. M. S. Multi-element determination of metals and metalloids in waters and waste waters, at trace concentration level, using electroanalytical stripping methods with environmentally friendly mercury free-electrodes: A review / G. M. S. Alves, L. S. Rocha, H. M. V. M. Soares // Talanta. – 2017. – Vol. 175. – P. 53-68.

147. Bobrowski, A. Morphology and electrochemical properties of the bismuth film electrode ex situ electrochemically plated from perchloric acid / A. Bobrowski, A.

Królicka, J. Zarebski // Electroanalysis. – 2010. – Vol. 22. – № 13. – P. 1421-1427.

148. Economou, A. Screen-printed electrodes modified with “green” metals for electrochemical stripping analysis of toxic elements / A. Economou // Sensors. – 2018. – Vol. 18. – № 4. – Article 1032.

149. Kong, D. Coexisted Inorganic Ions Influence on Crystal Morphology of Bismuth-Film-Modified Electrodes / D. Kong, Y. Chen, P. Wan, B. Men // The Electrochemical Society, Inc. Meeting Abstracts. – 2014. – Vol. MA2014-03. – № 4. – P. 520.

150. Królicka, A. Bismuth film electrode for adsorptive stripping voltammetry - Electrochemical and microscopic study / A. Królicka, A. Bobrowski // Electrochemistry Communications. – 2004. – Vol. 6. – № 2. – P. 99-104.

151. Qin, X. Influence of substrate temperature on the morphology and structure of bismuth thin films deposited by magnetron sputtering / X. Qin, C. Sui, L. Di // Vacuum. – 2019. – Vol. 166. – № 1. – P. 316-322.

152. Nunes, L. M. S. The influence of the electrodeposition conditions on the electroanalytical performance of the bismuth film electrode for lead determination / L. M. S. Nunes, R. C. Faria // Electroanalysis. – 2008. – Vol. 20. – № 20. – P. 2259-2263.

153. Barceló, C. Ex-situ Antimony Screen-printed Carbon Electrode for Voltammetric Determination of Ni(II)-ions in Waste water / C. Barceló, N. Serrano, C. Ariño, J. M. DíazCruz, M. Esteban // Electroanalysis. – 2016. – Vol. 28. – № 3. – P. 640-644.

154. Yang, M. Fern-shaped bismuth dendrites electrodeposited at hydrogen evolution potentials / M. Yang // Journal of Materials Chemistry. – 2011. – Vol. 21. – № 9. – P. 3119-3124.

155. Xiao, Z. L. Tuning the Architecture of Mesostructures by Electrodeposition / Z. L. Xiao, C. Y. Han, W. K. Kwok, H. H. Wang, U. Welp, J. Wang, G. W. Crabtree // Journal of the American Chemical Society. – 2004. – Vol. 126. – № 8. – P. 2316-2317.

156. Serrano, N. Coating methods, modifiers and applications of bismuth screen-printed electrodes / N. Serrano, A. Alberich, J. M. Díaz-Cruz, C. Ariño, M. Esteban // TrAC - Trends in Analytical Chemistry. – 2013. – Vol. 46. – P. 15-29.

157. Bobrowski, A. Antimony Film Electrode Prepared in Situ in Hydrogen Potassium Tartrate in Anodic Stripping Voltammetric Trace Detection of Cd(II), Pb(II), Zn(II), Tl(I), In(III) and Cu(II) / A. Bobrowski, M. Putek, J. Zarebski // Electroanalysis. – 2012. – Vol. 24. – № 5. – P. 1071-1078.

158. Hočevar, S. B. A study on operational parameters for advanced use of bismuth film electrode in anodic stripping voltammetry / S. B. Hočevar, B. Ogorevc, J. Wang, B. Pihlar // Electroanalysis. – 2002. – Vol. 14. – № 24. – P. 1707-1712.

159. Olsen, N. J. Antimony(III) sulfide complexes in aqueous solutions at 30 °C: A solubility and XAS study / N. J. Olsen, B. W. Mountain, T. M. Seward // Chemical Geology. – 2018. – Vol. 476. – P. 233-247.

160. Quintana, J. C. Part I: A comparative study of bismuth-modified screen-printed electrodes for lead detection / J. C. Quintana, F. Arduini, A. Amine, F. Punzo, G. L. Destri, C. Bianchini, D. Zane, A. Curulli // Analytica Chimica Acta. – 2011. – Vol. 707. – № 1-2. – P. 171-177.

161. Vladislavić, N. Morphological characterization of ex situ prepared bismuth film electrodes and their application in electroanalytical determination of the biomolecules / N. Vladislavić, M. Buzuk, S. Brinić, M. Buljac, M. Bralić // Journal of Solid State Electrochemistry. – 2016. – Vol. 20. – № 8. – P. 2241-2250.

162. Kadara, R. O. Development of disposable bulk-modified screen-printed electrode based on bismuth oxide for stripping chronopotentiometric analysis of lead (II) and cadmium (II) in soil and water samples / R. O. Kadara, I. E. Tothill // Analytica Chimica Acta. – 2008. – Vol. 623. – № 1. – P. 76-81.

163. Voigt, K. Electrodeposition of Versatile Nanostructured Sb/Sb2O3 Microcomposites: A Parameter Study / K. Voigt, C. Heubner, T. Liebmann, B. Matthey, M. Weiser, M. Schneider, A. Michaelis // Advanced Materials Interfaces. – 2020. – Vol. 7. – № 13. – P. 1-10.

164. Wang, J. Bismuth-coated screen-printed electrodes for stripping voltammetric measurements of trace lead / J. Wang, J. Lu, S. B. Hočevar, B. Ogorevc // Electroanalysis. – 2001. – Vol. 13. – № 1. – P. 13-16.

165. Hutton, E. A. Validation of bismuth film electrode for determination of cobalt and cadmium in soil extracts using ICP-MS / E. A. Hutton, J. T. Van Elteren, B. Ogorevc, M. R. Smyth // Talanta. – 2004. – Vol. 63. – № 4. – P. 849-855.

166. Wang, J. Effect of surface-active compounds on the stripping voltammetric response of bismuth film electrodes / J. Wang, R. P. Deo, S. Thongngamdee, B. Ogorevc // Electroanalysis. – 2001. – Vol. 13. – № 14. – P. 1153-1156.

167. Levent, A. Voltammetric Behavior of Testosterone on Bismuth Film Electrode: Highly Sensitive Determination in Pharmaceuticals and Human Urine by Square-Wave Adsorptive Stripping Voltammetry / A. Levent, A. Altun, S. Taş, Y. Yardım, Z. Şentürk // Electroanalysis. – 2015. – Vol. 27. – № 5. – P. 1219-1228.

168. Pauliukaite, R. Characterization and application of bismuth-film modified carbon film electrodes / R. Pauliukaite, C. M. A. Brett // Electroanalysis. – 2005. – Vol. 17. – № 15-16. – P. 1354-1359.

169. Hočevar, S. B. Reactivity at the film/solution interface of ex situ prepared bismuth film electrodes: A scanning electrochemical microscopy (SECM) and atomic force microscopy (AFA) investigation / S. B. Hočevar, S. Daniele, C. Bragato, B. Ogorevc // Electrochimica Acta. – 2007. – Vol. 53. – № 2. – P. 555-560.

170. Hutton, E. A. Ex situ preparation of bismuth film microelectrode for use in electrochemical stripping microanalysis / E. A. Hutton, S. B. Hočevar, B. Ogorevc // Analytica Chimica Acta. – 2005. – Vol. 537. – № 1-2. – P. 285-292.

171. Morfobos, M. Simultaneous determination of nickel(II) and cobalt(II) by square wave adsorptive stripping voltammetry on a rotating-disc bismuth-film electrode / M. Morfobos, A. Economou, A. Voulgaropoulos // Analytica Chimica Acta. – 2004. – Vol. 519. – № 1. – P. 57-64.

172. Hutton, E. A. Bismuth film electrode for simultaneous adsorptive stripping analysis of trace cobalt and nickel using constant current chronopotentiometric and voltammetric protocol / E. A. Hutton, S. B. Hočevar, B. Ogorevc, M. R. Smyth // Electrochemistry Communications. – 2003. – Vol. 5. – № 9. – P. 765-769.

173. Wang, J. Bismuth film electrodes for adsorptive stripping voltammetry of trace nickel / J. Wang, J. Lu // Electrochemistry Communications. – 2000. – Vol. 2. – № 6. – P. 390-393.

174. Kokkinos, C. Disposable mercury-free cell-on-a-chip devices with integrated microfabricated electrodes for the determination of trace nickel(II) by adsorptive stripping voltammetry / C. Kokkinos, A. Economou, I. Raptis, T. Speliotis // Analytica Chimica Acta. – 2008. – Vol. 622. – № 1-2. – P. 111-118.

175. Piankova, L. A. Bismuth nanoparticles in adsorptive stripping voltammetry of nickel / L. A. Piankova, N. A. Malakhova, N. Y. Stozhko, K. Z. Brainina, A. M. Murzakaev, O. R. Timoshenkova // Electrochemistry Communications. – 2011. – Vol. 13. – № 9. – P. 981-984.

176. Królicka, A. Study on Catalytic Adsorptive Stripping Voltammetry of Trace Cobalt at Bismuth Film Electrodes / A. Królicka, A. Bobrowski, K. Kalcher, J. Mocak, I. Svancara, K. Vytras // Electroanalysis. – 2003. – Vol. 15. – № 23-24. – P. 1859-1863.

177. Królicka, A. Effects of electroplating variables on the voltammetric properties of bismuth deposits plated potentiostatically / A. Królicka, A. Bobrowski, A. Kowal // Electroanalysis. – 2006. – Vol. 18. – № 17. – P. 1649-1657.

178. Svancara, I. A role of the plating regime in the deposition of bismuth films onto a carbon paste electrode. Microscopic study / I. Svancara, L. Baldrianova, M. Vlcek, R. Metelka, K. Vytras // Electroanalysis. – 2005. – Vol. 17. – № 2. – P. 120-126.

179. Zhong, H. Bismuth nanodendrites as a high performance electrocatalyst for selective conversion of CO2 to formate / H. Zhong, Y. Qiu, T. Zhang, X. Li, H. Zhang, X. Chen // Journal of Materials Chemistry A. – 2016. – Vol. 4. – № 36. – P. 13746-13753.

180. Wang, J. Bismuth-coated carbon electrodes for anodic stripping voltammetry / J. Wang, J. Lu, S. B. Hočevar, P. A. M. Farias, B. Ogorevc // Analytical Chemistry. – 2000. – Vol. 72. – № 14. – P. 3218-3222.

181. Lee, S. H. Effect of Plating Variables on Oxygen Evolution Reaction of Ni–Zn–Fe Electrodes for Alkaline Water Electrolysis / S. H. Lee, J. E. Kim, H. Joo, C. Park,

S. Jeong, K. Jung, Y. Kim, K. Kang // Catalysts. – 2022. – Vol. 12. – № 3. – 346 p.

182. Hirayama, H. Nucleation and growth of ultrathin Bi films / H. Hirayama // Advances in Physics: X. – 2021. – Vol. 6. – № 1. – Article 1845975.

183. Yang, M. Electrodeposition of bismuth onto glassy carbon electrodes from nitrate solutions / M. Yang, Z. Hu // Journal of Electroanalytical Chemistry. – 2005. – Vol. 583. – № 1. – P. 46-55.

184. Vladislavic´, N. Study of Bi film formation on different carbon based electrodes for possible applicability in electroanalytical determination of cysteine / N. Vladislavic´, S. Brinic´, Z. Grubacˇ, M. Buzuk // International Journal of Electrochemical Science. – 2014. – Vol. 9. – № 11. – P. 6020-6032.

185. Narasimman, P. Effect of surfactants on the electrodeposition of Ni-SiC composites / P. Narasimman, M. Pushpavanam, V. M. Periasamy // Portugaliae Electrochimica Acta. – 2011. – Vol. 30. – № 1. – P. 1-14.

186. Kefala, G. Determination of trace aluminium by adsorptive stripping voltammetry on a preplated bismuth-film electrode in the presence of cupferron / G. Kefala, A. Economou, M. Sofoniou // Talanta. – 2006. – Vol. 68. – № 3. – P. 1013-1019.

187. Hue, N. T. Determination of Chromium in Natural Water by Adsorptive Stripping Voltammetry Using in Situ Bismuth Film Electrode / N. T. Hue, N. V. Hop, H. T. Long, N. H. Phong, T. H. Uyen, L. Q Hung, N. N. Phuong // Journal of Environmental and Public Health. – 2020. – Vol. 2020. – № 1. – Article 1347836.

188. Guzsvány, V. Bismuth film electrode for the cathodic electrochemical determination of thiamethoxam / V. Guzsvány, M. Kádár, F. Gaál, L. Bjelica, K. Tóth // Electroanalysis. – 2006. – Vol. 18. – № 13-14. – P. 1363-1371.

189. Zidarič, T. Multi-pulse galvanostatic preparation of nanostructured bismuth film electrode for trace metal detection / T. Zidarič, V. Jovanovski, E. Menart, M. Zorko, M. Kolar, M. Veber, S. B. Hočevar // Sensors and Actuators, B: Chemical. – 2017. – Vol. 245. – P. 720-725.

190. Fu, R. Synthesis and characterization of triangular bismuth nanoplates / R.

Fu, S. Xu, Y. N. Lu, J. J. Zhu // Crystal Growth and Design. – 2005. – Vol. 5. – № 4. – P. 1379-1385.

191. Jovanovski, V. Ex situ prepared antimony film electrode for electrochemical stripping measurement of heavy metal ions / V. Jovanovski, S. B. Hočevar, B. Ogorevc // Electroanalysis. – 2009. – Vol. 21. – № 21. – P. 2321-2324.

192. Arancibia, V. Ex situ prepared nafion-coated antimony film electrode for adsorptive stripping voltammetry of model metal ions in the presence of pyrogallol red / V. Arancibia, E. Nagles, C. Rojas, M. Gómez // Sensors and Actuators, B: Chemical. – 2013. – Vol. 182. – P. 368-373.

193. Kokkinos, C. Novel disposable microfabricated antimony-film electrodes for adsorptive stripping analysis of trace Ni(II) / C. Kokkinos, A. Economou, I. Raptis, T. Speliotis // Electrochemistry Communications. – 2009. – Vol. 11. – № 2. – P. 250-253.

194. Nigović, B. Square-wave voltammetric determination of pantoprazole using exsitu plated antimony-film electrode / B. Nigović, S. B. Hočevar // Electrochimica Acta. – 2013. – Vol. 109. – P. 818-822.

195. Betancourth, J. M. Multivariate cathodic square wave stripping voltammetry optimization for nitro group compounds determination using antimony film electrodes / J. M. Betancourth, M. Cuellar, P. I. Ortiz, V. Pfaffen // Microchemical Journal. – 2018. – Vol. 139. – P. 139-149.

196. Sosa, V. Antimony film screen-printed carbon electrode for stripping analysis of Cd(II), Pb(II), and Cu(II) in natural samples / V. Sosa, C. Barceló, N. Serrano, C. Ariño, J. M. Díaz-Cruz, M. Esteban // Analytica Chimica Acta. – 2015. – Vol. 855. – P. 34-40.

197. Ashrafi, A. M. Codeposited antimony-bismuth film carbon paste electrodes for electrochemical stripping determination of trace heavy metals / A. M. Ashrafi, K. Vytřas // International Journal of Electrochemical Science. – 2013. – Vol. 8. – № 2. – P. 2095-2103.

198. Pérez-Ràfols, C. New approaches to antimony film screen-printed electrodes

using carbon- based nanomaterials substrates / C. Pérez-Ràfols, N. Serrano, J. M. Díaz-Cruz, C. Ariño, M. Esteban // Analytica chimica acta. – 2016. – Vol. 916. – P. 17-23.

299. Hilali, N. Comparison between modified and unmodified carbon paste electrodes for hexavalent chromium determination / N. Hilali, A. Ghanam, H. Mohammadi, A. Amine, J. J. Garcıa-Guzman, L. Cubillana-Aguilera, J. M. Palacios-Santander // Electroanalysis. – 2018. – Vol. 30. – № 11. – P. 2750-2759.

200. Scholz F. Electroanalytical Methods: Guide to Experiments and Applications, 2nd ed. – Berlin: Springer, 2010. – 359 p.

201. Ayala, M. C. Electrochemical modified electrode with bismuth film for ultrasensitive determination of aluminum (iii) / M. C. Ayala, L. L. López, A. Jaramillo-Botero, D. Valencia // Journal of Electroanalytical Chemistry. – 2022. – Vol. 919. – Article 116552.

202. Chooto, P. Cyclic Voltammetry and Its Applications / P. Chooto. – London: IntechOpen, 2019. – 1 p.

203. Pauliukaite, R. Characterization and applications of a bismuth bulk electrode / R. Pauliukaite, S. B. Hočevar, B. Ogorevc, J. Wang // Electroanalysis. – 2004. – Vol. 16. – № 9. – P. 719-723.

204. Bedin, K. C. Inexpensive bismuth-film electrode supported on pencil-lead graphite for determination of Pb(II) and Cd(II) Ions by anodic stripping voltammetry / K. C. Bedin, E. Y. Mitsuyasu, A. Ronix, A. L. Cazetta, O. Pezoti, V. C. Almeida // International Journal of Analytical Chemistry. – 2018. – Vol. 2018. – № 1. – Article 1473706.

205. Mayorga-Martinez, C. C. Bismuth nanoparticles for phenolic compounds biosensing application / C. C. Mayorga-Martinez, M. Cadevall, M. Guix, J. Ros, A. Merkoçi // Biosensors and Bioelectronics. – 2013. – Vol. 40. – № 1. – P. 57-62.

206. Randviir, E. P. A review of electrochemical impedance spectroscopy for bioanalytical sensors / E. P. Randviir, C. E. Banks // Analytical Methods. – 2022. – Vol. 14. – № 45. – P. 4602-4624.

207. Das, A. Shape-controlled synthesis of three-dimensional triangular bismuth

microstructures and sensing of H2O2 / A. Das, M. V. Sangaranarayanan // CrystEngComm. – 2016. – Vol. 18. – № 7. – P. 1147-1155.

208. Ortiz, B. Electrochemical modification of a carbon electrode using aromatic diazonium salts. 2. Electrochemistry of 4-nitrophenyl modified glassy carbon electrodes in aqueous media / B. Ortiz, C. Saby, G. Y. Champagne, D. Bélanger // Journal of Electroanalytical Chemistry. – 1998. – Vol. 455. – № 1-2. – P. 75-81.

209. Koç, Y. Investigation of electrochemical behavior of potassium ferricyanide / ferrocyanide redox probes on screen printed carbon electrode through cyclic voltammetry and electrochemical impedance spectroscopy / Y. Koç, U. Morali, S. Erol, H. Avci // Turkish Journal of Chemistry. – 2021. – Vol. 45. – № 6. – P. 1895-1915.

210. Yıldız, C. Highly sensitive direct simultaneous determination of zinc(II), cadmium(II), lead(II), and copper(II) based on in-situ-bismuth and mercury thin-film plated screen-printed carbon electrode / C. Yıldız, D. E. Bayraktepe, Z. Yazan // Monatshefte fur Chemie. – 2021. – Vol. 152. – № 12. – P. 1527-1537.

211. Wong, A. Voltammetric determination of 3-Methylmorphine using glassy carbon electrode modified with rGO and bismuth film / A. Wong, A. M. Santos, C. A. Proenca, T. A. Baldo, M. H. A. Feitosa, F. C. Moraes, M. D. P. T. Sotomayor // Biosensors. – 2022. – Vol. 12. – № 10. – 860 p.

212. Tohidinia, M. Poly(quercetin)-bismuth nanowires as a new modifier for simultaneous voltammetric determination of dihydroxybenzene isomers and nitrite / M. Tohidinia, M. Farsadrooh, S. Bahmanzadeh, N. Sabbaghi, M. Noroozifar // Royal Society of Chemistry Advances. – 2018. – Vol. 8. – № 3. – P. 1237-1245.

213. Czop, E. A study of in situ plated tin-film electrodes for the determination of trace metals by means of square-wave anodic stripping voltammetry / E. Czop, A. Economou, A. Bobrowski // Electrochimica Acta. – 2011. – Vol. 56. – № 5. – P. 2206-2212.

214. Petovar, B. A detailed electrochemical impedance spectroscopy study of a bismuth-film glassy carbon electrode for trace metal analysis / B. Petovar, K. Xhanari, M. Finšgar // Analytica Chimica Acta. – 2018. – Vol. 1004. – P. 10-21.

215. Finšgar, M. Copper-bismuth-film in situ electrodes for heavy metal detection / M. Finšgar, L. Kovačec // Microchemical Journal. – 2020. – Vol. 154. – P. 1-10. – Article 104635.

216. Gouveia-Caridade C. Electrochemical Impedance Characterization of Nafion-Coated Carbon Film Resistor Electrodes for Electroanalysis / C. Gouveia-Caridade, C. M. A. Brett // Electroanalysis. – 2005. – Vol. 17. – № 7. – P. 549-555.

217. Gouveia-Caridade, C. Influence of Nafion Coatings and Surfactant on the Stripping Voltammetry of Heavy Metals at Bismuth-Film Modified Carbon Film Electrodes / C. Gouveia-Caridade, R. Pauliukaite, C. M. A. Brett // Electroanalysis. – 2006. – Vol. 18. – № 9. – P. 854-861.

218. Newman J. Electrochemical systems, 3rd ed / J. Newman, K. E. Thomas-Alyea. – New Jersey: John Wiley & Sons, 2004. – P. 180-185.

219. Al-Harbi E. A. Fabrication and application of bismuth-film modified glassy carbon electrode as sensor for highly sensitive determination of cetirizine dihydrochloride in pharmaceutical products and water samples / E. A. Al-Harbi // International Journal of Electrochemical Science. – 2021. – Vol. 16. – № 10. – Article 211036.

220. Anik, Ü. The usage of a bismuth film electrode as transducer in glucose biosensing / Ü. Anik, S. Timur, M. Çubukçu, A. Merkoçi // Microchimica Acta. – 2008. – Vol. 160. – № 1-2. – P. 269-273.

221. Mardiana, U. Electropolymerized Neutral Red as Redox Mediator for Yeast Fuel Cell / U. Mardiana, C. Innocent, H. Jarrar, M. Cretin // International Journal of Electrochemical Science. – 2015. – Vol. 10. – № 11. – P. 8886-8898.

222. Naik, T. S. S. K. Modification of carbon paste electrode by electrochemical polymerization of neutral red and its catalytic capability towards the simultaneous determination of catechol and hydroquinone: A voltammetric study / T. S. S. K. Naik, B. E. K. Swamy // Journal of Electroanalytical Chemistry. – 2017. – Vol. 804. – P. 78-86.

223. Park, D. H. Electricity generation in microbial fuel cells using neutral red as an electronophore / D. H. Park, J. G. Zeikus // Applied and Environmental

Microbiology. – 2000. – Vol. 66. – № 4. – P. 1292-1297.

224. Kuzin, Y. Electrochemical DNA sensor based on carbon black-poly (neutral red) composite for detection of oxidative DNA damage / Y. Kuzin, D. Kappo, A. Porfireva, D. Shurpik, I. Stoikov, G. Evtugyn, T. Hianik // Sensors. – 2018. – Vol. 18. – № 10. – Article 3489.

225. Evtugyn, G. Electrochemical aptasensor based on polycarboxylic macrocycle modified with neutral red for aflatoxin B1 detection / G. Evtugyn, A. Porfireva, V. Stepanova, R. Sitdikov, I. Stoikov, D. Nikolelis, T. Hianik // Electroanalysis. – 2014. – Vol. 26. – № 10. – P. 2100-2109.

226. Smolko, V. Electrochemical Aptasensor Based on Poly (Neutral Red) and Carboxylated Pillar[5]arene for Sensitive Determination of Aflatoxin M1 / V. Smolko, D. Shurpik, A. Porfireva, G. Evtugyn, I. Stoikov, T. Hianik // Electroanalysis. – 2018. – Vol. 30. – № 3. – P. 486-496.

227. Hong, J. Neutral Red and Ferroin as Reversible and Rapid Redox Materials for Redox Flow Batteries / J. Hong, K. Kim // ChemSusChem. – 2018. – Vol. 11. – № 11. – P. 1866-1872.

228. Jeykumari, D. R. S. Covalent modification of multiwalled carbon nanotubes with neutral red for the fabrication of an amperometric hydrogen peroxide sensor / D. R. S. Jeykumari, S. S. Narayanan // Nanotechnology. – 2007. – Vol. 18. – № 12. – Article 125501.

229. Yang, J. Neutral red paired with metal sulfates for redox flow batteries / J. Yang, H. O. Seo, K. Kim // Journal of Electroanalytical Chemistry. – 2021. – Vol. 893. – Article 115333.

230. Walz Jr, F. G. Equilibrium studies on neutral red–DNA binding / F. G. Walz Jr, B. Terenna, D. Rolince // Biopolymers: Original Research on Biomolecules. – 1975. – Vol. 14. – № 4. – P. 825-837.

231. Halliday, C. S. Some electrochemical and photoelectrochemical properties of 3-Amino-7-dimethylamino-2-methylphenazine (Neutral Red) in aqueous solution / C. S. Halliday, D. B. Matthews // Australian Journal of Chemistry. – 1983. – Vol. 36. – № 3. – P. 507-516.

232. Bard, A. J. Electrochemical Methods: Fundamentals and Applications, 2nd ed / A. J. Bard, L. R. Faulkner. – New York: John Wiley & Sons, 1980. – 97 p.

233. Turyan, Y. I. Chemical Reactions in Polarography / Y. I. Turyan. – Moscow: Khimiya, 1980. – 87 p. [Russian]

234. Gumustas, M. The Role of and the Place of Method Validation in Drug Analysis Using Electroanalytical Techniques / M. Gumustas, S. A. Ozkan // The Open Analytical Chemistry Journal. – 2011. – Vol. 5. – № 1. – P. 1-21.

235. Pauliukaite, R. Characterisation of poly (neutral red) modified carbon film electrodes; application as a redox mediator for biosensors / R. Pauliukaite, M. E. Ghica, M. Barsan, C. M. A. Brett // Journal of Solid State Electrochemistry. – 2007. – Vol. 11. – P. 899-908.

236. Economou, A. Bismuth-film electrodes: Recent developments and potentialities for electroanalysis / A. Economou // TrAC - Trends in Analytical Chemistry. – 2005. – Vol. 24. – № 4. – P. 334-340.

237. Seifi, A. Highly sensitive and simultaneous electrochemical determination of lead and cadmium ions by poly(thionine)/MWCNTs-modified glassy carbon electrode in the presence of bismuth ions / A. Seifi, A. Afkhami, T. Madrakian // Journal of Applied Electrochemistry. – 2022. – Vol. 52. – № 10. – P. 1513-1523.

238. Kaur, B. Simultaneous determination of epinephrine, paracetamol, and folic acid using transition metal ion-exchanged polyaniline-zeolite organic-inorganic hybrid materials / B. Kaur, R. Srivastava // Sensors and Actuators, B: Chemical. – 2015. – Vol. 211. – P. 476-488.

239. Malakhova, N. Neutral Red as a redox probe for comparative evaluation of electrochemical performance of bismuth modified electrodes / N. Malakhova, A. B. Kifle, A. Ivoilova, N. Leonova, A. Kozitsina // Analytical Letters. – 2024. – Article 2314744. – P. 1-18.

240. Li, Z. High-performance solid-state supercapacitors based on graphene-ZnO hybrid nanocomposites / Z. Li, Z. Zhou, G. Yun, K. Shi, X. Lv, B. Yang. – 2013. – Vol. 8. – № 1. – Article 473.

241. Ranjan, B. Pseudocapacitive Storage in Molybdenum Oxynitride Nanostructures Reactively Sputtered on Stainless-Steel Mesh Towards an All-Solid-State Flexible Supercapacitor / B. Ranjan, D. Kaur // Small. – 2023. – Vol. 20. – № 20. – Article 2307723. – P. 1-17.

242. Stoynov, Z. B. Electrochemical Impedance / Z. B. Stoynov, B. M. Grafov, B. S. Savova-Stoynov, V. V. Elkin. – Moscow: Nauka; 1991. – 336 p. [Russian]

243. Kifle, A. B. Evaluation of electrochemical performance of antimony modified screen-printed carbon electrodes / A. B. Kifle, N. Malakhova, A. Ivoilova, N. Leonova, S. Saraeva, A. Kozitsina // Chimica Techno Acta. – 2024. – Vol. 11. – № 2. – Article 202411204.

244. Malakhova, N. Bismuth-coated screen-printed electrodes for the simple voltammetric determination of formaldehyde / N. Malakhova, P. Mozharovskaia, A. B. Kifle, A. Kozitsina // Analytical Methods. – 2022. – Vol. 14. – № 35. – P. 3423-3433.

245. Yates, F. Statistical tables for biological agricultural and medical research, 1st ed. / F. Yates. – London: Bookliver and Bookyd Ltd., 1938. – 90 p.

# Appendix A (Mandatory)

# Implementation information

федеральное государственное бюджетное
образовательное учреждение
высшего образования
«Уральский государственный
медицинский университет»
Министерства здравоохранения
Российской Федерации
(ФГБОУ ВО УГМУ Минздрава России)
ул. Репина, 3, г.Екатеринбург, 620028
Тел. (343) 371-34-90; факс 371-64-00
E-mail: usma@usma.ru
ИНН/КПП 6658017389/665801001

от _____ № _____
на № _____ от _____

**УТВЕРЖДАЮ:**
Ректор федерального государственного
бюджетного образовательного учреждения
высшего образования
«Уральский государственный медицинский
университет»
Министерства здравоохранения
Российской Федерации,
академик РАН,
доктор медицинских наук,
профессор
**Ковтун О.П.**

## АКТ

внедрения в учебный процесс ФГБОУ ВО УГМУ Минздрава России методики анализа фармпрепаратов на содержание формальдегида, разработанной в рамках научных исследований аспиранта Кифле Александра Берхане, обучающегося по направлению 04.06.01 – Химические науки на кафедре аналитической химии Химико-технологического института Уральского федерального университета имени первого Президента России Б.Н. Ельцина под руководством доктора химических наук, профессора, заведующего кафедрой Козициной А.Н.

Мы, нижеподписавшиеся, комиссия в составе: председателя - проректора по образовательной деятельности, кандидата медицинских наук, доцента Ушакова А.А., и членов - декана фармацевтического факультета, д.ф.н., профессора Андриановой Г.Н., и.о. зав. кафедрой фармации Мельниковой О.А. удостоверяем, что методика электрохимического анализа фармпрепаратов на содержание формальдегида внедрена и используется в учебном процессе при подготовке фармацевтических кадров на кафедре Фармации в рамках дисциплин «Аналитическая химия», «Общая и неорганическая химия».

Выполнение количественного контроля по разработанной методике является экологически безопасным, не требует применения дорогостоящих и агрессивных реагентов, не зависит от окраски раствора. При этом позволяет определять достаточно низкие концентрации формальдегида на уровне 0,02 мг/л.

Эффективность внедрения подтверждается развитием профессиональных компетенций обучающихся по вопросам, связанным с особенностями фармацевтического анализа электрохимическими методами, в частности методом инверсионной вольтамперометрии с использованием в качестве индикаторных электродов толстопленочных углеродсодержащих электродов, модифицированных висмутом.

Председатель:
Проректор по образовательной деятельности
к.м.н., доцент А.А. Ушаков

Члены комиссии:
Декан фармацевтического факультета, д.ф.н., профессор Г.Н. Андрианова

И.о. зав. кафедры фармации, д.ф.н., профессор О.А. Мельникова

Подпись к.м.н., доцента А.А. Ушакова, д.ф.н, профессора Г.Н. Андриановой, д.ф.н., профессора О.А. Мельниковой заверяю начальник управления кадрового обеспечения ФГБОУ ВО УГМУ Минздрава России _____ Н.А. Поляк